AD-A272 113 TION PAGE

Form Approved
OMB No. 0704-0188

1. AGENCY USE ONLY (Leave blank)	2. REPORT DATE	3. REPORT TYPE AND DATES COVERED
	10/12/93	ANNUAL TECH. REPORT - 11/1-90 - 10/31/93

4. TITLE AND SUBTITLE
INVESTIGATIONS OF HETEROJUNCTIONS AND MULTIPLE QUANTUM WELL STRUCTURES USING CRYSTALLINE ORGANIC SEMICONDUCTORS

5. FUNDING NUMBERS
AFOSR-91-0075

6. AUTHOR(S)
STEPHEN R. FORREST

7. PERFORMING ORGANIZATION NAME(S) AND ADDRESS(ES)
UNIVERSITY OF SOUTHERN CALIFORNIA
DEPARTMENT OF ELECTRICAL ENGINEERING
LOS ANGELES, CA 90089-0241

8. PERFORMING ORGANIZATION REPORT NUMBER
AFOSR-TR-

9. SPONSORING/MONITORING AGENCY NAME(S) AND ADDRESS(ES)
AFOSR
BOLLING AFB
WASHINGTON, DC 20332-6448

10. SPONSORING/MONITORING AGENCY REPORT NUMBER
2305/ES

11. SUPPLEMENTARY NOTES

12a. DISTRIBUTION/AVAILABILITY STATEMENT
APPROVED FOR PUBLIC RELEASE: DISTRIBUTION UNLIMITED

12b. DISTRIBUTION CODE

13. ABSTRACT *(Maximum 200 words)*

A new class of engineered materials based on crystalline organic semiconductors grown by the ultrahigh vacuum process of organic molecular beam deposition is described. The objective of this program is to investigate these materials and the conditions which lead to ordered growth between highly lattice mismatched van der Waals crystals into novel "quasi-epitaxial" structures. During the first year of the program, considerable progress has been made in understanding and exploiting this new class of materials. In particular, a simple model has been developed which describes the physical mechanisms underlying quasi-epitaxy. The electrical and optical properties of both single and multiple heterojunction structures grown using alternating layers of two different, lattice-mismatched organic molecules have been investigated in detail. It is found that the layers can be grown sufficiently thin (10 Å) to result in exciton confinement in organic multiple quantum wells. These and other quasi-epitaxially grown structures can lead to an entirely new family of optoelectronic devices with exciting new electronic and nonlinear optical characteristics.

14. SUBJECT TERMS	15. NUMBER OF PAGES 115
	16. PRICE CODE

17. SECURITY CLASSIFICATION OF REPORT	18. SECURITY CLASSIFICATION OF THIS PAGE	19. SECURITY CLASSIFICATION OF ABSTRACT	20. LIMITATION OF ABSTRACT
UNCLASSIFIED	UNCLASSIFIED	UNCLASSIFIED	UL

Investigations of Heterojunctions and Multiple Quantum Well Structure Using Crystalline Organic Semiconductors

AFOSR Contact: **AFOSR-91-0075**

Final Report: **1 Nov., 1990 - 31 Oct., 1992**

Principal Investigator: **Stephen R. Forrest**
Departments of Electrical Engineering and Materials Science
Center for Photonic Technology
University of Southern California
Los Angeles, CA 90089-0241

Abstract

A new class of engineered materials based on crystalline organic semiconductors grown by the ultrahigh vacuum process of organic molecular beam deposition is described. The objective of this program is to investigate these materials and the conditions which lead to ordered growth between highly lattice mismatched van der Waals crystals into novel "quasi-epitaxial" structures. During the first year of the program, considerable progress has been made in understanding and exploiting this new class of materials. In particular, a simple model has been developed which describes the physical mechanisms underlying quasi-epitaxy. The electrical and optical properties of both single and multiple heterojunction structures grown using alternating layers of two different, lattice-mismatched organic molecules have been investigated in detail. It is found that the layers can be grown sufficiently thin (10 Å) to result in exciton confinement in organic multiple quantum wells. These and other quasi-epitaxially grown structures can lead to an entirely new family of optoelectronic devices with exciting new electronic and nonlinear optical characteristics.

INVESTIGATIONS OF HETEROJUNCTIONS AND MULTIPLE QUANTUM WELL STRUCTURES USING CRYSTALLINE ORGANIC SEMICONDUCTORS

Grant No.: AFOSR-91-0075

P.I. Stephen R. Forrest
Department of Electrical Engineering
University of Southern California
Los Angeles, CA 90089

Final Report Summary

This reports on a highly successful two year program whose objective was to investigate the structural and optoelectronic properties of a novel engineered materials system: vacuum deposited semiconducting organic thin films. The program was terminated early due to the move of the PI from USC to Princeton. Hence, this final report concerns only the research done at USC over the shortened time frame of the project.

This research has led to the following breakthrough results:

1. Demonstration of the first organic thin film multiple quantum wells using the novel growth technique of organic molecular beam deposition (OMBD). This growth technology developed in our lab has set a standard now being investigated worldwide. Approximately 2 - 4 papers each month are appearing in Applied Physics Letters, with additional papers appearing in such journals as Physical Review Letters, Japanese Journal of Applied Physics, etc. Virtually all groups have adopted our terminology of OMBD and "quasi-epitaxy" (QE). This latter term refers to the growth of lattice-mismatched structures which are bonded by the flexible van der Waals forces. In addition, a large percentage of papers currently being published by other groups refer to two papers generated by our group, one of them done under this current contract:

"Evidence for Exciton Confinement in Crystalline Organic Multiple Quantum Wells", F. F. So and S. R. Forrest, Phys. Rev. Lett., **66**, 2649 (1991).

2. Discovery and analysis of exciton confinement in the first organic multiple quantum well structures. This work has numerous exciting potential applications in optical devices such as modulators, light emitters and detectors. We measured, for the first time, the exciton radius and recombination lifetime in organic MQW structures, and found that their energy was blue shifted, and their radiative lifetime reduced due to quantum effects.

3. Demonstration of monolayer control of organic thin film growth. Here, direct observation via scanning tunnelling microscopy of molecular layers, and their relation to the substrate was made. The results lead to the generation of a simple calculational model which is currently being used to predict the conditions and materials which lend themselves best to quasi-epitaxial growth.

Exchanges with Air Force Labs

In addition to these discoveries, we have fabricated several devices which take advantage of the unique optical and electronic properties of the organic thin films. Much of this device work was done with support and collaboration from Rome Air Development Center (Hanscom) which has closely followed the research, and in some cases has transferred some of our technology to their own labs. As an example, RADC issued an SBIR contract solicitation for a multipurpose ultrahigh vacuum system similar to our OMBD chamber as part of their desire to incorporate OMBD technology for their own use. This collaboration with RADC continues even at Princeton University due to the importance of moving this strategic technology into other domestic laboratories.

Personnel

The PI employed the following graduate students using AFOSR support during the course of this research:

Dr. F. F. So: PhD, USC, 1991. Currently employed at Motorola, Inc. Thesis title: "Growth and Characterization of Heterojunctions and Multiple Quantum Well Structures Based on Crystalline Organic Semiconductors".

E. I. Haskal: PhD, USC, expected 1994 (currently doing research at Princeton)

Y. Zhang: PhD, USC, expected 1994 (currently doing research at Princeton)

Two post-doctoral fellows were also supported under this contract:

Dr. D. Y. Zang. Currently employed at Metrolaser, Inc., Irvine, CA

Dr. P. E. Burrows. Currently employed as Member of Technical Staff, Advanced Technology Center for Photonics and Optoelectronic Materials, Princeton University.

Publications

Papers

1. "Optical Waveguides in Crystalline Organic Semiconductor Thin Films," D. Y. Zang, Y. Q. Shi, F. F. So, S. R. Forrest, and W. H. Steier, *Appl. Phys. Lett.*, 58, 562 (1991)

2. "Optical Nonlinearities in Crystalline Organic Multiple Quantum Wells," J. F. Lam, S. R. Forrest, and G. L. Tangonan, *Phys. Rev. Lett.*, 66, 1614 (1991)

3. "Evidence for Exciton Confinement in Crystalline Organic Multiple Quantum Wells," F. F. So and S. R. Forrest, *Phys. Rev. Lett.*, 66, 2649 (1991)

4. "Giant Anisoptropies in the Dielectric Properties of Quasi-Epitaxial Crystalline Organic Semiconductor Thin Films," D. Y. Zang, F. F. So, and S. R. Forrest, *Appl. Phys. Lett.*, 59, 823 (1991)

5. "Quasi-Epitaxially Grown Crystalline Organic Semiconductors: Structural, Electrical and Optical Properties," F. F. So and S. R. Forrest, (invited paper) *J. Nonlinear Optics*, 2, 205 (1992)

6. "All-Optical Modulation in Crystalline Organic Semiconductor Waveguides," D. Y. Zang and S. R. Forrest, *Appl. Phys. Lett.*, 60 189 (1992)

7. "Evolution of Quasi-Epitaxial Growth of a Crystalline Organic Semiconductor on Graphite," E. I. Haskal, F. F. So, P. E. Burrows, and S. R. Forrest, *Appl. Phys. Lett.*, 60, 3223 (1992)

8. "Observation and Modelling of Quasi-Epitaxial Growth of a Crystalline Organic Thin Film", P. E. Burrows, Y. Zhang, E. I. Haskal and S. R. Forrest, *Appl. Phys. Lett.*, 61, 2417 (1992).

Presentations at Professional Conferences

1. "Crystalline Organic Semiconductor Thin Film Optical Waveguides," D. Y. Zang, Y. Q. Shi, F. F. So, S. R. Forrest and W. H. Steier, *Optical Society of America Annual Meeting, Technical Digest*, Paper FD1, 232, Boston, MA (Nov. 4–9, 1990)

2. "Organic Molecular Beam Epitaxy," S. R. Forrest and F. F. So, (invited paper) *Frontiers of Organic MBE and STM*, Riken Institute of Physical and Chemical Research, Japan (Mar. 12–13, 1991)

3. "Crystalline Organic Semiconductor Thin Films Grown by Molecular Beam Deposition: A New Class of Engineered Materials for Optoelectronics," S. R. Forrest, F. F. So and D. Y. Zang, (invited paper) *Topical Meeting on Epitaxial Materials and In Situ Processing for Optoelectronic Devices*, Newport Beach, CA (July 29, 1991)

4. "Integrated Optoelectronic Devices Based on Organic/Inorganic Heterojunctions," S. R. Forrest and F. F. So, (invited paper) *Solid State Devices and Materials Conf.*, Yokohama, Japan (August, 1991)

5. "Thin Film Crystalline Organic Semiconductors: A New Class of Engineered Materials for Optoelectronics," F. F. So, D. Y. Zang and S. R. Forrest, (invited paper) *Materials Research Society Annual Meeting*, Paper N6.6, Boston, MA (Dec., 1991)

6. "Optical and Electronic Properties of Crystalline Organic Semiconductor Structures Grown by Organic MBE," S. R. Forrest and F. F. So, (invited paper) *Gordon Conf.*, Ventura, CA (Feb., 1992)

7. "The Optical Properties of Crystalline Organic Multiple Quantum Well Structures," S. R. Forrest, F. F. So and D. Y. Zang, (invited paper) *Charge Transfer in Restricted Geometries*, Rochester NY (July, 1991)

8. "Evidence for Quasi-epitaxial Growth of a Crystalline Organic Semiconductor on Graphite Using Scanning Tunnelling Microscopy," E. I. Haskal, S. R. Forrest and Y. J. Zhang, (invited paper) *24th Annual Symp., Amer. Vac. Soc.*, Pasadena, CA (Sept. 25, 1991)

9. "Optically Induced Modulation in Crystalline Organic Semiconductor Waveguides," D. Y. Zang and S. R. Forrest, *Conf. on Opt. Fiber Comm.*, San Jose, CA (Feb. 3–7, 1992)

10. "Crystalline Organic Semiconductor Waveguide Optical Directional Couplers and Switches," D. Y. Zang and S. R. Forrest, *Int. Photonics Res. Topical Mtg.*, New Orleans, LA (April 13–15, 1992)

In Appendix 1 we provide reprints of key papers published during the course of this research. In Appendix 2 we enclose excerpts from the first year annual report.

2. Introduction

Recent work in many laboratories worldwide [1-7] has demonstrated a new class of engineered materials with application to photonic devices. These materials are variously known as "van der Waals solids", "layered materials" or "quasi-epitaxial materials". The property which these materials have in common is that the cohesive force which bonds the various material layers together is the relatively weak van der Waals force. This results in an ability to layer materials which are highly lattice-mismatched without inducing defects in the crystal structure. One particularly interesting class of van der Waals solids with applications to a very broad range of optical and electronic devices is based on multilayered structures consisting of crystalline organic semiconductors [1]. These materials have been found to have excellent electrical and optical characteristics when grown by the ultrahigh vacuum process of organic molecular beam deposition (OMBD) onto other organic semiconductors, or even onto the surfaces of inorganic semiconductors such as Si, GaAs or InP [8,9]. For example, high bandwidth photodetectors consisting of layers of perylene-based compounds deposited on Si substrates have been demonstrated [8], as have field effect transistors based on organic/InP heterojunctions [10]. Furthermore, waveguides and other optical devices have been demonstrated using these quasi-epitaxially grown layers [11].

In this work, we discuss the structural, dielectric, conductive, and optical properties of this new and exciting class of engineered materials. In particular, we have demonstrated the growth of multiple quantum well (MQW) structures based solely on organic semiconductors. These structures have demonstrated quantum confinement of excitons [1,2], opening the door to a wide range of devices such as optical modulators and switches which can be tailored to match

a particular window in the visible and infrared spectral regions. Furthermore, we have observed giant anisotropies [3] in the dielectric and conductive properties of these epitaxial films which are a direct result of their crystal structure.

Due to the ease with which these materials can be grown into crystalline structures without regard to lattice match constraints, as well as due to the wide variety of materials which can be chosen for a given application, the process of OMBD of van der Waals solids opens the door to an unprecedented range of new challenges and opportunities to the materials scientist, both in the understanding of materials as well as in the ability to fabricate new devices for use in advanced optoelectronic systems.

The purpose of this paper is to review our recent results in the growth and characterization of quasi-epitaxial films of two different organic molecules, and to discuss the unique optical and electrical properties of the films and multilayer structures consisting of two different materials interleaved in very thin ($\geq$ 10 Å) layers.

The paper is organized as follows: In the following section we discuss the process of quasi-epitaxy. Both the techniques employed and a physical model for the growth process will be presented. In Sec. 3, we discuss the electrical properties as well as the conductivity mechanisms dominant in heterojunctions consisting of two, layered organic films. In Sec. 4, the optical properties of organic multiple quantum well (MQW) structures are considered in detail, and in Sec. 5 we discuss the future prospects for quasi-epitaxially grown organic semiconductors.

3. Structure of quasi-epitaxially grown films

Quasi-epitaxy (q-e) is the process whereby a film which is strongly lattice-mismatched to a substrate can be grown in a relatively defect-free, ordered layer. This seemingly contradictory state of affairs is a direct result of the weak nature of the van der Waals (vdW) interaction which is the cohesive force binding the constituent materials. Here, it is assumed that the internal binding energy of a given material is significantly greater than the binding energy of the dissimilar materials used in the layered structures. Although there is strain energy associated with the mismatch between adjoining layers, this energy is insufficient to induce defects within a particular layer.

In our experiments, we have used the archetype compound, 3, 4, 9, 10 perylenetetracarboxylic dianhydride (PTCDA) to study the mechanisms of q-e growth. The unit cell of PTCDA, or $C_{24}O_6H_8$, is shown in Fig. 1. The molecule forms tightly bound stacks, with an intermolecular spacing of only 3.21 Å. Furthermore, adjacent stacks are oriented (in the bulk crystal) with the long molecular axes at 90° with respect to each other. There are several physical implications which arise from the obvious asymmetries of this structure. For example, the close stacking distance gives rise to extensive π-orbital overlap between adjacent molecules within a stack, whereas almost no overlap of the molecular orbitals exist between the stacks. This results in large conductive and dielectric asymmetries along various crystalline axes, as will be discussed below.

The first demonstration of quasi-epitaxial growth of an organic semiconductor deposited onto a glass substrate was by Forrest, et al. in 1984 [12]. In that work, it was found that when PTCDA was deposited at a rate exceeding 50 Å/s onto a glass substrate held at room temperature, single crystalline thin films could be grown which extended several centimeters across the substrate surface. Following that initial work, Debe, et al. [13] demonstrated that other perylene derivatives similar to PTCDA could attain single crystallinity when deposited more slowly onto substrates held well below room temperature. More recently, we have found that PTCDA, and an analogous compound, 3,4,7,8 naphthalenetetracarboxylic dianhydride (NTCDA), or $C_{14}O_6H_8$, can both be grown quasi-epitaxially at a rate of 1 - 3 Å/s when deposited onto glass substrates held at approximately 90K [1]. Low substrate temperature during growth is required since the thermal energy of the molecules on the surface needs to be brought well below the intermolecular bond energy for ordered growth to be established.

Multilayer stacks of alternating layers of PTCDA and NTCDA also have recently been found to form ordered crystalline structures. This order is achieved even though the crystal structures of PTCDA and NTCDA are highly mismatched. In Fig. 2 we show a unit cell of NTCDA (c.f. Fig. 1). Here, it is seen that rather than forming planar stacks as in the case of PTCDA, NTCDA molecules stack in a herringbone habit, with an intermolecular spacing of 3.5 Å. In the herringbone structure, adjacent stacking axes are positioned at 90° with respect to each other, once again leading to anisotropies in the conductive and

dielectric properties of these crystals. However, the asymmetries are much less pronounced than those found in PTCDA.

In growing the multilayer stacks of PTCDA and NTCDA onto glass substrates, pre-purified powder samples of the materials were loaded into separate sublimation cells in the OMBD growth chamber which had a base pressure of 10^{-10} Torr. The materials were then alternately deposited by sequentially heating and shuttering each cell to a temperature high enough to sublime the molecules at a rate of 1 - 3 Å/s (approximately 400 °C for PTCDA and 250 °C for NTCDA) as determined using a crystal thickness monitor, while the temperature was kept well below the dissociation temperature for the particular molecule being deposited. Typically, from 1 - 20 layers of each material with individual layer thicknesses ranging from 10 Å to 1000 Å were grown in this fashion.

Evidence for crystalline order has been obtained using both x-ray diffraction as well as optical birefringence measurements [1]. In the case of x-ray diffraction, it was found that both PTCDA and NTCDA grew into their normal crystal stacking habits even though the layers alternated between the mismatched crystals of PTCDA and NTCDA. In a separate series of birefringence experiments, it was found that the optic axis of PTCDA in such multilayer structures was oriented in a single direction across broad wafer areas, and that the birefringence of each of the PTCDA layers in the stacks *added coherently*, even though the PTCDA layers were separated by intervening NTCDA layers. The experiment was accomplished by placing a multilayer sample on a glass substrate between crossed polarizers, and then measuring the intensity of the transmitted light through the polarizers as the sample was rotated about its optic axis which was oriented along the beam direction. By using a tightly focussed beam, this birefringence measurement determines the local orientation of the optic axis of PTCDA (NTCDA has only very weak birefringence and hence the probe is not sensitive to its presence in the stacks). This technique, therefore, is sensitive to the degree of crystalline order over the region covered by the beam diameter. The finding that the optic axis of PTCDA is oriented in the same direction across the wafer surface, and that the birefringence of a multilayer stack is equal in magnitude to a single PTCDA film of equal total thickness, indicates that the crystalline orientation of one PTCDA layer is the same as all the other PTCDA layers in a multilayer structure. By inference, the NTCDA layers must be likewise aligned. This

ordering, both across wafer surfaces as well as between layers in the stacks is evidence for quasi-epitaxy in the multilayer samples.

The process of q-e can be quantitatively understood if we require that a monolayer of one material must find a minimum energy configuration with the underlying crystal during growth. That is, when growth of material B is initiated on the surface of material A, the first few molecules B align themselves to A to minimize their individual molecular interaction energies. As the growth of layer B approaches a full monolayer, different islands of material B arising from nucleation at random sites across the surface of A will be out of registry with each other, although they may all be approximately aligned. As the spacing between islands is filled in with additional deposition of material B, the islands must shift slightly (but in a rigid manner) to accommodate these last, interstitial molecules. This process must occur without increasing the overall energy of the layer to the extent that a dislocation is generated. Note that this picture requires that the substrate temperature be high enough to allow for some surface mobility of the islands and molecules, yet not so high that the individual molecules are only very loosely bound to the surface. For this reason, deposition of q-e grown materials occurs on substrates cooled below room temperature.

One condition which must be fulfilled for the above scenario to occur is that the binding energy minimum between molecules A and B be very broad -- i.e. there is a range of positions which molecule B can have when aligned to molecule A which does not significantly change the total energy of the system. In this way, small shifts in position can be accommodated without significantly increasing the total crystal energy. We have tested this hypothesis by calculating the vdW bond energy between PTCDA (molecule A) and NTCDA (molecule B). These calculations are done using the atom-atom potential method [14]. In this method, we calculate (and minimize) the vdW energy between each pair of atoms in both the PTCDA and NTCDA molecules. The total bond energy is simply:

$$\Phi = \Sigma \phi_{ij} \qquad (1)$$

where ϕ_{ij} is the atom-atom potential between the ith and jth *atoms* in molecules A and B, respectively. This, in turn, is calculated using the Buckingham potential:

$$\phi_{ij} = -\alpha/r_{ij}^6 + \beta\exp(-\gamma r_{ij}). \qquad (2)$$

Here, r_{ij} is the distance between atoms i and j in molecule B, and α, β and γ are vdW atom-atom potential constants for the constituent atoms in the two molecules (C, O and H for PTCDA and NTCDA, for example). The constants used in the case of PTCDA and NTCDA are given in Table 1.

The accuracy of this method has been tested by calculating the minimum energy configuration of *bulk* PTCDA, and comparing the results to the measured crystal structure. Under this test, the model works surprisingly well. For example, the calculated intermolecular stacking distance is 3.26 Å as compared with the actual value of 3.21 Å. Furthermore, the model predicts that two molecules stack with their long axes aligned, but with their short (b) axes offset by 0.9 Å, as compared to 1.1 Å obtained from measurements. Finally, molecules in adjacent stacks favor a perpendicular to a parallel relative stack orientation by 40 meV, also consistent with observation (Fig. 1). Thus, we have some confidence that the atom-atom method is valid for predicting the stacking configuration of two different molecules such as PTCDA on NTCDA.

The results of this calculation for PTCDA/NTCDA multilayers are shown in Fig. 3. Here, the diagram shows contours of constant total energy, Φ, as a function of displacement of the two molecules placed in a planar stacking configuration. The contours are at 5 meV intervals, and position (0,0) corresponds to the center of an NTCDA molecule positioned directly over the center of a PTCDA molecule. Note that the intermolecular z-spacing of 3.2 Å was determined from a similar minimization procedure as that outlined above.

From the energy contour plot, we see that the energy minimum between PTCDA and NTCDA is indeed broad, allowing for nearly a 2 Å translation of one molecule with respect to another without any significant increase in Φ. Thus, we can conclude from this first order, somewhat simplified calculation, that our "picture" of the process of q-e is plausible. That is, we expect that once the islands are nucleated around the surface of the substrate, they are still free to rigidly translate to accommodate the arrival of the final molecules which fill in the interstices between neighboring islands. This shift occurs without inducing strain or polycrystalline growth.

While this model is still unsophisticated in many ways, it suggests the properties which molecules must possess before they can be grown into q-e structures. From these initial results, we infer that the process is, in fact, a very general property of vdW solid growth.

4. Organic Heterojunctions

It is well known that multiple quantum wells can be fabricated by alternately layering two inorganic semiconductors with different bandgaps. Thus, the question arises: Is it also possible to observe quantum confinement in fully organic multiple heterojunction structures? This question can only be answered once we understand the nature of a heterojunction between two organic semiconductors, and the role it plays in governing charge transport between the contacting layers. While there have been reports on the fabrication of organic heterojunctions (HJs) and their rectification characteristics [17,18], the charge transport mechanisms across such HJs are still not well understood. In this section, therefore, we describe the rectification characteristics of organic heterojunctions, and demonstrate that they can be understood in terms of a band model analogous to that used for inorganic semiconductors. That is, we show that charge transport over the energy barrier at the heterointerface is limited by the band-like thermionic emission of charge carriers. From the results of our experiments, we infer that, indeed, fully organic semiconductor multiple quantum well (MQW) structures have the potential for exhibiting many of the same physical properties as do inorganic semiconductor MQWs.

The inset of Fig. 4 shows a fully organic heterojunction device consisting of copper phthalocyanine (CuPc) and PTCDA. In this structure, indium-tin-oxide and indium are used as contacts to CuPc and PTCDA, respectively, since these materials have been found to have very low contact resistance to the corresponding organic layers. The rectification due to the heterojunction is evident from the bipolar current-voltage (J-V) characteristics shown in Fig. 4. Here, forward bias is achieved when PTCDA is negative with respect to CuPc.

We can understand the observation of rectification in the CuPc/PTCDA heterojunction in terms of the conventional theory for inorganic semiconductor HJs [19]. It should be noted, however, that charge transport in crystalline organic materials might alternatively be described by the hopping model, where the transport of localized carriers between adjacent molecules is a thermally activated process. In this case, therefore, the carrier mobility should have a strong temperature dependence. However, such a temperature dependence is not observed in organic crystals, therefore suggesting that charge transport is inconsistent with the hopping model. On the other hand, the use of band theory for some crystalline organic materials is justified by previous work on hole mobility measurements on ultra-high purity naphthalene and perylene crystals

[20]. In that work, Warta and Karl found that the hole mobility reaches a maximum value of 400 cm^2/V-s at 4.2 K in some materials. Furthermore, the hole mobility was found to increase linearly at low electric field, and saturates at high fields. The high field carrier velocity saturation is due to phonon emission, consistent with band theory. Further, the long carrier mean free path (as compared with the intermolecular stacking distance) in these crystalline organic materials estimated from the low temperature mobility data also supports the band description. Provided that we can use this model to describe the charge transport in PTCDA and CuPc, the transport theory for inorganic semiconductor heterojunctions can also be applied (with caution) to organic heterojunctions.

Using the treatment of Chang for isotype heterojunctions [21], the saturation current density for an HJ is given by:

$$J_S = BT^{1/2}\exp[- qV_{D2}/kT] \qquad (4)$$

where B is a pre-factor which depends on the density of acceptors and the hole effective mass in CuPc, kT is the Boltzmann energy at temperature T, V_{D2} is the diffusion potential on the depleted, CuPc side of the heterojunction, and q is the electron charge. The valence band discontinuity energy, ΔE_V, is then given by:

$$\Delta E_V = qV_{D1} + qV_{D2}. \qquad (5)$$

In the above equation, V_{D1} is the diffusion potential on the PTCDA side of the heterojunction. For simplicity, we assume that there is no significant difference in the effective hole densities of states and in the acceptor concentrations between CuPc and PTCDA.

From Eq. 4, it can be seen that J_S is thermally activated with energy qV_{D2}. In Fig. 5, we show the dependence of $\log(J_S)$ on 1/T for a CuPc/PTCDA heterojunction. Here, J_S is obtained by extrapolating both the forward and reverse bias currents to an applied voltage of V = 0. The activation energies for both forward and reverse bias are the same, yielding $V_{D2} = 0.51 \pm 0.05$ V. This value is consistent with that obtained from capacitance-voltage (C-V) measurements, where we find that $V_{D2} = 0.45 \pm 0.15$ V. Following the treatment of Chang, we obtain $V_{D1} = 0.01$ V, and hence the valence-band discontinuity energy for CuPc/PTCDA heterojunctions is $\Delta E_V = V_{D1} + V_{D2} = 0.52 \pm 0.05$ V.

Based on the electrical characteristics of the CuPc/PTCDA heterojunctions, a band diagram near the heterointerface is proposed in Fig. 6. Here the "bandgap" of CuPc is taken as 1.7 eV, and the "bandgap" of PTCDA is 2.2 eV. For the purposes of this discussion, the highest occupied molecular orbital (HOMO) is treated as the valence band, and the lowest unoccupied

molecular orbital (LUMO) is treated as the conduction band. The band offset, ΔE_V, is also shown in the figure. Note that, although the HOMO and LUMO are somewhat similar to bands in conventional semiconductors, the bandwidth typical of organic semiconductors is ~ 1 - 10 meV [22], whereas for inorganic semiconductors the bandwidth is ~ 1 eV. These factors have profound effects on the charge transport since both the density of states and carrier effective masses are significantly different for organic and inorganic semiconductors. We note too, that the band picture cannot be accurately applied to organic materials whose carrier mobility is significantly lower than PTCDA (where a hole mobility from 0.1 cm^2/V-s to 1 cm^2/V-s at room temperature is typical).

An alternative picture for the CuPc/PTCDA HJ based on molecular spectral levels is shown in Fig. 7. This diagram phenomenologically describes the processes of heterojunction transport using the hopping model, without invoking band structure. In the figure, the HOMO and LUMO bands are shown as functions of the configuration coordinate, Q (where the subscripts C and P refer to CuPc and PTCDA, respectively). Both the ground states (S_0) and first excited singlet states (S_1) are resolved into different vibronic levels (labeled 0, 1, 2, ...). As indicated in Fig. 7, the ground states (S_0) of CuPc and PTCDA are offset by an energy of ΔE_V. This is the energy required to transfer a hole from a CuPc to a PTCDA molecule across the heterojunction interface, and hence is just the band offset energy obtained from the C-V and J-V transport measurements. While this molecular level diagram is useful for understanding transport across the heterointerface, it fails to fully describe the transport within the layers. In that case, the band model is more useful for interpreting the macroscopic electrical characteristics of organic HJs. Whichever model is used, however, our results suggest that the organic HJ provides an energy barrier to charge transport similar to that observed in inorganic semiconductor HJs.

5. Optical properties organic multiple quantum wells

In the previous section, we demonstrated that semiconductor heterojunctions can be formed by layering two different crystalline organic thin films, and that the energy barrier at the interface controls the flow of charge across the HJ. By sandwiching an ultra-thin, small bandgap organic layer between two large bandgap organic layers, organic quantum well structures can then be realized. Due to the reduced dimensionality in such structures, charge carriers are confined between the barriers, hence strongly affecting the optical properties of the resulting materials. In the following, we describe the

optical properties of crystalline organic MQWs consisting of alternating, ultra-thin layers (between 10 Å and 200 Å thick) of PTCDA and NTCDA grown by OMBD. A schematic diagram of such a quantum well structure is shown in Fig. 8 where PTCDA is the well layer sandwiched between adjacent NTCDA (with a bandgap energy of 3.1 eV) barrier layers.

The room temperature optical absorption and low temperature (20 K) photoluminescence bands of a 5 period, symmetric PTCDA/NTCDA organic MQW sample with an individual layer thickness of 40 Å is shown in Fig. 9. The characteristic absorption spectra of both PTCDA and NTCDA are indicated in the figure. The absorption bands are due to exciton generation in the corresponding crystalline layers, and are relatively broad due to the strong exciton-phonon interaction characteristic of organic crystals [22]. The lowest energy singlet exciton absorption peak in PTCDA (indicated by the left-hand arrow) shifts to higher energy as the layer thickness is decreased, as shown by the data points in Fig. 10. No apparent shifts in the higher energy exciton lines were observed, possibly as a result of the broad nature of these absorption bands.

Since the electronic polarization energy is large (~ 1 eV) in crystalline organic materials, it plays a vital role in determining the exciton energy. Thus we might expect the presence of NTCDA molecules to influence the PTCDA exciton energy, as observed in our MQW samples. An alternative explanation for the blue shift is due to quantum confinement of excitons in a quantum well structure. We now discuss both models in detail.

The change of polarization energy of PTCDA due to the proximity of NTCDA molecules in closely spaced layers can be calculated using perturbation theory. A derivation of the perturbation to the exciton energy due to polarization effects is given in Appendix C. The results of the calculation show that the first order energy shift to the polarization energy increases linearly with the layer thickness, t. This effect, while being very short range, can actually increase the exciton energy with increasing well width, contrary to our observations. Hence, we can rule out this first order "energy offset" effect. On the other hand, the second order polarization energy correction is proportional to t^{-4}. As shown in Fig. 10, the data are not consistent with the results of the calculation since their energy dependence is considerably smaller than even t^{-2}. Hence, we conclude that the polarization model does not adequately explain the observed blue shift in the exciton line.

Quantum confinement provides an alternative explanation for the observed blue shift in the absorption spectrum [1,2]. Here, we use the variational method to evaluate the binding energy of an exciton in a quantum well. The Schrodinger equation for an exciton can be solved using the trial wavefunction:

$$\Psi_{tot} = \psi_e(z_e)\psi_h(z_h)\psi_{1s}(\rho\, z) \qquad (6)$$

where $\psi_{1s}(\rho,z)$ is the hydrogenic 1s wavefunction, $\rho = x^2 + y^2$, z_e and z_h are coordinates in the z-direction for the electron and hole, respectively, $\psi_e(z_e)$ and $\psi_h(z_h)$ are the exact solutions to the finite square well problem, and $z = z_e - z_h$. In Eq. 6, the hydrogenic state has the form:

$$\psi_{1s} = \exp\,[\,-\,(\rho^2/\alpha^2 + z^2/\beta^2)^{1/2}] \qquad (7)$$

Here, α is a variational parameter in the trial solution, and β is set equal to a_o, where a_o is the exciton Bohr radius in the bulk crystal. For crystalline organic MQW structures, typically $a_o << L_z$, where L_z is the quantum well width. In this case, therefore, it is reasonable to assume $\beta = a_o$, with α being the only variation parameter.

The parameters used in this model to fit the data in Fig. 10 are listed in Table 2. Here, the sum of V_e and V_h is equal to the difference in energy gaps of PTCDA and NTCDA. Of all the parameters used in the calculation, the results are most sensitive to the choice of m_h and the ratio, V_e/V_h. Using these parameters, a good fit to the experimental data is obtained for $m_h = 0.18m_o$, where m_o is the electron rest mass. A small value of m_h and a relatively large value of m_e were chosen in the calculation since PTCDA is predominantly a hole-transporting material. The effect of using different values of m_h are also shown for comparison in Fig. 10 indicating the sensitivity of the fit to this parameter. Note that our calculation implies that $V_e >> V_h$. This is consistent with electrical measurements made for PTCDA/NTCDA heterojunctions which do not exhibit significant rectification of the hole current at temperatures ranging from room temperature to about 90 K. This indicates that the energy barrier to hole transport is less than 100 meV. A best fit to the data is obtained assuming $V_h = 50$ meV, in accordance with these findings. The calculated values of α are also shown in Fig. 10. Here, α increases monotonically with increasing well width, and asymptotically approaches $a_o = 12$ Å.

The effect of quantum confinement of excitons in organic MQWs is further evident from exciton lifetime measurements, where we have found that the exciton lifetime decreases with decreasing layer thickness. For example, at L_z =

200 Å, the radiative lifetime is 10.8 ± 0.5 ns, decreasing to 5.7 ± 0.5 ns for L_z = 14 Å. In previous work, the decrease in lifetime in PTCDA/NTCDA MQWs has been attributed to the shrinkage of exciton volume due to quantum confinement [2]. This phenomenon, which is often observed in inorganic semiconductor heterostructures, results from an increased overlap of the electron and hole wavefunctions, thus enhancing the probability for exciton recombination. It can be shown [2] that the shrinkage in exciton volume can be used to quantitatively explain the exciton lifetime data using the parameters given in Table 2, and taking the wavefunction given in Eq. 6 and 7.

The most important conclusion drawn from the above experiments is that we have observed effects of exciton quantum confinement in crystalline organic multiple quantum wells for the first time. From the results of variational calculations, the exciton Bohr radius in PTCDA is determined to be ~12 Å, implying that the exciton wavefunction extends to 3 - 4 nearest neighbors. We can therefore conclude that excitons in the crystalline organic materials studied here are Wannier-like [16] rather than Frenkel-like.

6. Giant anistropies in crystalline organic films deposited by OMBD

We have measured the indices of refraction and dielectric constants along different directions in thin films of the crystalline organic semiconductor; 3,4, 9, 10 perylenetetracarboxylic dianhydride. The films were deposited via organic molecular beam deposition, resulting in highly ordered, "quasi-epitaxial" films. Due to inherent asymmetries in the molecular crystal structure, the ordering of the films results in giant anistropies in their dielectric properties. For example, the index of refraction measured at a wavelength of λ = 1.064 μm in the direction perpendicular to the substrate plane is $n_\perp$ = 1.36 ± 0.01, whereas parallel to the plane, $n_\parallel$ = 2.017 ± 0.005, resulting in an index difference of Δn = 0.66. Furthermore, the dielectric constant of the films measured between 100 Hz and 10 MHz is $\varepsilon_\perp = 1.9 \pm 0.1$ and $\varepsilon_\parallel = 4.5 \pm 0.2$. To our knowledge, these are the largest index anisotropies ever measured for thin films. In this section, we also discuss a guided wave polarization-selective device which takes advantage of the large dielectric anisotropies characteristic of the thin organic films.

One would expect that the dielectric properties of highly ordered films would also have a considerable degree of anisotropy along different crystalline directions. The molecules form planar stacks, with a distance of 3.21 Å between

molecules in the stack. Typically, the films consist of such stacks tilted at $\phi = 11^o$ from the substrate normal. The long axes of molecules in adjacent stacks are rotated by 90° to the long axis of a molecule in the stack at the center of the unit cell. The off-resonance dielectric constant of a material at frequency, ω, is given by:

$$\varepsilon - 1 = \frac{4\pi N q^2 f_j}{m^* (\omega_j^2 - \omega^2)} \qquad (8)$$

where N is the molecular number density, ω_j is the dipole transition frequency, q is the electronic charge, and m* is the electron effective mass. The oscillator strength of the dipole transition from level o to j is given by $f_j = 2m^* h\omega |x_{oj}|^2/h^2$, where x_{oj} is the electron position expectation value, and h is Planck's constant divided by 2π. Assuming that the largest contribution to the dipole moment of the molecule is due to the p-orbitals, and that the electron within a given orbital is completely delocallized, then we can make the approximation that $f_{j\perp}/f_{j||} \sim |x_{oj\perp}|^2/|x_{oj||}|^2 \sim d^2/L^2$. Here, $d \cong 3.2$ Å is the extent of the π-orbital system perpendicular to the molecular plane, and L is its extent in the plane, which is approximately equal to the length of the perylene molecular core of PTCDA (i.e. $L \cong 6.9$ Å). Hence, provided that there is perfect crystalline alignment throughout the thin film, we can expect an anisotropy in ε between directions perpendicular and parallel to the thin film plane (and hence approximately perpendicular and parallel to the molecular stacking axis) of $(\varepsilon_\perp - 1)/(\varepsilon_{||} - 1) \sim d^2/L^2 \sim 0.22$. This value is only an approximation, since we are assuming that m* is isotropic [22], and that the dipole moment is due to a completely delocallized electron in the extended p-system. Nevertheless, it is shown below that this value is close to the measured anisotropy in e for highly ordered, quasi-epitaxial films of PTCDA.

To measure the dielectric constant along different film directions, capacitors oriented along the various film axes were fabricated on quartz substrates. For measuring the capacitance along the in-plane direction, interdigitated patterns of Cr-Au contacts were employed. Here, a thin layer (~ 150 Å) of Cr was deposited, followed by a 0.7 μm thick Au layer which forms a current-blocking contact to PTCDA [15]. Next, the contacts were patterned into 2 mm long interdigitated electrodes with 2μm spacing and finger width. In addition, some electrode sets were positioned perpendicular to other sets to

determine if there were significant asymmetries in the capacitance in the two in-plane directions. Next, purified PTCDA was deposited via organic molecular beam deposition (OMBD) onto a quartz substrate which was maintained at a temperature of approximately 90K during growth. The PTCDA thickness was 0.9 μm, filling the spaces between the electrode fingers. As has been discussed previously [1], deposition under these conditions ensures that the resulting film is single crystalline, independent of the substrate material employed.

The capacitance measured between 100 Hz and 10 MHz for one set of electrode pairs using this in-plane geometry is shown in Fig. 11. The capacitance is independent of frequency over the measurement range, indicating that the films are relatively free of traps. Traps tend to affect the capacitance when their emission rate is comparable to the test frequency.

The capacitance of a co-planar strip line lying on a quartz substrate with dielectric constant ε_S is given by [23]: $C = (\varepsilon_S + \varepsilon_F)\varepsilon_0[FK(k)]l/2$, where ε_0 is the permittivity of free space, l is the finger length, F = 16 is the number of finger pairs, K is the ratio of two complete elliptic integrals of the first kind, and k is a geometrical parameter related to the finger width and spacing. Here, we assume quartz fills one half plane, and a material with dielectric constant e_F the other. The ratio of capacitances of the pattern measured before (C_{wo}) and after (C_w) deposition of the PTCDA thin film is then simply:

$$C_{wo}/C_w = (\varepsilon_S + 1)/(\varepsilon_S + \varepsilon_{||}) \qquad (9).$$

We note that the small amount of electric field penetration above the PTCDA film can lead to deviations from Eq. (9). However, since the PTCDA thickness was larger than that of the contact fingers, this error leads to an insignificant underestimate of $\varepsilon_{||}$. We obtain in-plane dielectric constants for PTCDA of $\varepsilon_{||}$ = 4.6± 0.2 and 4.3± 0.2 for the two perpendicular orientations of the patterns. Since these values are within each other's error limits, we assume that the dielectric constants along the two directions is not significantly different, leading to $\varepsilon_{||}$ = 4.5± 0.2.

To measure $\varepsilon_\perp$, a parallel plate geometry was used, where the back contact was formed using a broad Cr-Au contact deposited on glass. This was followed by deposition of a 0.9 μm thick layer of PTCDA. Top contact to the PTCDA was made using circular Au pads of area 2.5 x 10^{-4} cm^2. Using this geometry, it is found that $\varepsilon_\perp = 1.9 \pm 0.1$ over the same frequency range as that

used to measure $e_{||}$. From these data we obtain $(\varepsilon_\perp - 1)/(\varepsilon_{||} - 1) = 0.26$ which is close to our theoretical estimate of 0.22 for perfectly oriented crystalline films.

In earlier measurements of $\varepsilon_\perp$ for PTCDA deposited under conditions leading to polycrystalline growth, it was found that [15] $\varepsilon_\perp = 3.6 \pm 0.4$. Assuming a homogeneous medium was being analyzed in that case, then the spatially averaged dielectric constant is $\varepsilon \equiv (2\varepsilon_{||} + \varepsilon_\perp)/3$. Using the values of e obtained in this work, we find $\varepsilon \equiv 3.6$. This is in agreement with the former value, indicating that the films deposited on room temperature substrates using standard vacuum sublimation techniques are structurally randomized, whereas deposition via OMBD on cold substrates results in films which have nearly perfect crystalline structure across broad areas.

Since $\varepsilon_\infty = n^2$, where n is the refractive index of the film, and ε_∞ is the thin film dielectric constant at optical frequencies, we also expect to observe asymmetries in n as a result of the ordering of the quasi-epitaxial films of PTCDA. In earlier work [11], we measured an in-plane refractive index of $n_{||} = 2.017 \pm 0.005$. In this work, therefore, we measure only $n_\perp$.

Determination of $n_\perp$ proceeds by measuring the reflectivity from the thin film as a function of beam incident angle using several film thicknesses and light wavelengths. Considering an *isotropic* homogeneous thin film sandwiched between two semi-infinite media, the reflectivity is given by [24]:

$$R = \frac{r_{12}^2 + r_{23}^2 + 2r_{12}r_{23}\cos 2\beta}{1 + r_{12}^2 r_{23}^2 + 2r_{12}r_{23}\cos 2\beta} \qquad (10)$$

where $\beta = 2\pi n_2 t \cos\theta_2/\lambda$. Here, n_2 is the refractive index measured along the refractive angle θ_2 in the thin film of thickness, t. Also, r_{12} (r_{23}) is the reflectivity at the interface between medium 1 (3) and medium 2. The reflectivity maxima and minima for a given index, n_2, occur at angles θ_2 which satisfy $n_2 t = m\lambda/4\cos\theta_2$, where m is the integer order of the extremum. If the film thickness is accurately determined, the refractive index can thence be obtained by measuring the angles corresponding to reflectivity extrema as predicted by these equations.

To extend this technique to anisotropic thin films, the incident light polarization is made parallel to the plane of incidence; i.e. it is a TM-polarized wave. Furthermore, using birefringence measurements discussed previously [1], the optical b-axis is located, and is also oriented parallel to the incident light polarization vector. When the incident angle (θ_1) of the beam to the film is

changed, this is equivalent to a rotation of the angle θ_2 in an index ellipsoid with axes of length $n_{||} = n_b$ and $n_\perp$, as shown in the inset in Fig. 12. Here, n_b is the index along the b-axis. From this figure, it can be shown that the index $n_2^2 = n_{||}^2 + (1 - n_{||}^2/n_\perp^2)\sin^2\theta_1$, from which $n_\perp$ is easily extracted.

A typical measurement result made at $\lambda = 1.064$ μm for a 1.25 μm thick PTCDA film together with a theoretical calculation using Eq. (10) is shown in Fig. 12. The experimental setup consists of a YAG laser providing the incident beam. A large area detector is positioned near the top film surface to measure the reflected light intensity. The PTCDA is deposited on a quartz substrate at low temperatures to achieve crystalline order. Also, the back surface of the quartz is frosted to minimize reflections from the quartz/air interface. It can be seen that the positions of the theoretical extrema match those obtained experimentally, although the magnitude of the reflected signal is sometimes different than predicted due to unwanted reflections from surface imperfections and the quartz/air interface. Similar fits are obtained for a film thickness of 1.13 μm, and at $\lambda = 1.3$ μm, and the results are listed in Table 3. From these data, we obtain $n_\perp = 1.36 \pm 0.01$ at $\lambda = 1.064$ μm, giving $\Delta n = n_{||} - n_\perp = 0.66$ which apparently is the largest value of Δn reported for thin films far from their absorption edge (which for PTCDA lies at $\lambda \equiv 6000$ Å [15]). Very little dispersion is observed in n measured at $\lambda = 1.064$ μm and 1.3 μm, as indicated by the data in Table 3.

It is interesting to compare the asymmetries measured for the dielectric constant and the index of refraction. Ignoring dispersion between the frequencies at which these parameters were determined, we find that $\varepsilon_{||}/\varepsilon_\perp = 2.4 \equiv (n_{||}/n_\perp)^2 = 2.2$. This is truly a remarkable agreement given the widely different conditions under which the various measurements were made. Indeed, we see that the low frequency dielectric constant is approximately equal to n^2 for each of the various film directions.

A waveguide polarizer was fabricated to take advantage of the large birefringence characteristic of OMBD-grown PTCDA thin films. Thus, 2 μm wide PTCDA rib waveguides were made of lengths of 1.5 and 10 mm. The guides were fabricated by first spinning a 1 μm thick film of the photoresist AZ 1400 (with $n_{PR} = 1.61$) onto the (100) surface of an InP wafer (with $n_s = 3.27$ at $\lambda = 1.064$ μm). Next, 2 μm wide ridges were photolithographically patterned in the AZ 1400, followed by deposition of approximately 1 μm of PTCDA. The regions where PTCDA was deposited onto the photoresist ridges form the

guides to TE modes (where $n_{||} > n_{PR}$), but not to TM modes (where $n_{\perp} < n_{PR}$). Elsewhere, PTCDA is directly deposited on the large index InP substrate where guiding does not occur. The substrates were cleaved along (110) planes, thus allowing for end-fire coupling of light into the cleaved facets. Similar guides have previously been measured to have a loss of <2.5 dB/cm [6].

Due to the selective guiding of TE over TM modes, the PTCDA waveguides form a strongly polarizing medium. To measure the TM/TE extinction ratio, $\lambda = 1.064$ μm light from a diode-pumped YAG laser was coupled into and out of the guides using microscope objective lenses. The input light polarization was continuously rotated through 360° using a quarter wave plate placed between the laser and the sample. In addition, a Glan-Thomson polarizer (GTP) with an extinction ratio > 50 dB was placed in front of the laser. This set up, shown in the inset of Fig. 13, ensures a constant coupling efficiency of a highly polarized beam along any direction. The out-coupled light was passed through a second GTP which analyzed the light prior to being detected using a Si CCD camera.

Measurement results for the 10 mm long device are shown in Fig. 13. Here, both the TE and TM components of the output light beam are plotted versus the input light polarization angle. An extinction ratio of TM/TE < -48 dB was obtained, where the measurement accuracy was limited by the GTP. Similar results were obtained for the 1.5 mm guide, in which an extinction ratio of TM/TE « - 25 dB was measured. The accuracy of this measurement was limited by light scattered over the top of the short guide. The propagation loss of the short guide was found to be < 0.4 dB.

In summary of this part of the work, extremely large anisotropies in dielectric properties have been observed in crystalline organic thin films of the compound, PTCDA. The anisotropies in both the dielectric constant and index of refraction for these films is a result of their nearly perfect crystalline order achieved via OMBD on cold substrates. Similar results are expected for other anisotropic organic semiconductor crystals deposited using the OMBD technique. Furthermore, a TE-pass waveguide polarizer with a high TM polarization extinction and low TE propagation loss was demonstrated. Since such polarizing guides can be deposited on conventional semiconductor substrates, these films have uses such as optical isolators integrated with semiconductor lasers or amplifiers.

7. *Resonant nonlinear effects in crystalline organic films*

In this work, we demonstrated all-optical modulation in crystalline organic semiconductor waveguides grown by the ultrahigh vacuum process of organic molecular beam deposition. Two light beams with wavelengths of 1.06 μm and 0.514 μm were used as the guided and the pump light sources, respectively. A refractive index change of 5.4×10^{-5} at 1.06 μm was observed at a pump intensity of 1.0 W/cm^2. This large nonlinear effect is attributed to free electron-hole pairs produced by the dissociation of excitons generated by the short wavelength beam. A carrier lifetime of (17 ± 1) μs which determines the modulator switching time is in good agreement with theoretical predictions. To our knowledge, this is the first observation of free carrier induced index modulation in crystalline organic waveguides.

Charge transport in molecular semiconductors is thought to be initiated via excitonic transitions [25]. Here, free electron-hole pairs are generated in a second order process via dissociation of photogenerated excitons at surfaces or bulk material impurities. That is, given a molecule in ground state S_o, a dominant channel for free carrier production due to absorption of light of energy hw, is $S_o + h\omega \rightarrow S^*$, followed by $S^* + M \rightarrow e^- + h^+$. Here, S^* is the excited singlet exciton state of the molecule, M represents an impurity or interface, and e^- and h^+ are the free electron and holes, respectively. The absorbed light must have a photon energy greater than the exciton transition energy (typically 1.5 – 3 eV). Since the process is second order, the quantum efficiency (h) for electron-hole generation is usually ≤1%. Assuming that there is a refractive index change (Δn) associated with the optical generation of free carriers (via excitons), the Drude model gives:

$$\Delta n = \frac{-e^2 N}{2 n m^* \varepsilon_O \omega^2} \qquad (11)$$

where e is the electronic charge, N is the free carrier density induced by the optical beam, n is the refractive index in the dark, m^* is the effective carrier mass, ε_O is the permittivity in vacuum, and w is the light frequency. A steady state solution of the continuity equation for N gives:

$$\Delta n = n_2 I = \frac{-e^2 \alpha \tau \eta I}{2 n m^* \varepsilon_O \omega^3} \qquad (12)$$

Here, α is the absorption coefficient, I is the optical intensity, τ is the free carrier lifetime, and h is Planck's constant divided by 2π. Note that the NLO coefficient,

n_2, given by Eq. (12) is only due to the free carrier concentration (not the exciton population), and is intensity dependent.

To fabricate the waveguide devices in which n_2 was measured, a 1μm-thick, AZ 1400 photoresist layer (with n_p = 1.61) was first spun onto the surface of a cleaned and polished (100) InP substrate. Next, a series of 2 μm wide strips were patterned onto the photoresist along the (110) direction by standard photolithographic techniques. A 1 μm thick crystalline PTCDA layer was then deposited onto both the InP substrate and the photoresist ridges using the ultrahigh vacuum (~10^{-9} Torr) process of organic molecular beam deposition [2]. Deposition proceeds by heating a pre-purified source of PTCDA to 450 °C to achieve a deposition rate of approximately 3 Å/s, while the substrate temperature is maintained at 90 K. It has previously been found that thin film deposition under these conditions results in single crystalline growth of PTCDA on the photoresist strips into low loss (< 2.5 dB), TE-mode waveguides [3]. To form waveguide facets, the InP substrate was cleaved along the (110) direction. The facet surfaces are sufficiently smooth to allow for observation of Fabry-Perot resonances as the index of the guide is thermally or optically varied.

In the experiments, 1.06 μm wavelength light from a YAG laser was coupled into and out of the waveguide using two microscope objective lenses (see inset, Fig. 14). A high speed $In_{0.53}Ga_{0.47}As$ avalanche photodetector (APD) was used to detect the light signal. To ensure a constant coupling efficiency, a TV camera monitored the beam spot position using a beam splitter placed in front of the APD. The waveguide was placed on a copper block mounted on a thermoelectric cooler. Using a thermocouple and a temperature controller, the temperature of the waveguide device was controlled to within ±0.05 °C.

The 2μm wide PTCDA rib waveguide allowed for propagation of a single TE_{00} mode. The waveguide, with its cleaved facets, acts as a lossy Fabry-Perot resonator with a transmission function of:

$$P(\delta) = \frac{(1-R)^2 e^{-\alpha L}}{(1-Re^{-\alpha L})^2 + 4Re^{-\alpha L}\sin^2\frac{\delta}{2}} \qquad (13)$$

where a is the absorption coefficient, L is the device length (1.62 mm), R is the reflection coefficient at the waveguide facets which is calculated to equal 0.11 considering only Fresnel reflections, and d is the phase shift defined as: $d = d_O +$

$\Delta\delta = 4\pi L/\lambda\ (n+\Delta n)$. When the temperature,T, is varied, the transmitted intensity *varied periodically (see Fig. 14) as is characteristic of a* Fabry-Perot resonator. A complete fringe (two adjacent maxima) corresponding to a phase difference of Dd = 2π was observed for a temperature change of 2 °C, from which we obtain $(1/n)\Delta n/\Delta T = (8.1 \pm 0.5) \times 10^{-5} K^{-1}$. Using Eq. (13), however, a maximum transmission modulation of ~50% was expected, compared to an observed modulation of only 10%. This smaller than expected modulation is possibly due to imperfect waveguide facets which lower the finesse of the resonator.

To measure the all-optical modulation characteristics of the guide, a pump light beam of 0.514 μm wavelength with a diameter of=1 mm directly illuminated the surface of the PTCDA waveguide, while the 1.06 μm beam was end-fire coupled into the waveguide, as in the case of $\Delta n/\Delta T$ measurements. In order to avoid thermally induced intensity changes from the pump, the device temperature was precisely maintained at 22.1 °C using the thermoelectric cooler. The pump-induced intensity changes are shown in Fig. 15. Here, the transmitted intensity is *decreased* nearly linearly proportional to the pump intensity at a temperature of 22.1 °C. In contrast, the transmitted intensity due to a temperature rise at 22.1 °C is *increased* (Fig. 14).

While we suggest that the pump power dependence of $P(\delta)$ is due to an optically induced index change, it is nevertheless important to consider other competing processes. The most significant contributions to Δn are thermally induced index changes and optically induced absorption effects. To differentiate between these various mechanisms, we have investigated the modulation behavior at very low pump light intensities (< 1 W/cm^2) over a wide temperature range (16 °C – 37 °C). Three observations exclude the possibility of thermal effects: Firstly, the changes in transmitted intensity under a constant pump power could either be increased or decreased, *depending on temperature. However,* the sign of the optically induced change of transmitted intensity was always *opposite* to the thermally induced changes over the entire temperature range explored. For instance, at a certain temperature, if the transmitted intensity was *decreased* due to pump light illumination, it was *increased* due to a temperature rise. This is similar to observations for inorganic semiconductors [26] in which nonlinear effects were attributed to index changes due to excitons.

A further observation ruling out thermal effects is that the temperature increase is calculated to be ~0.03 °C under a maximum pump light intensity of 1 W/cm^2. This calculation assumes a steady state thermal conductivity of 0.1, 0.007

and 0.8 W/cm-K for PTCDA, AZ1400 and InP, respectively. Such a small temperature rise does not significantly contribute to the intensity modulation, as inferred from Fig. 14. Finally, the transient thermal relaxation time was calculated to be >13 ms, which is three orders of magnitude larger than the measured modulation time of 17 μs, as shown below. A very low amplitude "tail" in the modulation response with a time constant of ~6 ms was observed at the highest pump intensities. We attribute this latter time constant to be characteristic of very small thermal effects, whereas the shorter time constant results from significantly larger carrier lifetime effects.

The second "parasitic" effect to be considered is pump induced absorption changes, $\Delta\alpha$. Using Eq. (13), it can be shown that the change of transmitted light intensity, ΔP, in the limit of $aL<<1$, is given by: $\Delta P = -A\,\Delta\alpha$, where A is a constant. Since the waveguide used in our experiment had $\alpha L = 0.092$, this expression is valid. Thus, if the optically induced intensity change is due to $\Delta\alpha$, we should see a constant decrease of the transmitted intensity under a constant pump light illumination, *independent* of temperature. However, as noted above, the sign of the observed change varied, dependent on temperature. In addition, the absorption change due to the optically induced plasma is given by $\Delta\alpha/\Delta n = 2/c\tau$, where τ is the carrier lifetime and c is the velocity of light. For PTCDA, $\Delta\alpha/\Delta n = 4.2 \times 10^{-6}$ cm^{-1}, and absorption changes are insignificant. We conclude, therefore, that the modulation is due to an intensity dependent refractive index, rather than a change in the absorption coefficient.

Since both optically and the thermally induced modulation is caused by the changes in refractive index, the thermal measurements can be used to determine $\Delta n = n_2 I$ [27]. That is, since the thermal measurements indicated that an output intensity change of 10% corresponds to a p-phase change (Fig. 14), then the 2% decrease in transmitted intensity induced by a pump power of $I = 0.98$ W/cm^2 corresponds to $\Delta\delta = \pi/5$. Using the relationship: $\Delta\delta = 4\pi(n_2 I)L'/\lambda$ we get $n_2 = 5.4 \times 10^{-5}$ cm^2/W, where $L' = 1$ mm is the interaction length. Here, 22.1 °C was chosen as the measurement temperature since the optically induced intensity change is nearly linear over a small range of pump intensity (<1W/cm^2). Of course, the measurement can be made equally well at other temperatures.

That n_2 can be explained by the presence of optically generated free carriers was verified By comparing the measured carrier lifetime to theoretical predictions we verified that n_2 is indeed due to an optically generated plasma. Here, t was directly measured from the transient response time of the 1.06 μm

wavelength beam due to a pulsed 0.514 μm pump beam. Using a measurement system with a response time of < 1 μs, the rise and fall times of the 1.06 μm beam were found to be 18 μs and 16 μs, respectively (Fig. 16). For comparison, from the steady state measurements of n_2, using Eq. (2) we obtain $\tau = (14 \pm 1)$ μs, which is very close to the measurement. The constants used in the calculation for PTCDA are: $\alpha = 4.6 \times 10^5$ cm^{-1} at $\lambda = 0.514$ μm as obtained from absorbance measurements, a hole effective mass for PTCDA of $m^* = 0.18\ m_e$ (where m_e electron rest mass) [2], and a quantum efficiency of $\eta = 0.01$ [28]. The presence of electrons was ignored since their effective mass is at least an order of magnitude larger than that of holes [2]. In this case, Eq. (12) implies that their effect on Δn is negligible.

In Table 4 we list the resonant nonlinear properties of some typical inorganic semiconductors, along with one organic polymer, and PTCDA. From this table, n_2 of PTCDA is one of the highest observed to date. However, the response time (τ) is comparatively long. To reduce the carrier lifetime for high speed applications, organic multiple quantum well structures [12] are potentially useful. However, decreasing the carrier lifetime might also reduce h, thereby ultimately decreasing n_2. Alternatively, one can reduce τ by electrically injecting holes from contacts, and then sweep them out using an applied electric field.

In the conclusion, we report the apparently first observation of free carrier-induced nonlinear effects in crystalline organic semiconductors. An intensity-dependent refractive index of $n_2 = 5.4 \times 10^{-5}$ cm^2/W has been measured, and is among the highest values reported for practical optical device materials.

8. Future Prospects for Quasi-Epitaxial Organic Structures

Our results for the charge transport and optical properties of these novel layered structures provide an unusually large range of possibilities for materials and device physicists. That is, crystalline organic compounds have proven to be an exciting class of materials from the standpoint of providing a model system for understanding fundamental transport properties in van der Waals solids. In addition, their environmental stability, compositional versatility and combination of physical properties which bridge the materials spectrum between semiconductors and insulators opens the prospect for a broad new class of engineered materials for use in future generation optoelectronic device applications. To summarize our findings to date, crystalline organic compounds

have several properties which, taken together, make them unique in the known spectrum of materials:

1. Many crystalline materials bonded by vdW forces can be grown into ordered "quasi-epitaxial" films on substrates or other films without regard to lattice matching requirements.

2. The anisotropic crystalline structure of the films results in giant anisotropies in their conductive and dielectric properties. As an example, PTCDA films have a conductivity anisotropy of ~ 10^6, and a birefringence of $\Delta n = 0.66$. These properties are advantageous for a broad range of devices. Recently, polarization-selective waveguides employing the large birefringence of PTCDA have been demonstrated [3].

3. Heterojunctions consisting of an organic film in contact with an inorganic semiconductor substrate exhibit electrical and optical characteristics which are often the optimal combination of these properties for the particular HJ materials.

4. Heterojunctions consisting of two organic films in contact with each other often exhibit electrical and optical properties analogous in many ways to fully inorganic heterojunctions.

5. Evidence for quantum confinement in very thin layer organic multiple quantum well structures has furthered our understanding of the nature of excitons in crystalline organic materials. Given that excitons in these materials have been the focus of study for over 40 years [33,34], in many ways they are the key to our understanding the physics of vdW solids in general. In addition, the observation of quantum confinement suggests that many devices based on organic MQWs are becoming a realistic possibility. One example of such a device would be an organic MQW optical modulator which could be made to cover all regions of the UV, visible or near IR spectral regions, depending on the choice of organic compounds employed.

6. The large exciton-phonon coupling strength characteristic of organic semiconductors can lead to exciting, very large nonlinear optical effects. For example, Lam and co-workers [35] predicted that organic MQWs have large $\chi^{(3)}$ effects, and are therefore potentially useful for a broad range of applications which are unattainable using the polymers and photorefractive materials studied today. They have shown that quasi-epitaxially grown crystalline organic thin films and MQWs with large Franck-Condon (FC) shift energies exhibit an intensity-dependent absorption and index of refraction at relatively low input powers. Here, the FC shift is the energy difference between

the lowest energy absorption and the highest energy luminescence spectral peaks, and is proportional to the square of the exciton-phonon coupling strength. As shown by the arrows in Fig. 10, the PTCDA/NTCDA MQW structure with 40 Å layer thickness has FC = 4050 cm^{-1}, which to our knowledge is the largest yet observed for organic semiconductors.

To understand the nonlinear optical properties of organic MQWs, the Hamiltonian for organic MQWs under illumination can be written [35]:

$$H = h(\omega_x - \omega_l)a^+a - h\lambda Qa^+a + h\omega_o b^+b - \mu a^+E - \mu aE^* \qquad (14)$$

where ω_x, ω_l, and ω_o are the exciton, incident light and phonon frequencies, respectively, and λ is the exciton-phonon coupling constant, $\mu = qa_o$ is the exciton dipole moment, E is the external electrical field, and a^+a and b^+b are the exciton and phonon populations, respectively. Also, $Q = b^+ + b$ is the phonon amplitude.

The origin of the optical nonlinearities in organic MQWs lies in the second term of Eq. 14, which is proportional to the exciton-phonon coupling strength, λ, given by:

$$\lambda = \sqrt{\omega_o(FC)} \qquad (15)$$

The second term in Eq. 14 "renormalizes" the exciton energy, ω_x, by $-h\lambda Q$. As the incident optical field intensity increases, the exciton population increases, resulting in a decrease in the energy of the exciton absorption peak. Such an effect leads to an intensity dependent absorption, and hence an intensity dependent index of refraction through the Kramers-Kroenig effect. Note that if the incident light beam is detuned from the exciton peak on the low side of ω_x by a factor of $\omega_l - \omega_x$, then the absorption peak energy is shifted toward the pump light energy, which decreases the detuning. This increases the absorption with increasing incident light intensity, leading to optical bistability.

The two-wave mixing gain for a weak probe beam interacting with a strong pump beam for PTCDA/NTCDA MQW structures predicted by the time dependent solution of Schrodinger's Equation and using Eq. 14 is shown in Fig. 17. The horizontal axis corresponds to the (Rabi frequency)^2 which is proportional to the incident optical power in the pump beam, and the absorption or gain in the low intensity beam is plotted on the vertical axis. In the plot, the absorption becomes negative (i.e. gain) for a Rabi frequency of $\sqrt{60}$, corresponding to a power density of ~ 100 W/cm^2 for PTCDA. Also, a steep

increase in exciton population (hence absorption) occurs at a Rabi frequency as low as 20. Thus, strong nonlinear absorption is expected at power densities well below 50 W/cm^2. The results of the calculation indicate that crystalline organic materials with a large FC shift exhibit unusual optical nonlinearities which are unattainable with other classes of materials. With the ability to grow MQW structures and tailor their optical properties, the use of this new class of engineered materials for photonic applications can thus be widened.

References

1. F. F. So, S. R. Forrest, Y. Q. Shi and W. H. Steier, "Quasi-epitaxial growth of organic multiple quantum well structures by organic molecular beam deposition", Appl. Phys. Lett., **56**, 674 (1990).

2. F. F. So and S. R. Forrest, "Evidence for Exciton Confinement in Crystalline Organic Multiple Quantum Wells", Phys. Rev. Lett., **66**, 2649 (1991).

3. D. Y. Zang, F. F. So and S. R. Forrest, "Giant Anisotropies in the Dielectric Properties of Quasi-Epitaxial Crystalline Organic Semiconductor Thin Films", Appl. Phys. Lett. **58**, 562 (1991).

4. A. J. Dann, H. Hoshi and Y. Maruyama, "The structure and properties of phthalocyanine films grown by the molecular beam epitaxy technique. I. Preparation and characterization", J. Appl. Phys., **67**, 1371 (1990).

5. M. Hara, H. Sasabe, A. Yamada, and A. F. Garito, "Epitaxial growth of organic thin films by organic molecular beam epitaxy", Japan. J. Appl. Phys., **28**, L306 (1989).

6. K. Ueno, K. Saiki, T. Shimada and A. Koma, "Epitaxial growth of transition metal dichalcogenides on cleaved faces of mica", J. Vac. Sci. Technol., **A8**, 68 (1990).

7. A. Koma, K. Saiki and Y. Sato, "Heteroepitaxy of a two dimensional material on a three dimensional material", Appl. Surf. Sci. **41/42**, 451 (1989).

8. F. F. So and S. R. Forrest, "Organic-on-Inorganic Semiconductor Photodetector", IEEE Trans. Electron. Dev., **36**, 66 (1988).

9. S. R. Forrest, M. L. Kaplan and P. H. Schmidt, "Organic Thin-Film Techniques for Semiconductor Wafer Diagnostics", Ann. Rev. Mat. Sci., **17**, 189 (1987).

10. C.-L. Cheng, S. R. Forrest, M. L. Kaplan, P. H. Schmidt and B. Tell, "Novel Organic-on-InP Field-Effect Transistor", Appl. Phys. Lett., **47**, 1217 (1985).

11. D. Y. Zang, Y. Q. Shi, F. F. So, S. R. Forrest and W. H. Steier, "Optical waveguides in crystalline organic semiconductor thin films", Appl. Phys. Lett. **58**, 562 (1990).

12. S. R. Forrest, M. L. Kaplan and P. H. Schmidt, "Organic-on-Inorganic Semiconductor Contact Barrier Diodes. II. Dependence on organic film and metal contact properties", J. Appl. Phys. , **56,** 543 (1984).

13. M. K. Debe, K. K. Lam, J. C. Liu and R. J. Poirer, "Vacuum vapor deposited thin films of a perylene dicarboximide derivative: Microstructure versus deposition parameters", J. Vac. Sci. Technol., **A6**, 1907 (1988).

14. A. I. Kitaigorodsky, Molecular Crystals and Molecules, Academic, NY (1973).
15. S. R. Forrest, M. L. Kaplan and P. H. Schmidt, "Organic-on-Inorganic Semiconductor Contact Barrier Diodes. I. Theory wiith Applications to Organic Thin Films and Prototype Devices", J. Appl. Phys. , **55,** 1492 (1984).
16. P. J. Bounds and W. Siebrand, "Charge-transfer Excitons in Anthracene Crystals and Their Role in Optical Charge Carrier Generation", Chem. Phys. Lett.,**75**, 414 (1980).
17. C. Adachi, T. Tsutsui and S. Saito, "Organic electroluminescent device having a hole conductor as an emitting layer", Appl. Phys. Lett., **55**, 1139 (1989).
18. C. W. Tang, "Two-layer organic photovoltaic cell", Appl. Phys. Lett., **48**, 183 (1986).
19. "Optical and electrical properties of istotype crystalline molecular organic heterojunctions", S. R. Forrest, L. Y. Leu, F. F. So and W. Y. Yoon, J. Appl. Phys., **66**, 5908 (1989).
20. W. Warta and N. Karl, "Hot holes in naphthalene: High, electric-field-dependent mobilities", Phys. Rev., **B32**, 1172 (1985).
21. L. L. Chang, "The conduction properties of Ge-$GaAs_{1-x}P_x$ n-n heterojunctions", Solid State Electron., **8**, 721 (1965).
22. E. A. Silinsh, Organic Molecular Crystals, Springer-Verlag, Berlin (1980).
23. W. R. Smythe, Static and Dynamic Electricity, McGraw-Hill, NY 109 (1950).
24. M. Born and E. Wolf, The Principles of Optics, 6th Ed., Pergamon Press, Oxford, pp. 51 - 63 (1980).
25. R. F. Chaiken and D. R. Kearns, J. Chem. Phys., 45, 3966 (1966).
26. H. M. Gibbs, S. L. McCall, T. N. C. Venkatesan, A. C. Gossard, A. P. Passner, and W. Wiegman, Appl. Phys. Lett., 35, 451 (1979)
27. M. C. Gabriel, H. A. Haus and E. P. Ippen, J. Lightwave Technol., LT-4, 1482 (1986).
28. C. Arbour, N. R. Armstrong, R. Brina, G. Collins, J. Danziger, J. -P. Dodelet, P. Lee, K. W. Nebesney, J. Pankow, and S. Waite, Mol. Cryst. & Liq. Cryst., 183, 307 (1990)
29. D. A. B. Miller, C. T. Seaton, M. E. Prise, and C. D. Smith, Phys. Rev. Lett., 47, 197 (1981)
30. C. D. Poole and E. Garmire, Appl. Phys. Lett., 44, 363 (1984)

31. R. A. Fisher, Optical Phase Conjugation, R. K. Jain and M. B. Klein, Ed. ,Ch. 10, Academic Press, NY, p.369, (1983)
32. J. L. Oudar, I. Abram, and C. Minot, Appl. Phys. Lett., 44, 689 (1984)
33. A. F. Garito and J. W. Wu, Nonlinear Properties of Organic Materials, II, SPIE, 1147, 2 (1989)
34. N. Karl, "Studies of Organic Semiconductors for 40 Years-III", Mol. Cryst. Liq. Cryst., **171**, 31 (1989).
35. J. F. Lam, S. R. Forrest and G. L. Tangonan, "Optical Nonlinearities in Crystalline Organic Semiconductors", Phys. Rev. Lett., **66**, 1614 (1991).

APPENDIX A

TRIP REPORT

FRONTIER FORUM ON ORGANIC MBE AND STM

Riken Institute of Physical and Chemical Research
Wako, Saitama, Japan
March 11 - 13, 1991

S. R. Forrest
University of Southern California

This topical conference, or "forum" is held semi-annually by the Nonlinear Optics Group at Riken. This group is directed by Professor A. Garito at the University of Pennsylvania, with local direction provided by Professor Sasabe.

Riken is a very forward-looking and respected basic research organization in Japan. Research carried out at Riken is done by both permanent and temporary Japanese staff, and by foreign visitors. Indeed, even some of the groups are directed by non-Japanese, such as Professor Garito. Many of the temporary Japanese researchers are on loan from universities and industry, and hence Riken works very closely with both sectors of the Japanese research establishment. In many ways, what happens at Riken is picked up and followed closely by Japanese industry. There does not appear to be any organization in the U.S. which is comparable to Riken.

CNRS in France is somewhat similar in structure and goals.
The forum was attended by over 100 visitors mostly from Japanese industry. Papers on both MBE and STM were presented from Japanese researchers at Riken, in academia and industry. Invited papers by foreign researchers from DuPont, the University of Munich, the University of Pennsylvania, and the University of Southern California were also presented. A few invited papers from Europe and the U.S. were also cancelled due to the Persian Gulf war. A full program of the conference with abstracts is attached.

Taken together, a quality of the presentations was superb, with a great deal happening in the field of organic MBE and STM. I will give a few of the highlights below:

Organic MBE

Virtually all of the Japanese OMBE research centers around the growth of the phthalocyanines (Pc's) on alkali halide or metal dichalcogenide (mdc) (e.g. $MoSe_2$) substrates. The work basically follows the lead of Professor Koma at University of Tokyo who, for the last three years, has concentrated on growing VOPc and PbPc epitaxially onto $MoSe_2$ substrates. Also, he has successfully grown

a wide range of mdc's and alkali halides onto each other. His primary analysis tool is RHEED, with some x-ray diffraction and STM. To achieve epitaxy, extraordinarily low growth rates of from 0.01 ~ 0.1Å/s are required on low temperature substrates. No electrical or optical characterization of the films has been accomplished.

Surprisingly, Tanigaki at NEC deposits GaPcCl and Ga-Tetraphenyl porphorin - Cl on substrates held at 200°c to achieve epitaxy. Tanigaki has also shown a clear dependance of single crystal growth on base pressure, with "perfect" growth only occurring at $3x10^{-9}$ Torr.

One exciting development is that Koma claims to have grown NaCl <u>on top</u> of Pc's, opening up the door to heteroepitaxial superlattices bonded by Van der Waals' forces.

The DuPont effort is also quite sizeable. Here the emphasis is almost completely on growing and microscopically analyzing various epitaxial combinations of the mdc's. Again, no electrical or optical characterization of the materials has been done, although the DuPont group is doing some rudimentary calculational analysis of the basic reasons behind the observation of Van der Waals epitaxy.

The USC group's work is qualitatively different than all of the other work presented. Its primary focus is on growth of fully organic MQW structures and organic/inorganic heterojunctions based on the polyacenes (e.g. perylene and napthalene). The growth rates are high (1-3Å/s) and the substrate temperatures are <u>very</u> low (90K). This work appeared to present the first exciton size measurements using organic MQWs, and also concerned itself with predicting very large non linear optical effects in crystalline organic MQW structures. The work was clearly distinct from the Japanese and DuPont research in that it subjected the samples to both optical and electrical analysis, and overall was somewhat more applications-oriented than the other work presented. Another difference was that the structural techniques emphasized use of x-ray and optical information as opposed to RHEED analysis of the grown structures.

In addition to the papers, I learned a considerable amount about the OMBE efforts both at Riken in particular, and worldwide in general. The Riken OMBE group involves approximately 10 PhD level researchers. Two or three actually work on materials growth, while the balance work on materials characterization. Here, particular emphasis is on measuring the NLO properties of the films using lasers operating over a wide range of wavelengths (YAG, HeNe, Ar, CO_2, etc.). Also, a femtosecond laser setup is in operation using a colliding beam technique. Thus far, the optics group is awaiting samples from the OMBE group, whose films are still too thin to be useful.

Furthermore, Dr. Hara at Riken indicates that every major electronics company in Japan has either already installed or has purchased an OMBE system. These companies include Hitachi, Sony, NEC, KDD, Mitsubishi, Sharp, Sanyo, etc. The common system supplier is Vieetech -- a Japanese MBE company associated with Thermionics in the U.S. During FY 1990 alone, Vieetech took 13 orders from Japanese companies for OMBD systems! According to Hara, orders were still coming in, but were being refused since Vieetech was unable to keep up with production requirements. All systems ordered used the somewhat flawed but nevertheless functional Riken design.

According to Dr. Hara, each OMBE industrial group consisted of approximately 5 researchers at the Ph.D. (or equivalent) level. Discussions with Dr. Koma indicated that a similar number were involved in his group. At least two other professors from Japanese educational institutions are involved in OMBE since they approached me at the conference. If we presume the number of members of these latter groups is approximately three, then the total number of Japanese researchers now getting involved in OMBE is estimated at:

```
  75 Industrial
  10 Riken
  11 University
-----
  96 Total
```

This compares with ~ 5-10 in Germany (a new group at Tubingen is complementing the Stuttgart work) and ~ 6-7 in the U.S. (4 at USC and ~ 2 at University of Arizona).

The focus of this massive Japanese effort is still unclear. For the time being, most appear to be interested in following Riken's lead to "see what the future holds". All are aware of the vast potential of Van der Waals epitaxy in being able to engineer materials without the constraints of lattice match.

Organic STM

Riken (Dr. Hara) has taken a lead in recognizing the importance of STM in understanding OMBE films. Their work at elucidating liquid crystal structures using this technique is clear from the paper attached. Hara has 4 STMs in his laboratory and 1 atomic force microscope. One of his STMs is connected through a UHV mobile "trolley" to his OMBE system. The STM connected in this way is also mounted in a UHV system, although it has not been successfully used at this time.

Typically, layers analyzed were ~ 1-3 monolayers thick, and were grown on graphite or MoS_2 substrates. Effects on image quality due to tip composition, tip geometry and observational parameters (e.g. voltage and current) were all extensively discussed.

This part of the conference was important to the USC work in that we are currently attempting to interpret PTCDA images generated using the Digital Instruments Nanoscope II STM. Indeed a large proportion of the data presented at the conference were obtained using this instrument.

Perhaps the most beautiful STM work was presented by Dr. Heckl at the University of Munich. He presented extensive studies of DNA, liquid crystals and other organic molecules.

It appears that the work of the Riken group is making an important and long lasting linkage between STM and OMBE. They are interested in this linkage both for its application to resolving structural detail, and also for its use in "machining" microstructures consisting of organic molecules manipulated by the STM tip.

In summary, I feel it is of utmost importance to maintain contact between the Riken group (and hence the broader Japanese research establishment) and our group at USC. To date, we have independently followed somewhat different "evolutionary trends" in OMBE, both of which have their separate strengths and weaknesses. By maintaining contact, we can learn a considerable amount from the Japanese effort. To this end, I have invited Dr. Hara to visit USC during his visit to the Digital Instruments STM Users meeting in June. Further, I hope to attend the NLO meeting at the University of Pennsylvania (co-sponsored by Riken and University of Pennsylvania) in April. Finally, I have invited Dr. Paul Burrows, a Riken post-doc from the U.K., to visit and work in our laboratory once he finishes his "tour of duty" at Riken in the summer of 1991.

It was a very valuable experience for me to attend this forum, and hope to do so again at this same time next year.

"Frontier Forum"

The First Symposium on "*Nanoscopic*" Science & Technology for Low-Dimensional Materials

"Frontiers of Organic MBE & STM"

March 12-13, 1991

Nishina Memorial Hall and Laser Conference Room
RIKEN, Saitama JAPAN

Under the Auspices of
Frontier Research Program
The Institute of Physical & Chemical Research
RIKEN

Final Program and Abstract Brochure

"Frontier Forum" Final Announcement

"*Nanoscopic*" Science & Technology for Low-Dimensional Materials

"Frontiers of Organic MBE & STM"

March 12-13, 1991
Frontier Research Program
RIKEN Institute of Physical & Chemical Research
Wako, Saitama 351-01, JAPAN

The purpose of this "Frontier Forum" is to bring together recent advances in "*Nanoscopic*" science and technology for fabrication and fundamental study of low-dimensional materials. The topics will focus on novel application of Molecular Beam Epitaxy (MBE) and Scanning Tunneling Microscopy (STM) techniques, especially for organic molecular systems. The official language is English.

March 12 (Tue), Nishina Memorial Hall

9:30-10:00 Coffee Mixer

10:05-10:15(10) R. KUBO, Director-General of the Frontier Research Program
"Opening Address"

(10:15-12:30 Chairperson: M.HARA)

10:15-11:00(35+10) A. KOMA (Univ. of Tokyo) ----------3
"Van Der Waals Epitaxy and Organic MBE"

11:00-11:45(35+10) H. TADA (Univ. of Tokyo) ----------4
"Structural Analysis of Ultrathin Films of Metal-Phthalocyanines by RHEED"

11:45-12:30(35+10) K. TANIGAKI (NEC) ----------5
"Thin Film Crystals of Phthalocyanines and Porphyrins"

12:30-13:45 Lunch & Tea Break

(13:45-15:15 Chairperson: A.YAMADA)

13:45-14:30(35+10) P.E. BURROWS (RIKEN) ----------6
"A New Concept of Molecular Electronics: from Inchworm Memory to Organic Quantum Well"

14:30-15:15(35+10) S.R. FORREST (USC) ----------7
"Quasi-Epitaxial Growth of Organic Multiple Quantum Well Structures by Organic MBE"

15:15-15:30 Coffee Break

(15:30-17:00 Chairperson: P.E.BURROWS)

15:30-16:15(35+10) O. NISHIKAWA (Tokyo Inst. of Tech.) ----------8
"Tunneling Microscopies: from FEM to STS"

16:15-16:45(25+5) M. HARA (RIKEN) ----------9
"Organic MBE and Organic STM for Nanoscopic Materials"

16:45-17:00(15) A. YAMADA, Coordinator of Lab for NLO & Advanced Materials
"Materials for The Future"

17:30-20:00 Party, Dining Room

March 13 (Wed), Laser Conf Room

9:30-10:00 Coffee Mixer

10:05-10:15(10) H. SASABE, Coordinator of Lab for Bioelectronic Materials
"Opening Address"

(10:15-12:30 Chairperson: H.SASABE)

10:15-11:00(35+10) Y. IWAKABE (Hitachi) ----------10
"Direct Observation of Anchoring Structures of Liquid Crystal Molecules by STM"

11:00-11:45(35+10) W. MIZUTANI (ETL) ----------11
"A Model of Imaging Mechanism and Its Applications"

11:45-12:30(35+10) M. HARA (RIKEN) ----------12
"STM Imaging of Organic and Biological Molecules"

12:30-13:45 Lunch & Tea Break

(13:45-15:15 Chairperson: A.F.GARITO)

13:45-14:30(35+10) W.M. HECKL (IBM Munich) ----------13
"STM and SFM on Small Organic Molecules"

14:30-15:15(35+10) F.S. OHUCHI (DuPont Wilmington) ----------14
"Surface Physics and Chemistry of MBE Grown Low-Dimensional Materials: Surface Analysis with STM"

15:15-15:45(30) A.F. GARITO, Head of Lab for NLO & Advanced Materials
"Closing Remarks"

March 11 (Mon) "Lab Tour" for invited speakers, Frontier Bldg

15:00-17:00(120) Frontier Experimental Bldg
18:00 Mixer for invited speakers, Frontier Guest House

Honorary Chair: R. KUBO, Director-General of the Frontier Research Program

Organizing Chairs: H. SASABE, A.F. GARITO & A. YAMADA

For further information on this forum, please contact:

Masahiko HARA, Dr., Research Scientist
Frontier Research Program
RIKEN (The Institute of Physical & Chemical Research)
Wako, Saitama 351-01, JAPAN
Fax:+81-484-65-8048 or +81-484-62-4699
Tel:+81-484-62-1111 ext.6322 or 6324
or 6331 (Ms. NAKAGAWA)

Van der Waals Epitaxy and Organic MBE

Atsushi Koma
Department of Chemistry, University of Tokyo
Tokyo 113, JAPAN
TEL/FAX +81-3-5689-0654

Heteroepitaxial growth of ultrathin films of organic materials has potential applications in such new fields as nonlinear optics, molecular electronics and molecular biology. But there have been no good epitaxial growth method which is applicable to organic materials. Here we will introduce new concepts in heteroepitaxial growth of organic material films.

Usually there appear dangling bonds on a clean surface of a substrate. This makes it difficult to grow good heteroepitaxial film without good lattice match in the constituent materials, resulting in very limited combinations of substrate and overgrown materials. There are, however, materials having no dangling bonds on their clean surfaces, on which epitaxial growth proceeds via van der Waals forces. We call that kind of epitaxy van der Waals epitaxy [1]. Good heterostructures can be grown even between materials having large lattice mismatch in the van der Waals epitaxy. We have proven almost all layered materials can be heteroepitaxially grown on another layered materials regardless of their lattice matching conditions. This idea is especially useful in heteroepitaxial growth of organic materials, since many organic materials crystallize in forms of van der Waals crystals. Actually we have demonstrated ordered films of various metal phthalocyanines and coronene can be grown on a cleaved face of MoS_2, which has typical van der Waals nature. This method seems to be applicable to many other organic materials, although the substrate should be cooled for the materials with high vapor pressures.

In some cases electrostatic interactions help the epitaxial growth. This is especially true in the preparation of films of polar organic materials. For example good VO-phthalocyanine film can be grown on various alkali halide substrates. Here electrostatic interactions with alkaline or halogen ions help to orient polar VO-phthalocyanine molecules on alkali halide substrates [2].

[1] A. Koma, K. Sunouchi and T. Miyajima, J. Vac. Sci. Technol., B3 (1985) 724.
[2] H. Tada, K. Saiki and A. Koma, Jpn. J. Appl. Phys., 30 (1991) L306.

Structural Analysis of Ultrathin Films of Metal-Phthalocyanines by Reflection High Energy Electron Diffraction

H. TADA, M. SAKURAI, T. MORIOKA and A. KOMA
Dept. of Chem., Fac. of Sci., Univ. of Tokyo

Ultrathin films of some metal-phthalocyanines (MPc, M=VO, Pb, AlCl, and Cu, Pc=$C_{32}H_{16}N_8$) have been grown heteroepitaxially on cleaved faces of alkali halides (KBr, KCl, and NaCl) and MoS_2 by molecular beam epitaxy (MBE). Their structures were investigated *in situ* by reflection high energy electron diffraction (RHEED). Figure 1 shows the RHEED pattern of VOPc ultrathin film grown on KBr. The incident beam is parallel to the [100] direction of the substrate. Sharp streaks originating from ordered VOPc film are observed. The interval is one third of that between substrate streaks. Taking into account the RHEED patterns observed from various directions, VOPc molecules are found to form a single domain square lattice as shown in Fig. 2. On the other hand, they form two equivalent square lattices on KCl and NaCl. From these results that VOPc molecules are arranged differently depending upon the lattice constants of alkali halides, it is considered that the arrangement is primarily governed by the electrostatic interaction between VOPc molecule and the substrate. Van der Waals interaction between neighboring molecules seem to play a role to determine molecular distances and arrangement directions. Ultrathin films of PbPc and AlClPc molecules grown on alkali halides gave almost the same RHEED patterns, whereas CuPc films gave ordered dot patterns due to the formation of α-type crystalline islands. Thus metal-phthalocyanines with pyramidal molecular structures seem to be preferable to form smooth heteroepitaxial films on alkali halide substrates. They are apt to line up along [210] direction of the substrate, and they are considered to be stable when the molecular distances are about 14 Å.

CuPc ultrathin film grown on MoS_2 gave streaky RHEED patterns, and then CuPc molecules are found to form square lattices with molecular distance of 13.7 Å. Most organic ultrathin films prepared on MoS_2 so far (MPc, coronene, perylene, MNA) gave streaky RHEED patterns. The molecules seem to be closely packed in the first layer on MoS_2.

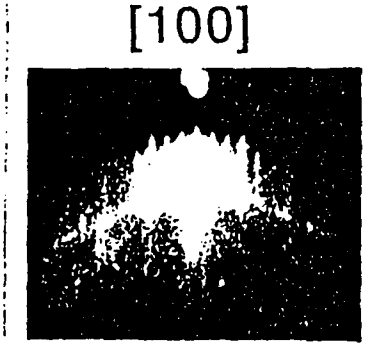

Fig.1. RHEED pattern of VOPc ultrathin film grown on KBr.

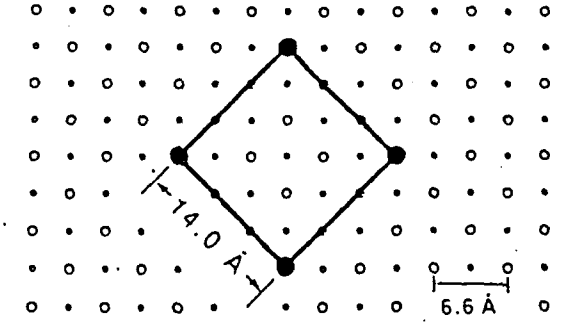

Fig.2. Possible arrangement of VOPc on KBr : (●) VO^{2+}, (o) K^+, (o) Br^-.

Thin Film Crystals of Phthalocyanines and Porphyrins

Katsumi Tanigaki, Sadanori Kuroshima and Thomas W. Ebbesen
Fundamental Research Laboratories, NEC Corporation,
34 Miyukigaoka Tsukuba, Ibaraki 305, Japan
Tel:81-298-50-1138, Fax:81-298-56-2326

Phthalocyanine and porphyrin families are promising molecules for electronics. Especially thin film crystals of these molecules have possibilities to open the way for their advanced applications as nanoscopic and low-dimensional materials [1]. Recent progress in the technology of thin film crystal growth by *molecular beam epitaxy (MBE)* is now being applied to organic molecules.

We have applied MBE technique for thin film crystal growth focusing on phthalocyanines and porphyrins containing III-V elements in the periodic table. This is because d_2sp_3/sp_3d_2 hybrid orbitals formed with tetragonally-positioned four nitrogen atoms and a central element are thought to play an important role for the artificial molecular assembly in the direction perpendicular to the molecular plane. In this presentation, we report thin film crystals of a phthalocyanine (Pc) and a mesotetraphenylporphyrin (TPPr) containing gallium (typical III element) as a central element and chlorine as a ligand, monochloro(phthalocyaninato)gallium (GaPcCl) and monochloro(mesotetraphenylporphyrinato)gallium (GaTPPrCl).

Precise control of the growth condition by organic MBE gives thin film single crystals of GaPcCl and GaTPPrCl on a KBr substrate over 2mmx2mm area. TEM and X-ray analyses of these thin film crystals reveal that their structure is body-centered tetragonal (BCT) with lattice parameters of a=9.9 Å and c=13.4 Å. Crystal analysis data of a bulk single crystal of GaTPPrCl grown with a vapor-phase apparatus support the determined BCT structure, being tetragonal, space group I4/m, with a=13.5 Å, c=9.9 Å for Z=2. The GaTPPrCl thin film density (ρ=1.324) measured by buoyancy is also in good agreement with the calculated one from the BCT structure. Direct TEM lattice image of GaTPPrCl is demonstrated with a computer simulation. These results indicate that Organic MBE will be useful in controlling an architecture of molecular assembly and should open a new field from the technological point of view.

Reference

[1] C. W. Dirk, T. Inabe, K. F. Schoch, and T. J. Marks, J. Am. Chem. Soc., 105, 1539 (1983).

A New Concept of Molecular Electronics: From Inchworm Memory To Organic Quantum Well.

P.E. Burrows, M. Hara, H. Sasabe, A. Yamada & A.F.Garito.
Frontier Research Program, Riken Institute, Hirosawa 2-1, Wako-shi, Japan.
E.G. Wilson.
Queen Mary & Westfield College, Mile End Road, London E1 4NS, England.

If the present trend continues, the size of electronic devices will decrease to the size of organic molecules by early next century.[1] This has prompted a plethora of device concepts utilising single molecules or polymer chains, but there has been little experimental evidence that manipulation and external contacting of such devices is feasible, or that the reliability of single molecule devices could be made sufficiently high.

A new device concept is presented, the inchworm memory[2], which stores information as charge on a three-dimensional stack of ultra-thin, high electron affinity sheets of conjugated organic molecules alternated with low electron affinity sheets of "insulator" molecules. This device offers information storage on a molecular scale without the need for lithography at molecular dimensions. A possible design for such a memory, utilising thin films of phthalocyanine molecules, is presented.

Organic Molecular Beam Epitaxy (OMBE) is a possible route to the production of such devices. Results are presented from metallo-phthalocyanine layers, grown heteroepitaxially on graphite under a base pressure of 2×10^{-10} torr by the OMBE technique with *in situ* RHEED monitoring. The orientational order of the initial stages was clearly determined by STM even in air. The combination of surface-sensitive diffraction methods with real space imaging by STM allows direct studies of epitaxial layers at the atomic scale. Preliminary evidence of organic RHEED intensity oscillations during film growth is presented.

[1] F.L. Carter (Ed.), *Molecular Electronic Devices I,II,* Marcel Dekker, New York (1982,1987).

[2] P.E. Burrows & E.G. Wilson, J. Mol. Elec. 6, 209 (1990).

Quasi-Epitaxial Growth of Organic Multiple Quantum Well Structures by Organic Molecular Beam Deposition

S. R. Forrest, F. F. So, and D. Y. Zang
Departments of Electrical Engineering and Materials Science
Center for Photonic Technology
University of Southern California
Los Angeles, CA 90089-0241

Abstract

We report on the growth and characterization of thin films and multiple quantum wells consisting of alternating layers of crystalline organic semiconductors. We have found that two compounds, namely PTCDA (a "narrow band-gap" perylene-based material) and NTCDA (a "wide band gap" naphthalene derivative) can be deposited in crystalline form on a wide variety of substrates using the UHV process of organic molecular beam deposition (OMBD). Furthermore, stacks of alternating layers of PTCDA and NTCDA can be grown in a completely ordered manner, thereby forming the first crystalline organic MQW structures.

The optical properties of the thin films and the MQWs have both been studied. Measurements of the PTCDA exciton spectrum suggest that the charge-transfer (CT) exciton can be quantum confined in PTCDA/NTCDA MQWs. Solution of Schrodinger's Equation for an exciton confined to a quantum well, both the blue shift of the exciton spectrum, and the decrease in its radiative lifetime with decreasing PTCDA layer thickness (from 10Å - 200 Å) can be explained assuming that the CT exciton is "Wannier-like" with a radius of 12 Å. Furthermore, solutions of the Davydov Hamiltonian for these MQWs predict large nonlinear optical effects in the PTCDA absorption coefficient resulting from the large exciton-phonon coupling characteristic of organic molecular semiconductors. This opens up the possibility that organic MQWs can be useful as light modulators, or for energy transfer in two-wave mixing experiments.

Due to the perfection of the deposited thin films, we have successfully fabricated very low loss optical waveguides to TE mode propagation. On the other hand, due to giant anisotropies discovered in the dielectric properties of these films (i.e. the birefringence of PTCDA is 0.66), TM modes are not guided, leading to naturally polarizing thin film waveguide devices.

This work was supported in part by the Air Force Office of Scientific Research, Rome Air Development Center and the 3M Corp.

TUNNELING MICROSCOPIES -- FROM FEM TO STS --

Osamu NISHIKAWA, Masahiko TOMITORI & Fumikazu IWAWAKI

Department of Materials Science and Engineering
The Graduate School at Nagatsuta
Tokyo Institute of Technology
4259 Nagatsuta, Midori-ku, Yokohama 227 Japan
Phone: 81-45-922-1111 Ext.2621, Fax: 81-45-922-5173

A field emission microscope (FEM), a field ion microscope (FIM) and a scanning tunneling microscope (STM) utilize electron tunneling and have realized the atomically high resolution imaging. The high resolution has been attained by confining the tunneling area to the size of an atom. Unique features of the microscopes are:

1. Direct projection of atomic arrangement of a tip apex by FIM and topographic depiction of individual atoms on a flat specimen surface by STM.
2. Electron spectroscopy of a small apex area with FEM (field emission electron energy spectroscopy: FEES) and individual surface atoms with STM (scanning tunneling spectroscopy: STS).
3. Mass analysis of individual apex atoms by an atom-probe(A-P), the combined instrument of an FIM and a mass spectrometer.

Although the performance of the microscopes appears peerless, there are many restrictions such as:

1. Extremely small specimens of FEM and FIM: Shperical apex of a sharp tip.
2. Highly sensitivity of STM images and STS spectra to the apex profile and composition of a scanning tip.
3. Incomprehensible tunneling characteristics of polymers and biomolecules.

Unique features and imposed restrictions of the microscopies will be discussed based on the experimental results.

Organic MBE and Organic STM for "*Nanoscopic*" Materials

*M. Hara, P. E. Burrows, H. Sasabe, A. Yamada & A. F. Garito**
Frontier Research Program,
The Institute of Physical and Chemical Research (RIKEN),
Wako, Saitama 351-01, JAPAN
Tel:+81-484-62-1111, Fax:+81-484-65-8048
*Permanent Address: Department of Physics, University of Pennsylvania, Philadelphia, PA 19101, USA.

Application of molecular beam epitaxy (MBE) and scanning tunneling microscopy (STM), especially for organic molecular systems, has been drawing our attention as a novel approach to realizing novel material structures which exhibit important electronic and photonic properties. The following is an outline of our work in progress, including an overview of the new concept embraced by "*nanoscopic*" science and technology.

1. Nanoscopic Fabrication

MBE has long been successful as an ultrahigh vacuum (UHV) deposition technique for fabricating multilayer thin film structures, even in the organic molecular field. In an extreme case, however, heteroepitaxial growth of organic ultrathin films on single crystal substrates can be attained by usual adsorption, even in air, like a single crystal growth by nature. From the numerous observations of the organic layer growth, it has been realized that the anchoring sites at the interface are the most important factors to manipulate the adsorbates and control the surface structures. From this point of view, the combination of the MBE and/or adsorption techniques with surface modification by STM will provide a new technique for "*nanoscopic*" fabrication of low-dimensional materials, which allows "molecular planting" at the atomic scale.

2. Nanoscopic Modification

Since the single atom positioning was reported by Eigler and Schweizer, considerable interest has centered on utilizing STM for pinning individual molecules. It has been well-known, however, that strict conditions such as low-temperature STM under UHV is required to obtain reproducibility. It is still more realistic, to some extent, to utilize the STM for lithography rather than manipulation. By introducing the micro-focusing technique, the STM controlled sub-nanoscopic electron beam will develop the possibilities, in principle, for the ultimate in "*nanoscopic*" modification.

3. Nanoscopic-Characterization

The STM has opened a completely new approach to organic molecules with ultrahigh resolution. More recently, the STM technique has been shown to provide outstanding capability not only in structural analysis but also in visualization of functional parts such as chiral centers and dipoles in individual molecules. This kind of "*nanoscopic*" characterization is indeed encouraging to the possibilities for the novel application of the STM as an input/output part in next-generation molecular devices.

Direct Observation of Anchoring Structures of Liquid Crystal Molecules by Scanning Tunneling Microscopy

Y. Iwakabe, M. Hara†, K. Kondo, K. Tochigi, A. Mukoh, A.F. Garito†*, H. Sasabe†and Y. Yamada†

Hitachi Research Laboratory, Hitachi Ltd., Hitachi, Ibaraki 319-12
†Frontier Research Program, The Institute of Physical and Chemical Research (RIKEN) Wako, Saitama 351-01

Scanning tunneling microscopy (STM) has been attracting much interest as a useful tool for the study of the molecular alignment on substrate at a atomic scale. The anchoring structures of liquid crystals, n- alkylcyanobiphenyl (mCB=8-12), on substrate are directly observed by STM in order to analyze the alignment mechanism of liquid crystals.

1. The substrate dependence of the anchoring structure of liquid crystal

The anchoring structures of smectic liquid crystal 8CB are observed condensed on graphite or MoS_2 [1]. In contrast to the bilayer structure on graphite, the liquid crystal 8CB on MoS_2 exhibits a periodic monolayer structure which suggests that the anchoring structure can be varied by the substrate structure.

2. The molecular structure dependence of the anchoring structure of liquid crystal

The anchoring structures of smectic liquid crystals 8CB, 10CB, 12CB are observed condensed on MoS_2 [2]. For 8CB, the anchoring structure is of the periodic monolayer type, while 10CB and 12CB take a bilayer structure. These structures on MoS_2 depend on the length of the alkyl group in contrast to those on graphite.

3. The relationship between bulk alignment and anchoring structure of liquid crystal

The anchoring structure of the liquid crystal is governed, to a large extent, by the balance of molecular-molecular and substrate-molecular interaction. The balance depend on the degree of freedom for the anchoring of alkyl chains.

*Permanent Address: Department of Physics, University of Pennsylvania, Philadelphia, PA 19104, USA

[1] M. Hara *et al.*: Nature 344 (1990) 228
[2] Y. Iwakabe *et al.* : Jpn. J. Appl. Phys. 29 (1990) L2243

A Model of Imaging Mechanism and Its Applications

Wataru Mizutani

Electrotechnical Laboratory, Umezono 1-1-4, Tsukuba 305, Japan

The interpretation of scanning tunneling microscopy (STM) images of adsorbed molecules is still controversial. Recently, a resonant tunneling model was proposed to interpret the experimental results of STM observation of liquid crystals[1]. Tunneling current comparable with the experiments can be calculated based on the model.

The following physical aspect of the model is now under investigation. One of the remarkable effects which should be studied is charging of molecules induced by electron tunneling. Provided that the individual molecule is observed, the energy increase by the single electron tunneling is estimated to be about 1 eV. On the other hand, the life time of the extra electron in the molecule is calculated to be 10^{-16} seconds. Therefore, the product $\Delta E \cdot \tau \sim 10^{-35}$ is less than $\hbar \sim 10^{-34}$, which means that the process is allowed by the indeterminacy principle. However, the energy levels of the molecule become uncertain during that time, and it is not so explicit that the resonant tunneling should occur under such an extreme condition. Probably the quantum many-particle effect should be considered to analyze the behavior of the electrons in the molecule, but such a theory applicable to STM is not proposed so far.

The model is applicable to other experimental results, i.e., a change in the molecular arrangement of a liquid crystal due to the bias voltage[2], and the observation of other adsorbed materials. There remain, however, some factors incomprehensible and needs for further modifications, especially taking into account of quantum chemistry.

1) W. Mizutani et al.: Appl. Phys. Lett. 56 (1990) 1974.
2) W. Mizutani et al.: J.Vac.Sci.Technol.A, April/May (1991).

STM Imaging of Organic and Biological Molecules

M.Hara, P.E.Burrows, H.Sasabe, A.Yamada & A.F.Garito
& The Organic STM Group
Frontier Research Program, The Institute of Physical and Chemical Research (RIKEN), Wako, Saitama 351-01, JAPAN
Y.Iwakabe, K.Tochigi & A.Mukoh
*Hitachi Res Lab, Hitachi Ltd, Hitachi, Ibaraki 319-12, JAPAN
T.Umemoto, H.Takezoe & A.Fukuda
**Dept of Org & Poly Mat, Tokyo Inst of Tech, O-okayama, Tokyo 152, JAPAN
M.Miyazawa, T.Sagara & K.Niki
***Dept of Phys Chem, Yokohama Natl Univ, Hodogaya, Yokohama 240, JAPAN

We present a wide variety of organic and biological molecules which have been imaged with STM in air.

1. Heteroepitaxially Grown Phthalocyanine Monolayers

The combination of diffraction methods with real apace imaging of STM allows direct studies of epitaxial layers at the atomic scale. Metallophthalocyanine monolayers were grown heteroepitaxially on graphite under 2 x 10^{-10} torr by the organic MBE technique with *in situ* RHEED monitoring. From STM images of the phthalocyanine layer and the substrate beneath the organic layer, the orientational correlation between the organic layer and the substrate surface was clearly determined in real space.

*2. Novel Anchoring Structures and Phase Transitions in Liquid Crystals**

While STM images of liquid crystal molecules have been reported with high resolution, only graphite has been used as a substrate so far. We replaced the graphite with MoS_2 and observed by STM an entirely new "2 x 4" anchoring structure for *n*-alkyl cyanobiphenyls. Furthermore, the results suggest that a possibility exists to study the phase transition mechanisms using the STM imaging.

*3. Visualization of Functional Parts in Ferroelectric Liquid Crystals***

The STM technique has been shown to provide outstanding results not only in structural analysis but also in visualization of functional parts such as chiral centers and dipoles in organic molecules. By carefully controlling deposition parameters in the sample preparation step, it is possible to distinguish between methyl and ethyl moiety around chiral carbons and orientations of dipoles in individual molecules.

*4. Novel Guest-Host Anchoring Method for STM Visualization of Biological Macromolecules****

Serious problems have been encountered in trying to obtain unambiguous STM images of biological macromolecules, mainly because of lack of reliable deposition methods on atomically flat substrates. The molecules must not be packed into dense aggregates, but must be distributed in a two-dimensional plane, *i.e.* sub-monolayer. Thus during deposition, high molecular mobility on the surface is desirable, while moderate anchoring is required during scanning. Here we introduce a novel and easy deposition method, "Guest-Host Anchoring" of biological macromolecules with clear discrimination against artifacts.

Surface phases of small organic molecules observed by tunneling microscopy

W.M. Heckl *, G. Binnig +, D.P.E. Smith+ and H. Klagges *

* University Munich, Schellingstr. 4, D-8000 München 40
+ IBM Research, Physics Group Munich

The two dimensional order formed by epitaxial growth of small organic molecules on the surface of graphite and molybdenum disulfide can be investigated with nearly atomic resolution by scanning tunneling microscopy (STM). We will discuss the structure, the registry, the adsorption and imaging mechanism as well as lattice defects and dynamical aspects of the interfacial layer. We will concentrate on DNA bases and show some additional examples of amphiphilic molecules and hexadecylpyrene as a fluorophore.

Several recent studies have reported on the possibility of imaging DNA by Scanning Tunneling Microscopy. However the ultimate goal, that is to read the code of the strands, has not yet been achieved. In order to do so it must be possible to clearly recognize and distinguish between the four different bases which comprise the genetic code. One essential requirement for imaging small organic molecules by STM is to find experimental preparation conditions where the molecules stick firmly to the substrate and form a layer with great stability in order to withstand the forces of the STM tip during imaging. Compared to the binding of complete DNA strands to the basal planes of MoS_2 or graphite the adsorption of "naked" nucleotide bases is favoured by their greater hydrophobicity and by their ability to register with the substrate forming a two dimensional ordered array. We found that the two-dimensional lattice formed by adenine, guanine and thymine, three of the four bases which comprise the genetic code of DNA, is nearly identical on the surface of the graphite and the molybdenum difsulfide substrate. The resolution of molecular details is superior in the case of the graphite substrate. By the aid of molecular orbital calculations, which allow for the comparison of predicted electron densities with the observed STM contrast, we propose the interfacial structure of guanine to be composed of linear strands of guanine molecules with alternating orientation linked together by hydrogen bonds.

Lit. W.M. Heckl et al.: Nature, submitted

D.P.E. Smith and W.M. Heckl, Nature, Vol. 346, No. 6285, 616 - 617, 1990

Materials Science Perspective on Surface Chemistry and Physics of Low Dimensional Layered Materials

Fumio S. Ohuchi
E.I.DuPont de Nemours and Company
Central Research and Development Department
Experimental Station
Wilmington, Delaware 19880-0356

Abstract

The potential for new materials with tailored bulk, surface and interface properties has motivated many recent investigations concerned with fabricating composite systems comprised of dissimilar materials. We have been developing processes involved in layered materials through tightly controlled atomic and electronic structure at the interfaces.

A route to new materials by exploiting atomically abrupt nature of layered compound materials and their reactivity to metals is described first, then a variation of molecular beam epitaxy, called van der Waals epitaxy, will be followed. Both methods have utilized unique natures of low dimensionality of the materials, and are rich in surface physics and chemistry.

The interactions of group IB metals (Cu, Ag and Au) with van der Waals surfaces of layered semiconducting materials have led new classes of material systems that have not been obtained by other methods. The peculiarity of interaction lies in the fact that the host structure is forced into a lattice distortion by electronic driving force from surface reaction and intercalation. Difference in the surface symmetry also influences the nucleation and growth of the metal atoms, which in turn demonstrates the decoration of atoms over the surface.

Lattice mismatching difficulties that limit the choice of materials in conventional MBE of three dimensional systems are circumvented in the van der Waals epitaxial process. Demonstrated are epitaxial growth of layered materials with lattice mismatching exceeding more than $\pm$18%. STM provided real space images of the morphology of the epitaxial layer and showed novel structures resulting from the large lattice mismatch where the epilayer atoms are commensulated. The flexibility for fabricating multilayer structures containing different materials selected for their specific properties, rather than their lattice matching requirement, has been discussed.

Appendix C: Polarization effects in organic MQWs

Consider an exciton with a Bohr radius a_o generated at point P in a PTCDA layer of thickness t sandwiched between two NTCDA layers with the same thickness, as shown in Fig. 18. The change in exciton potential due to the presence of an NTCDA molecule at point N on the NTCDA surface is:

$$\Delta\varphi = \Delta\mu\cos\theta'/\varepsilon_p|\mathbf{R}-\mathbf{r}|^2 \qquad \text{(A-1)}$$

where $\Delta\mu = \mu_P - \mu_N$, with μ_P (μ_N) the dipole moment per unit volume of PTCDA (NTCDA), ε_p is the dielectric constant of PTCDA, **R** is a vector between points P and N, θ' is the angle between **R** and the normal to the NTCDA plane, and the charge density of the exciton is described by the spherical coordinates: r, θ, and ϕ. Using Taylor's series expansion and dropping the higher order terms in Eq. A-1, the change in potential is:

$$\Delta\varphi = \Delta\mu\cos\theta'/(\varepsilon_p R^2)[1 + (2r/R)\cos\theta\cos\theta'] \qquad \text{(A-2)}$$

Here we assume the ground state exciton wavefunction to be a hydrogenic 1s state, and the first term to be proportional to the first order perturbation Hamiltonian. Therefore, the first order polarization energy correction is:

$$E^{(1)} = \langle 1s \mid H^{(1)} \mid 1s\rangle = q\Delta\mu\cos\theta'/(\varepsilon_p R^2) \qquad \text{(A-3)}$$

On the other hand, assuming ψ_n is the excited state wavefunction and $H^{(2)}$ is the second term in Eq. A-2, then the second order energy is:

$$E^{(2)} = \sum_n \mid \langle n|H^{(2)}| 1s\rangle \mid^2 / (E_n - E_{1s}) \qquad \text{(A-4)}$$

Here, n denotes the nth excited state wavefunction, and E_n and E_{1s} are the excited and ground state energies, respectively.

The first order polarization energy can be evaluated by integrating $E^{(1)}$ in Eq. A-3 over all space to obtain:

$$\langle E^{(1)}_{tot}\rangle = A'(\Delta\mu/\varepsilon_p)t \qquad \text{(A-5)}$$

where A' is a numerical constant. Similarly, ignoring the higher order term, the second order polarization energy can be evaluated:

$$\langle E^{(2)}_{tot}\rangle = A''\Delta\mu^2 a_o^2\delta/(\varepsilon_p t^4) \qquad \text{(A-6)}$$

where A" is also a numerical constant, and δ is the thickness of the PTCDA/NTCDA heterointerface region. Therefore, the first order energy correction to the polarization energy due to the presence of the NTCDA layers increases linearly with t, and the second order term is proportional to t^{-4}.

Table 1 – van der Waals Coefficients[1]

Bond Interaction	α (meV-Å^6)	β (meV)	γ (Å^{-1})
H-H	1.96	432	4.54
C-H	5.51	3735	4.57
C-C	15.7	39400	4.59
O-O	9.41	5860	4.59
C=O-O=C	16.1	9110	4.59
H-O	3.92	1160	4.57
H-O=C	5.29	1500	4.57
C-O	12.1	15200	4.59
C-O=C	15.9	19000	4.59

[1]Values for α, β and γ taken from A. Abe, R. L. Jernigan and P.J. Flory, J. Am. Chem. Soc., 88, 631 (1966); and R. A. Scott and H. A. Scheraga, J. Chem. Phys., 42, 2209 (1965).

Table 2. Variational calculation parameters

Parameter	Symbol	Unit	Value
Hole mass	m_h	m_o	0.18
Election mas	m_e	m_o	10.0
Electron potential	V_e	meV	900
Hole potential	V_h	meV	50
Reiative dielectric constant of PTCDA	ε_p		3.6

Table 3: Reflectivity data for PTCDA thin films

λ (μm)	Sample Thickness	Incident Angle[a]	$n_{\perp}$ (Cal.)
1.064	1.13	29°	1.354 (m=8)
1.319	1.25	47°	1.364 (m=8)
1.064	1.13	41°	1.343 (m=6)
1.319	1.25	55.5°	1.346 (m=6)

[a] Corresponding to the reflectivity minimum.

Table 4: Resonant Nonlinear Properties of Some Typical Materials

Material	Energy Gap (eV)	λ (μm)	Response Time	Temp. (K)	n_2 (cm^2/W)	Refs.
InSb	0.18	5.5	0.3 μs	80	10^{-3}	[29]
InAs	0.40	3.1	0.2 μs	80	$2x10^{-5}$	[30]
Si	1.12	1.06	—	300	$1.2x10^{-10}$	[31]
GaAs	1.42	0.81	30 ps	80	$8.6x10^{-10}$	[32]
SINC*		0.81	—	300	10^{-7}	[33]
PTCDA	2.2	0.514	16μs	295	$5.4x10^{-5}$	This work

* SINC is silicon naphthalocyanine oligomer, which is a random glassy polymer.

Figure Captions

Fig. 1: Two views of a unit cell of PTCDA.

Fig. 2: Two views of a unit cell of NTCDA.

Fig. 3: Plot of contours of constant van der Waals energy between a PTCDA and NTCDA molecule. Each contour corresponds to an increase in energy of 5 meV as one moves from the central position (0,0) to the edges. Each axis spans a distance of ± 2Å from the position where an NTCDA molecule is centered directly over the center of a PTCDA molecule, with an interplanar stacking distance of 3.2 Å.

Fig. 4: Bipolar current voltage characteristics of a CuPc/PTCDA heterojunction sample. **Inset:** Cross-sectional view of the CuPc/PTCDA test structure.

Fig. 5: Saturation current versus temperature for a CuPc/PTCDA heterojunction.

Fig. 6: Proposed band diagram of a CuPc/PTCDA heterojunction in the region of the heterointerface.

Fig. 7: Proposed molecular level scheme of a CuPc/PTCDA heterojunction.

Fig. 8: Schematic view of a PTCDA/NTCDA multiple quantum well structure.

Fig. 9: Room temperature absorption and 20K luminescence spectra for a 5 period, 40 Å symmetric PTCDA/NTCDA MQW. The luminescence spectrum is obtained by pumping the MQW sample using 554 nm light from an Ar ion laser.

Fig. 10: Singlet exciton energy as a function of PTCDA well width for PTCDA/NTCDA MQWs. Fits to the data are obtained using parameters given in Table 2, and are described in the text. Also shown is the exciton radius, α, as a function of well width.

Fig. 11: Capacitance measured versus frequency for a horizontal, interdigitated capacitor with PTCDA serving as the dielectric.

Inset: Two views of a unit cell of PTCDA.

Fig. 12: Reflectance at λ = 1.064 μm versus incident beam angle for a 1.25 μm thick PTCDA film on a quartz substrate. Data is shown as closed circles, and theory is shown as a solid line.

Inset: Index of refraction ellipsoid for PTCDA showing the relationship between the indices along different thin film directions.

Fig. 13: Transmitted light intensity for TE and TM waves in a 10 mm long, 2 μm wide PTCDA rib waveguide as a function of incident angle of polarization. Measurements are made at λ = 1.064 μm.

Inset: Experimental set-up used to characterize the PTCDA waveguide-polarizer under study.

Fig. 14: Temperature dependent intensity measured in a PTCDA Fabry-Perot waveguide resonator at λ = 1.06 μm with a length of 1.62 mm and a width of 2 μm.

Inset: The experimental set-up, 1: Argon laser (λ = 0.514 μm), 2: AO modulator, 3: Ring YAG laser (λ = 1.06 μm), 4: Glan-Thompson Polarizer, 5: Thermoelectric cooler and thermocouple, 6: TV Camera, 7: Monitor, 8: Iris, 9: APD, 10: Oscilloscope.

Fig. 15: Intensity of guided light (λ = 1.06 μm) versus pump light intensity (λ = 0.514 μm) in a PTCDA waveguide with the same parameters in Fig. 1.

Fig. 16: Rise and fall times of the 1.06 μm wavelength beam due to modulation of the λ = 0.514 μm beam.

Fig. 17: Nonlinear absorption in a weak probe beam of several PTCDA/NTCDA MQW structures as a function of pump beam intensity (which is proportional to the square of the Rabi Frequency).

Fig. 18: Geometry used for calculating the polarization energy of a PTCDA exciton sandwiched between two NTCDA layers separated by distance t.

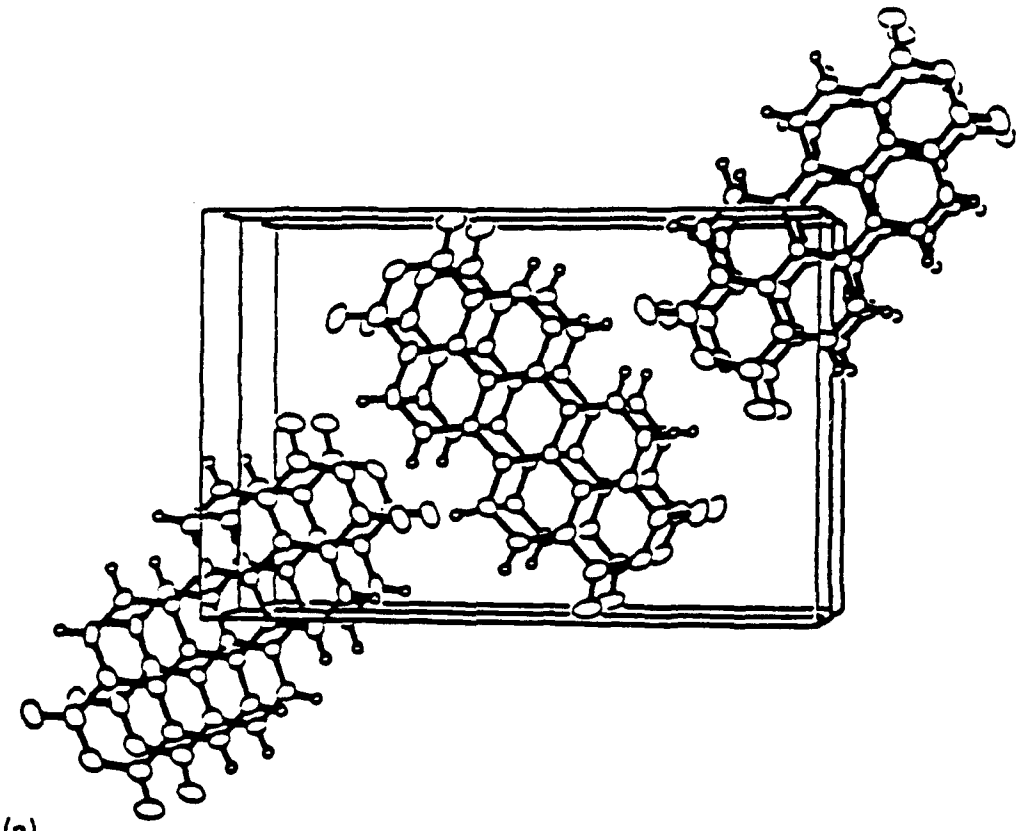

(a)

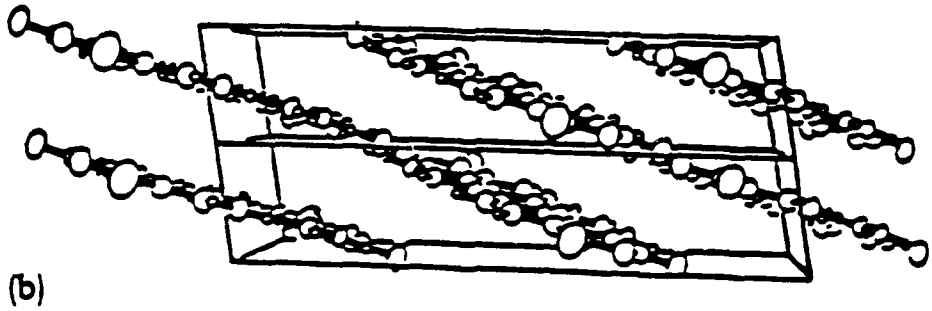

(b)

Fig. 1

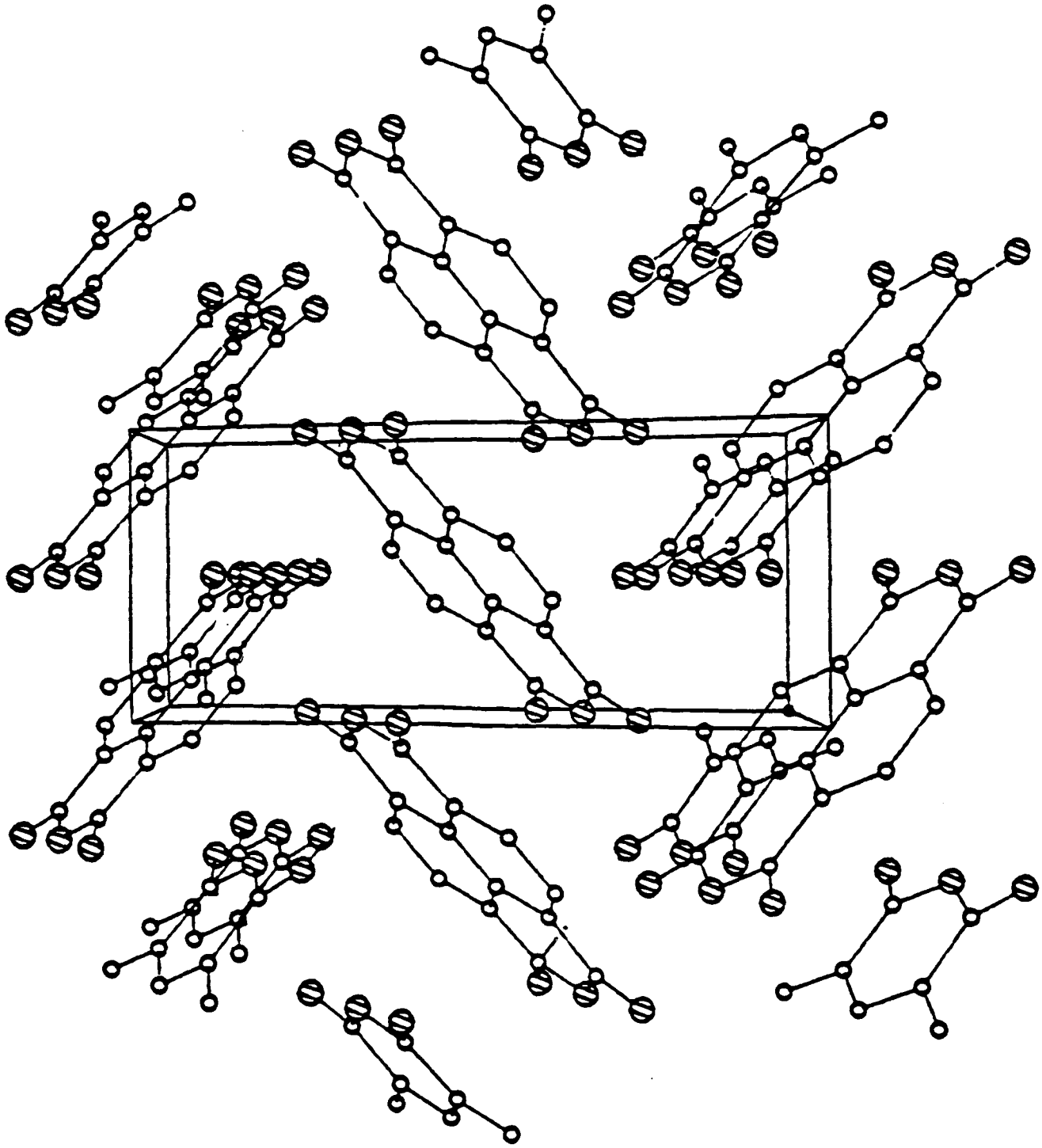

Fig. 2

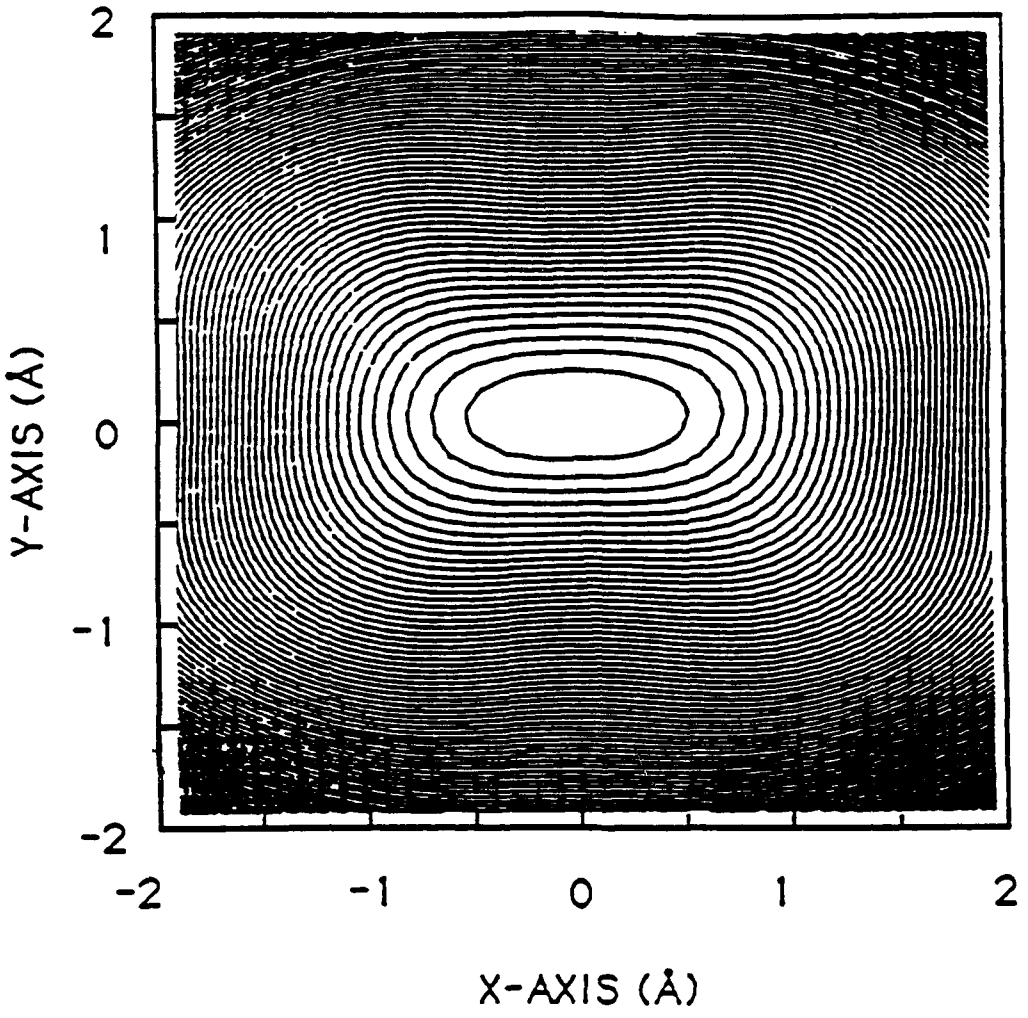

Fig. 3

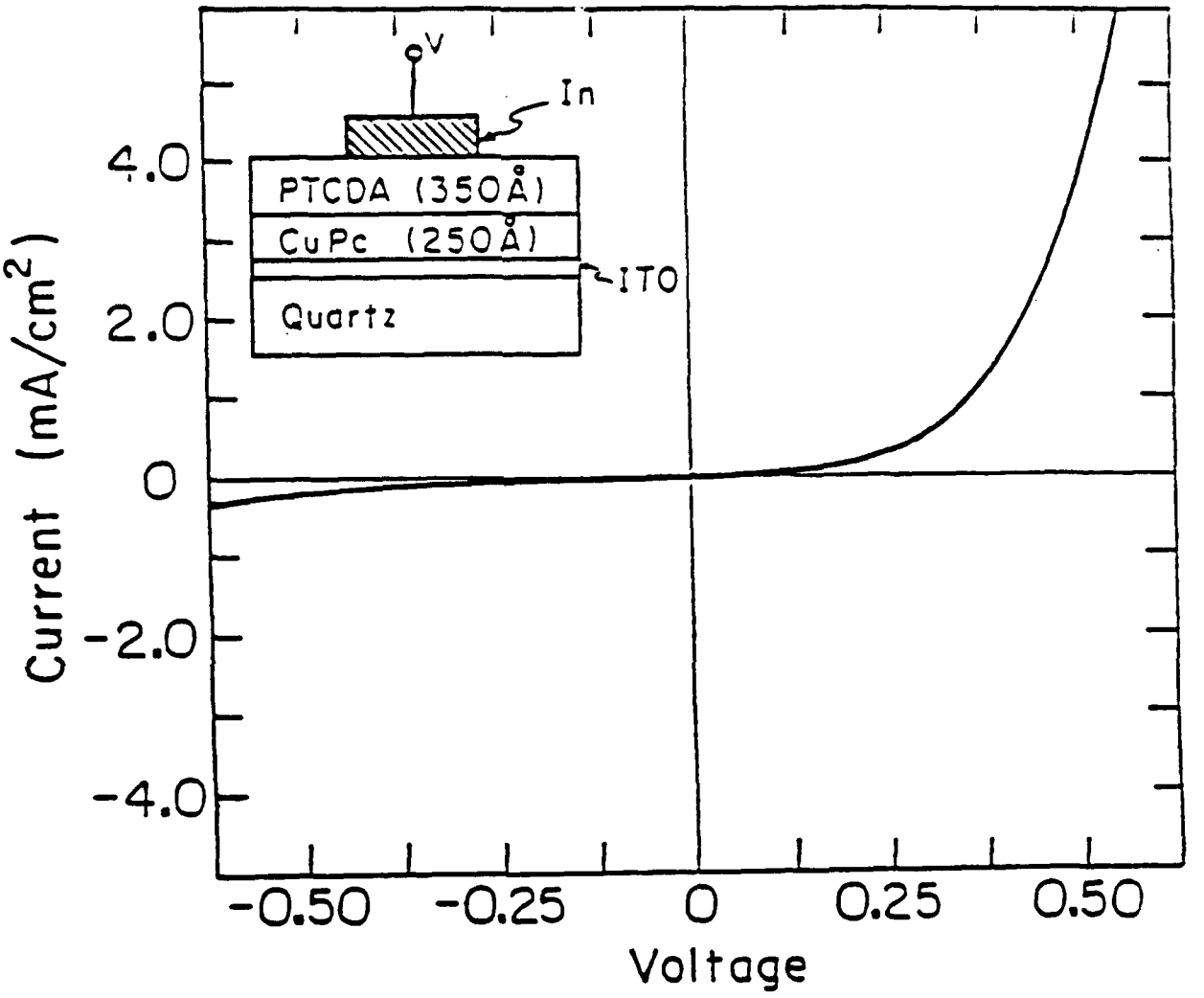
V
In
PTCDA (350Å)
CuPc (250Å)
ITO
Quartz
4.0
2.0
0
-2.0
-4.0
Current (mA/cm²)
-0.50
-0.25
0
0.25
0.50
Voltage

Fig. 4

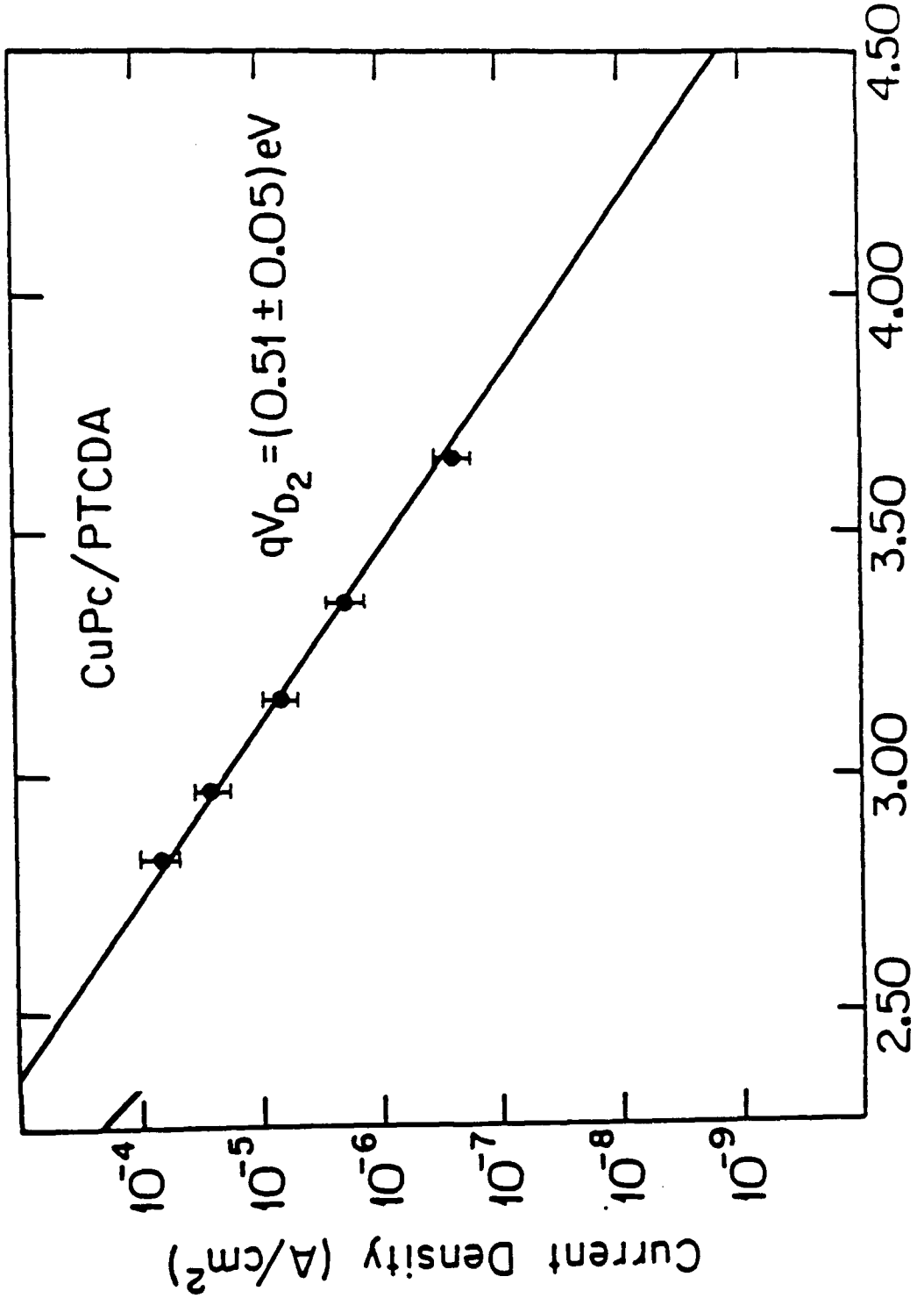
CuPc/PTCDA
qV_{D_2}=(0.51±0.05)eV
Current Density (A/cm²)
10^{-4}
10^{-5}
10^{-6}
10^{-7}
10^{-8}
10^{-9}
2.50
3.00
3.50
4.00
4.50
1000/T (1/K)

Fig. 5

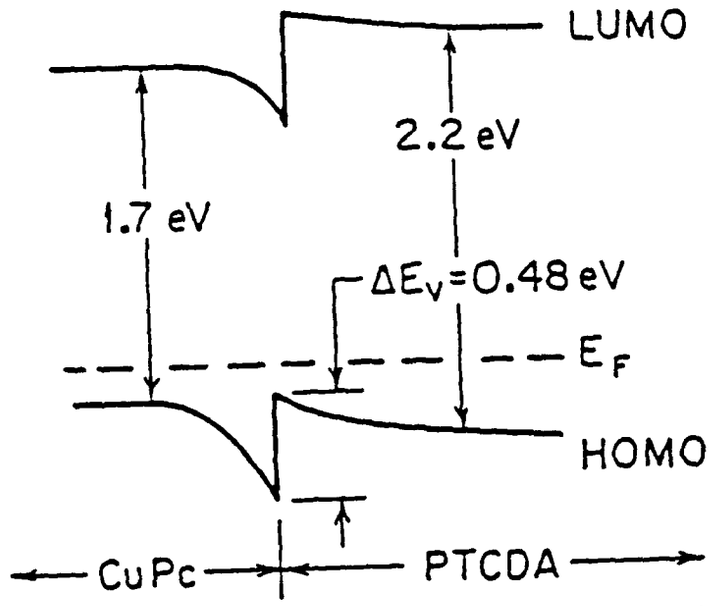

Fig. 6

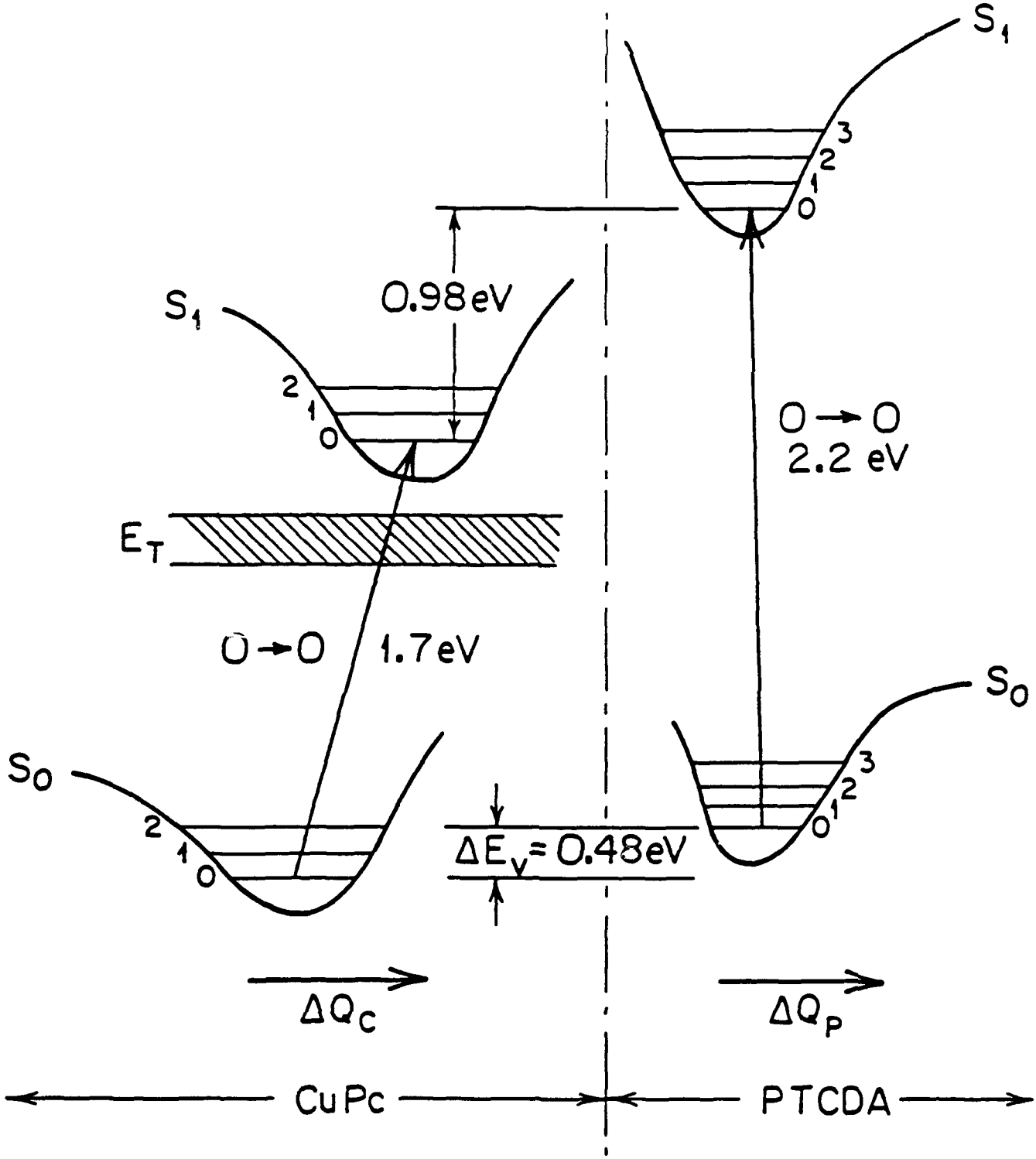
S1
3
2
1
0
0.98eV
S1
2
1
0
O → O
2.2 eV
ET
O → O 1.7eV
S0
S0
2
1
0
3
2
1
0
ΔEV = 0.48eV
ΔQC
ΔQP
CuPc
PTCDA

Fig. 7

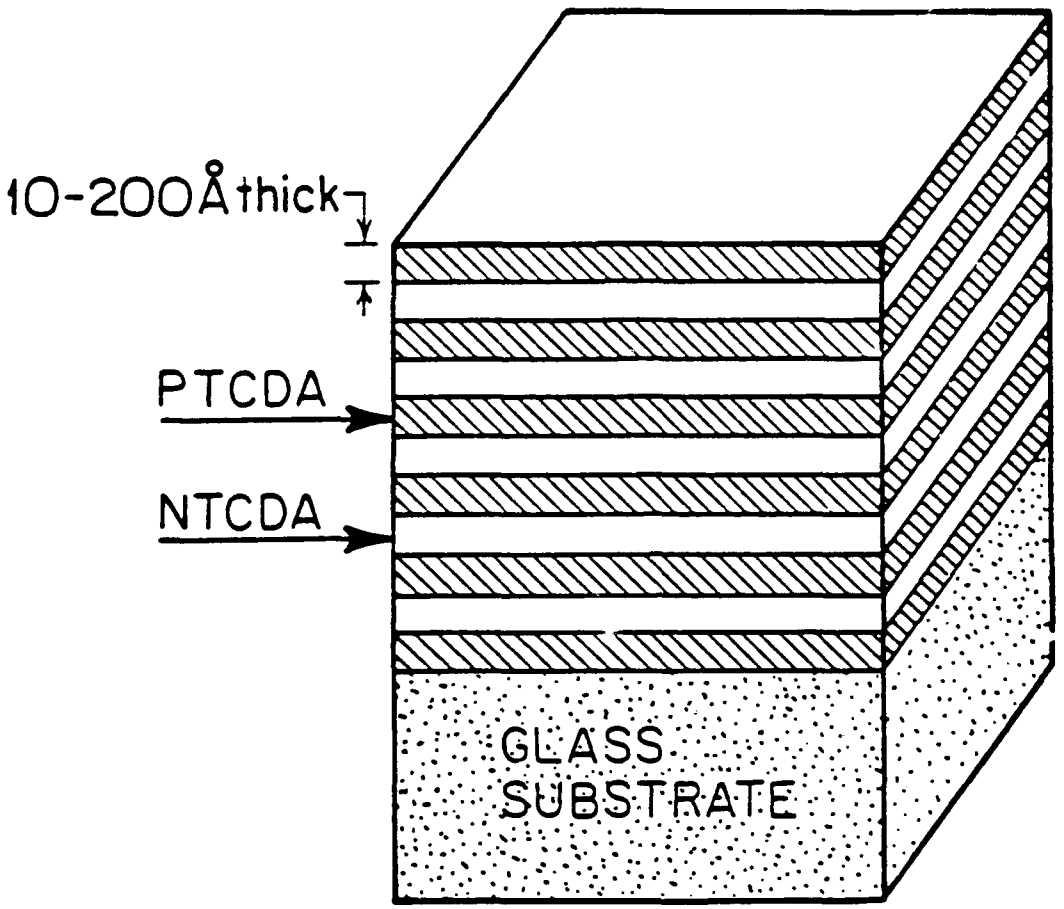

Fig. 8

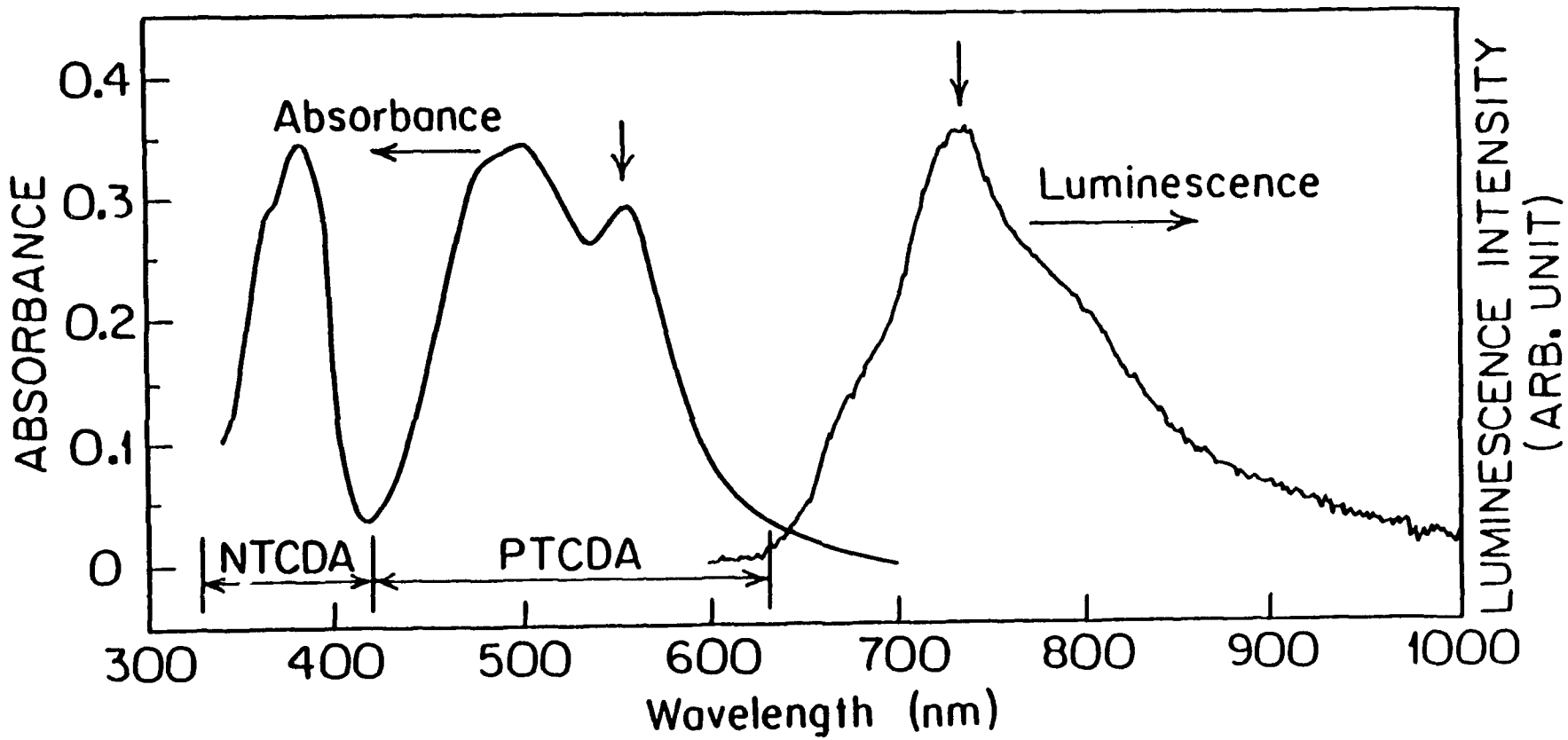
Absorbance
Luminescence
ABSORBANCE
LUMINESCENCE INTENSITY
(ARB. UNIT)
0.4
0.3
0.2
0.1
0
NTCDA
PTCDA
300
400
500
600
700
800
900
1000
Wavelength (nm)

Fig. 9

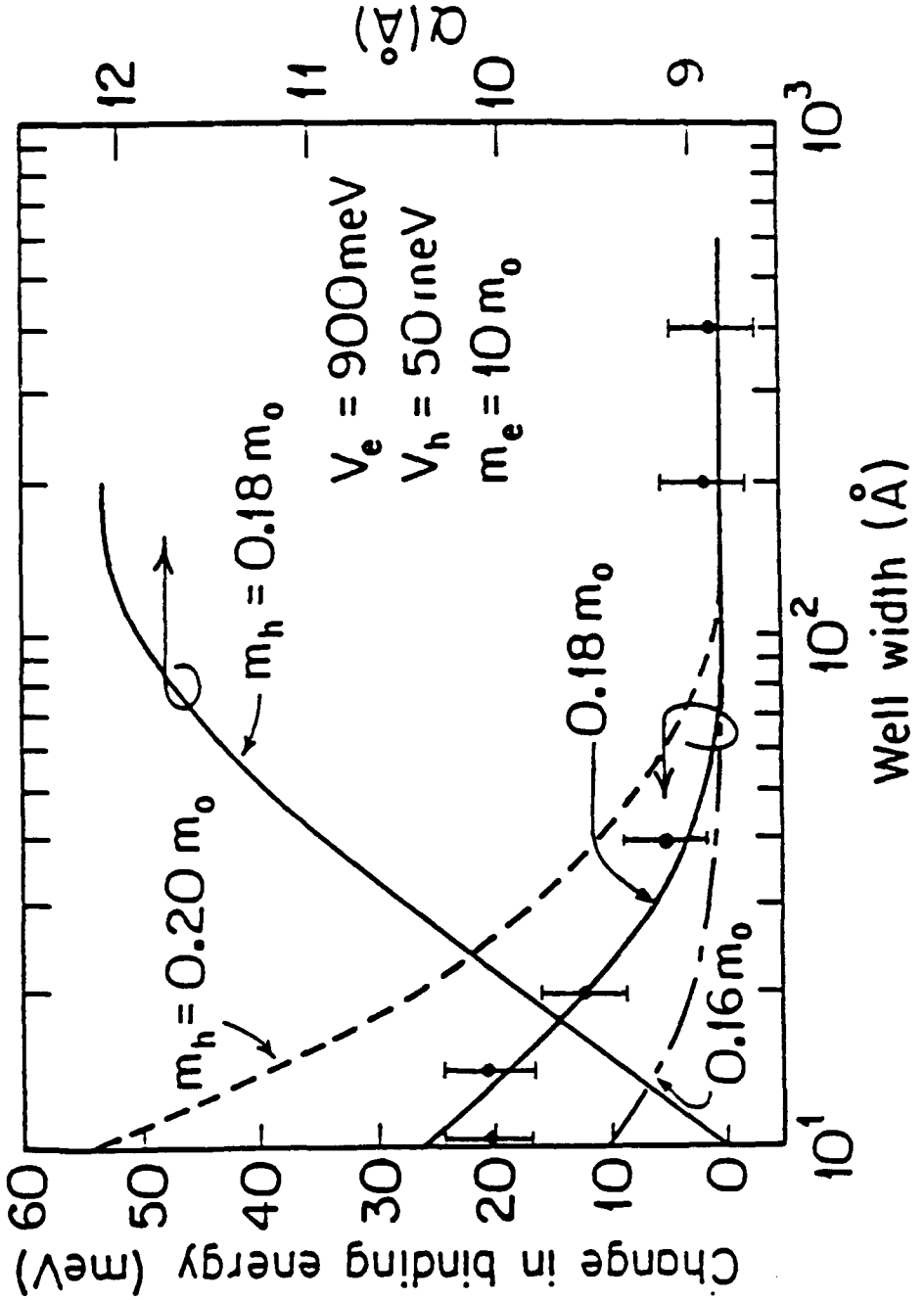
Change in binding energy (meV)
60
50
40
30
20
10
0
10^1
10^2
10^3
Well width (Å)
12
11
10
9
α(Å)
V_e = 900meV
V_h = 50meV
m_e = 10 m_o
m_h = 0.18 m_o
m_h = 0.20 m_o
0.18 m_o
0.16 m_o

Fig. 10

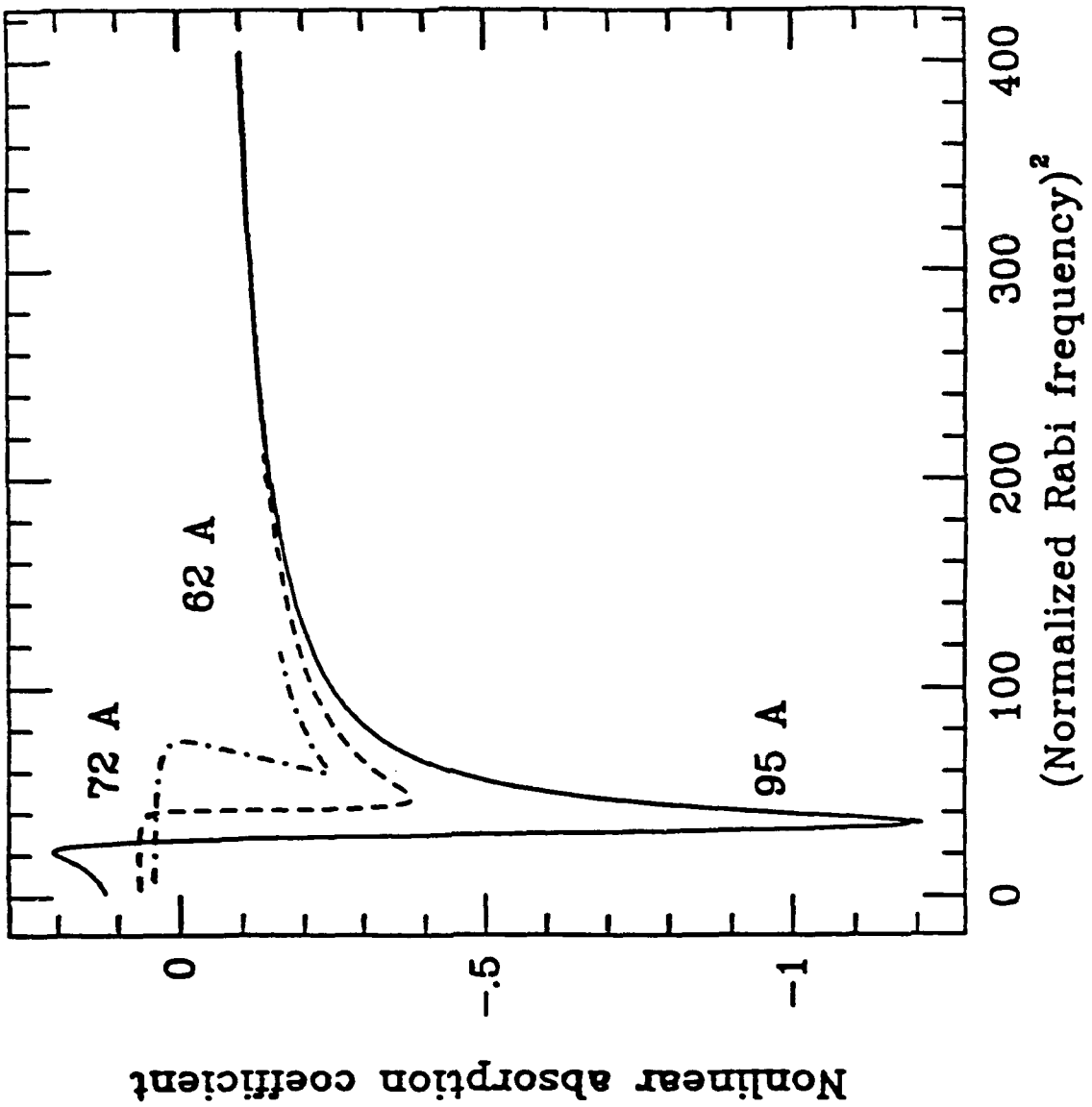
Nonlinear absorption coefficient
0
-.5
-1
0
100
200
300
400
(Normalized Rabi frequency)²
72 A
82 A
95 A

Fig. 11

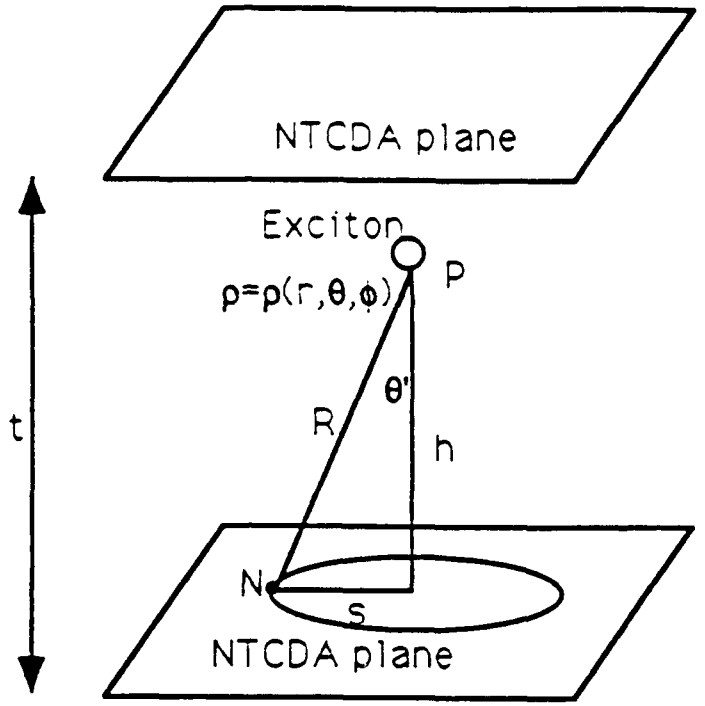

Fig. 12

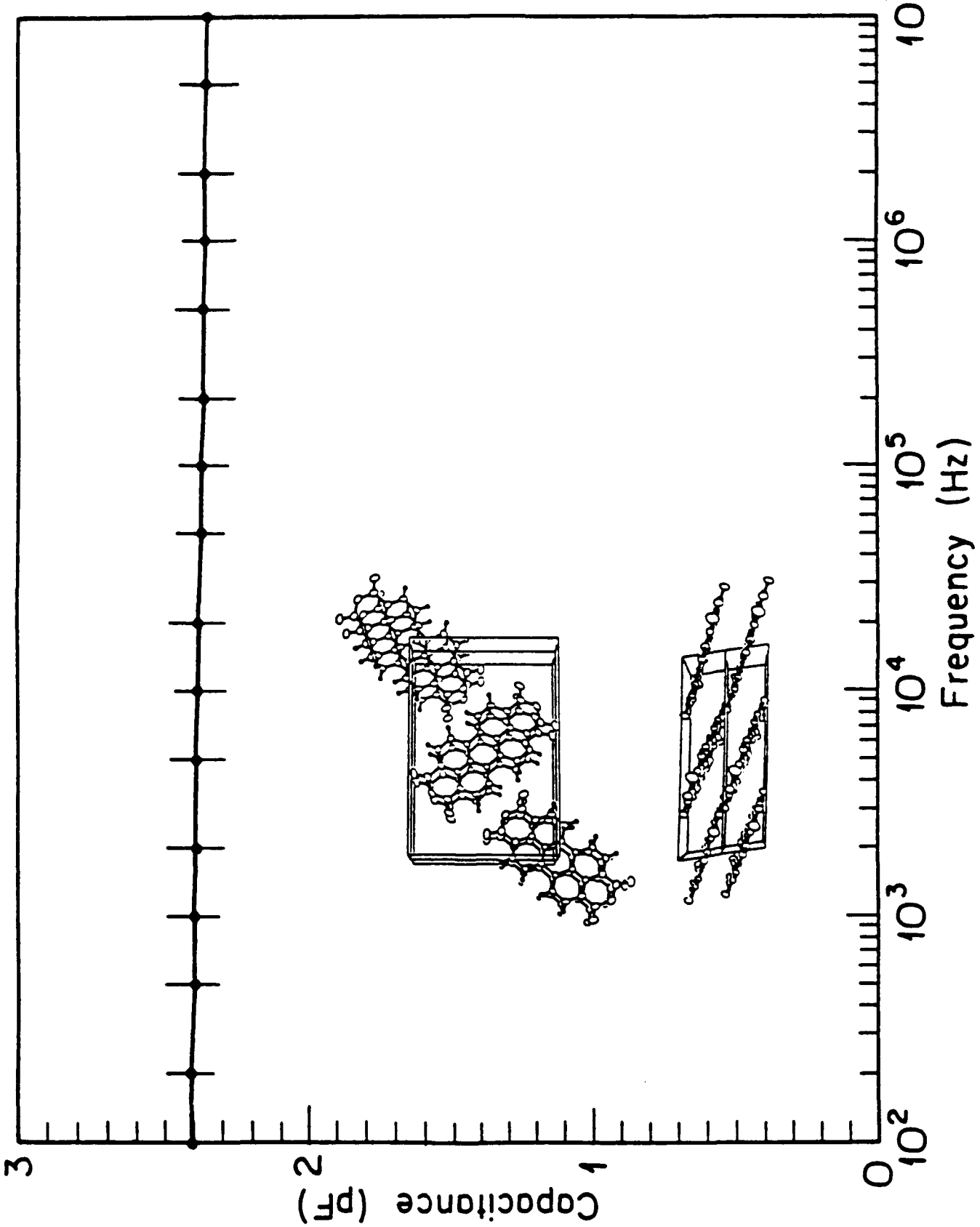

Fig. 13

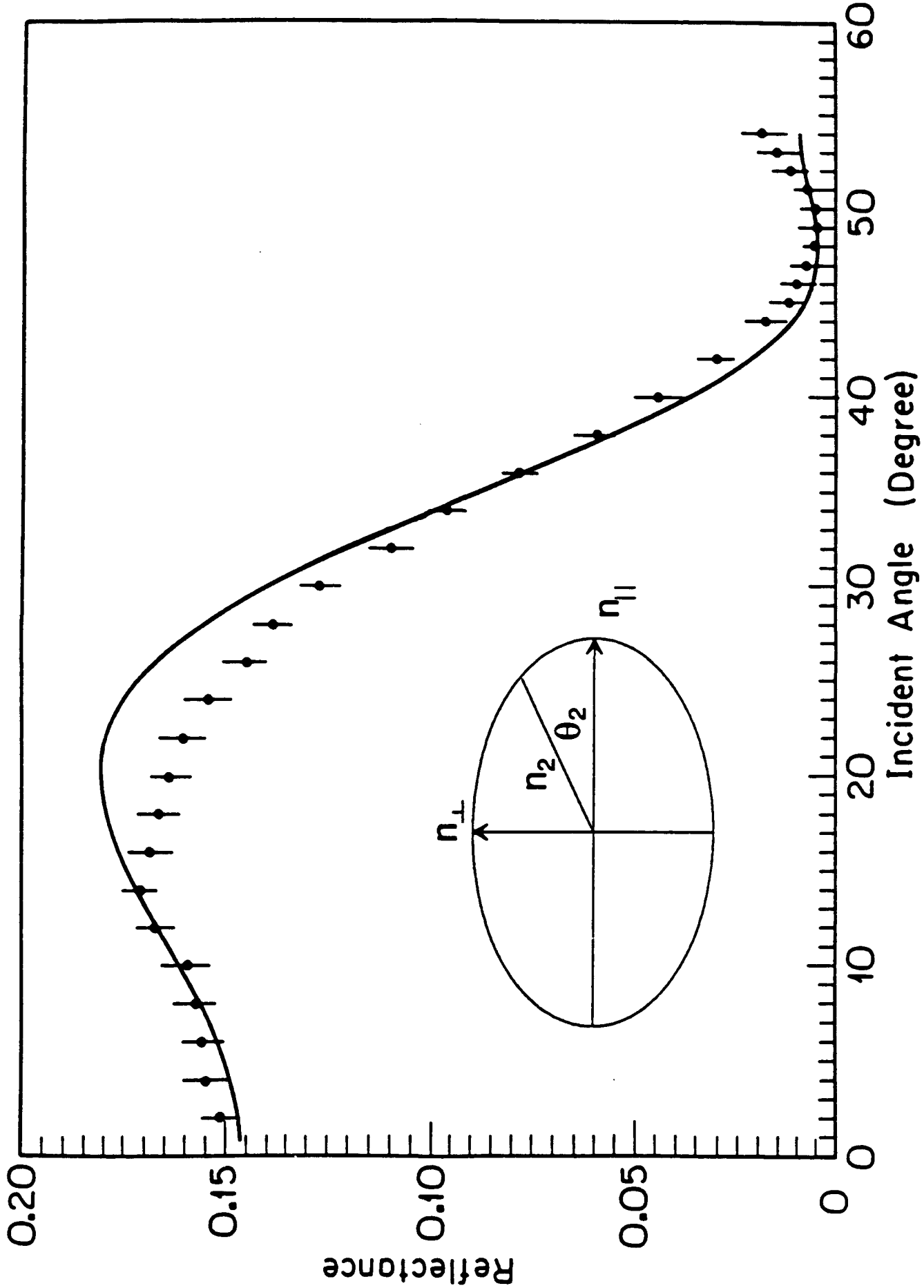
Reflectance
0.20
0.15
0.10
0.05
0
10
20
30
40
50
60
Incident Angle (Degree)
$n_{\perp}$
n_2
θ_2
$n_{\parallel}$

Fig. 14

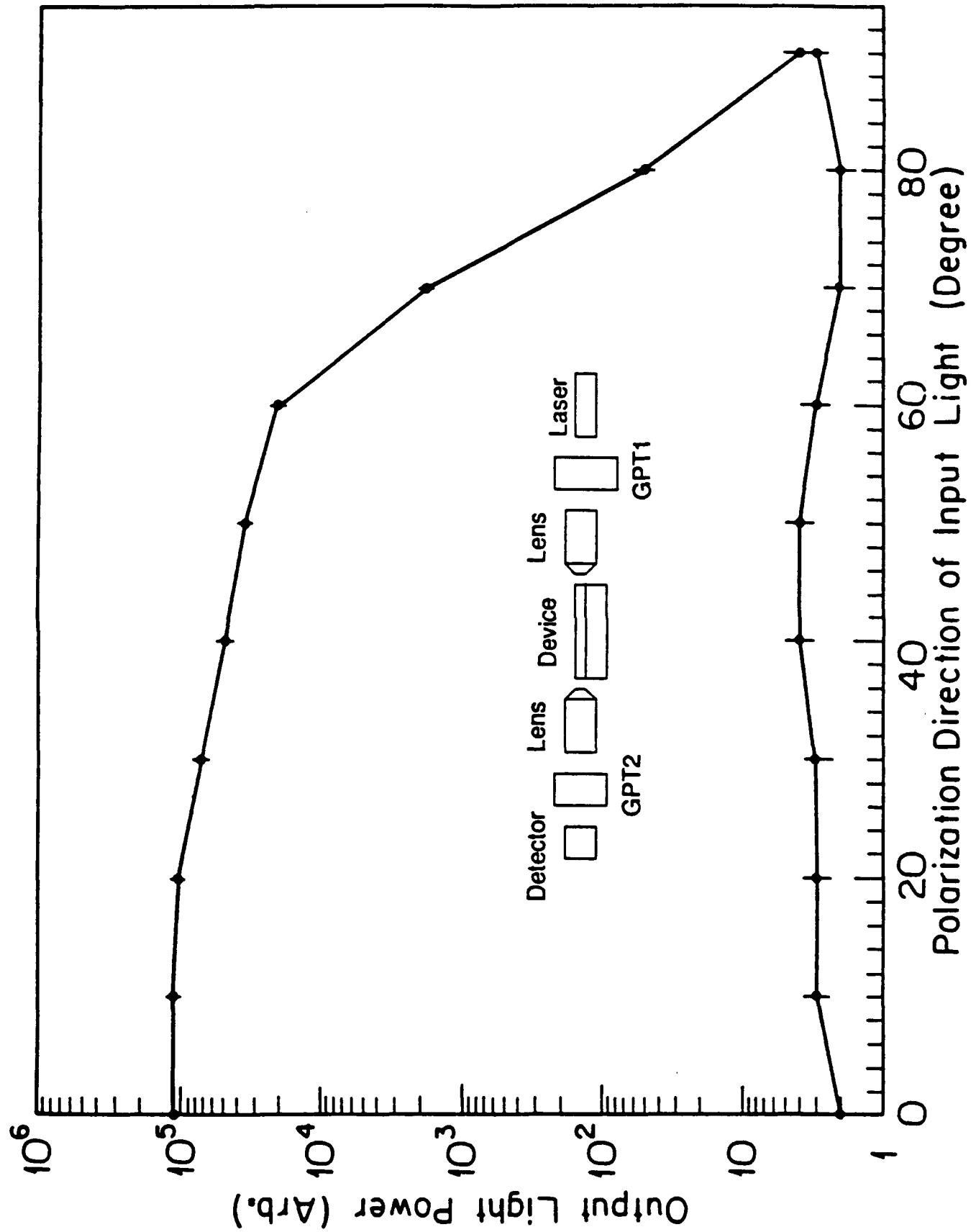
Output Light Power (Arb.)
10^6
10^5
10^4
10^3
10^2
10
1
0
20
40
60
80
Polarization Direction of Input Light (Degree)
Detector
Lens
GPT2
Device
Lens
GPT1
Laser

Fig. 15

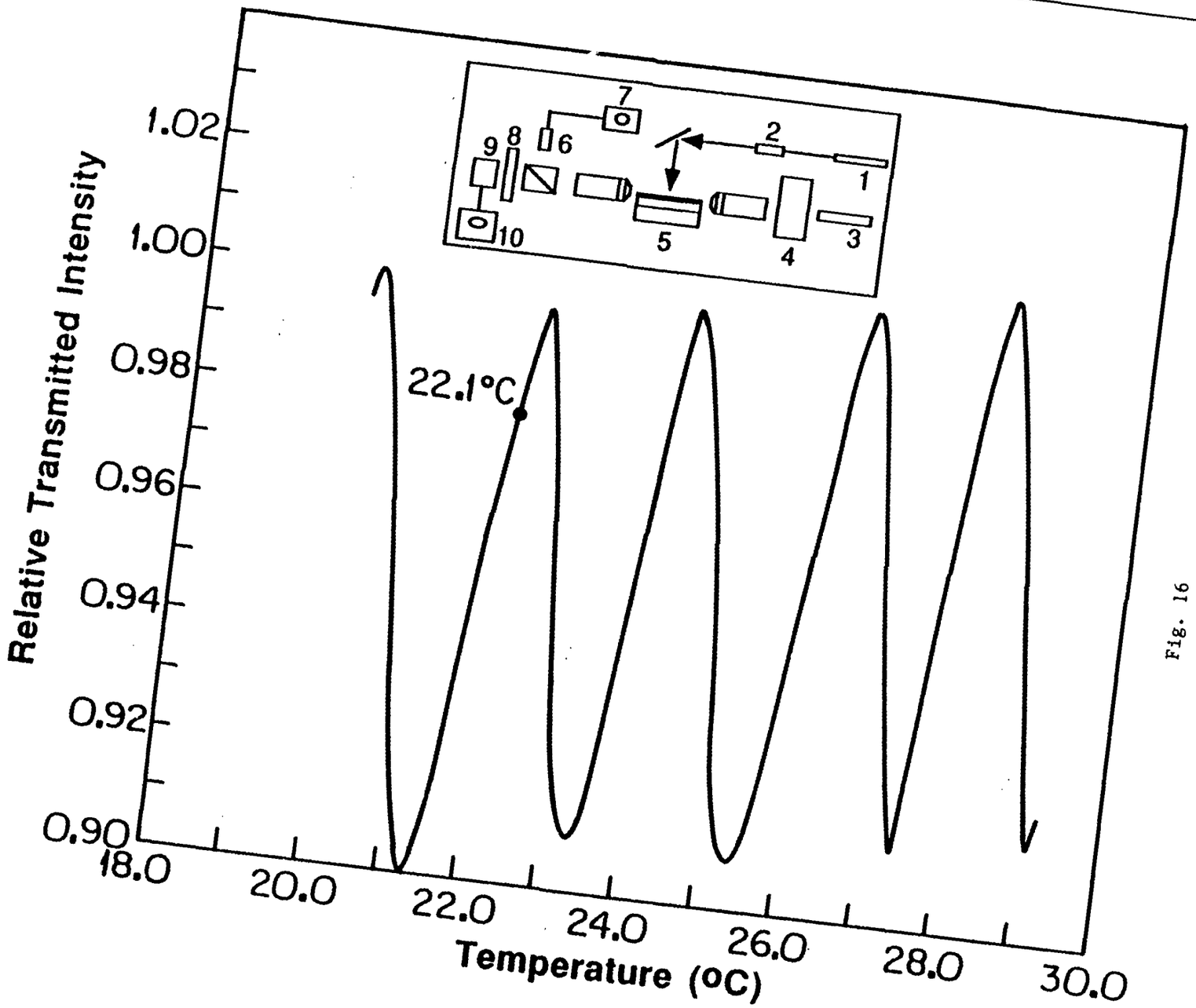
Relative Transmitted Intensity
1.02
1.00
0.98
0.96
0.94
0.92
0.90
22.1°C
18.0
20.0
22.0
24.0
26.0
28.0
30.0
Temperature (oC)
7
2
9
8
6
1
10
5
4
3

Fig. 16

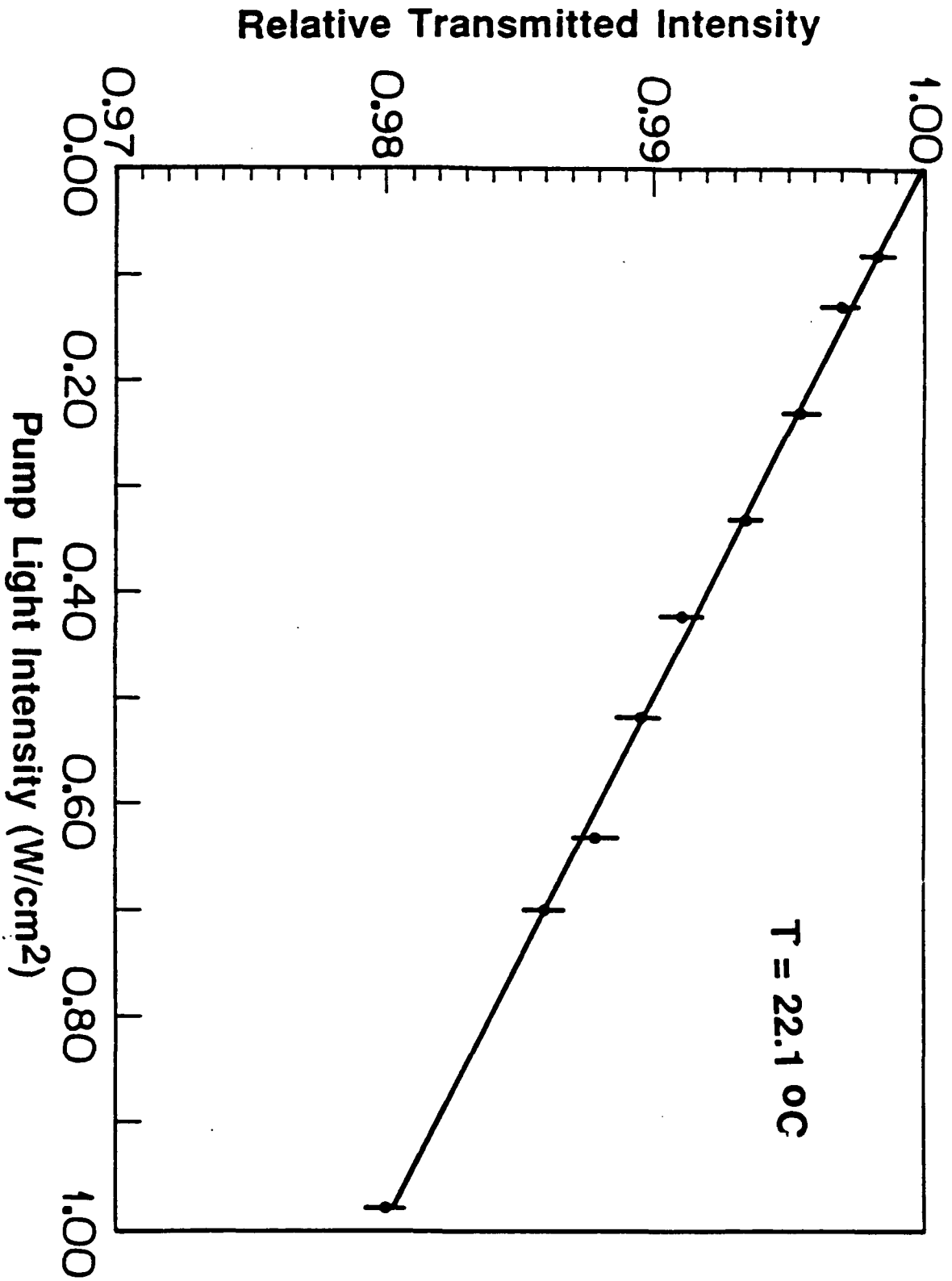
Relative Transmitted Intensity
0.97
0.98
0.99
1.00
0.00
0.20
0.40
0.60
0.80
1.00
Pump Light Intensity (W/cm2)
T = 22.1 oC

Fig. 17

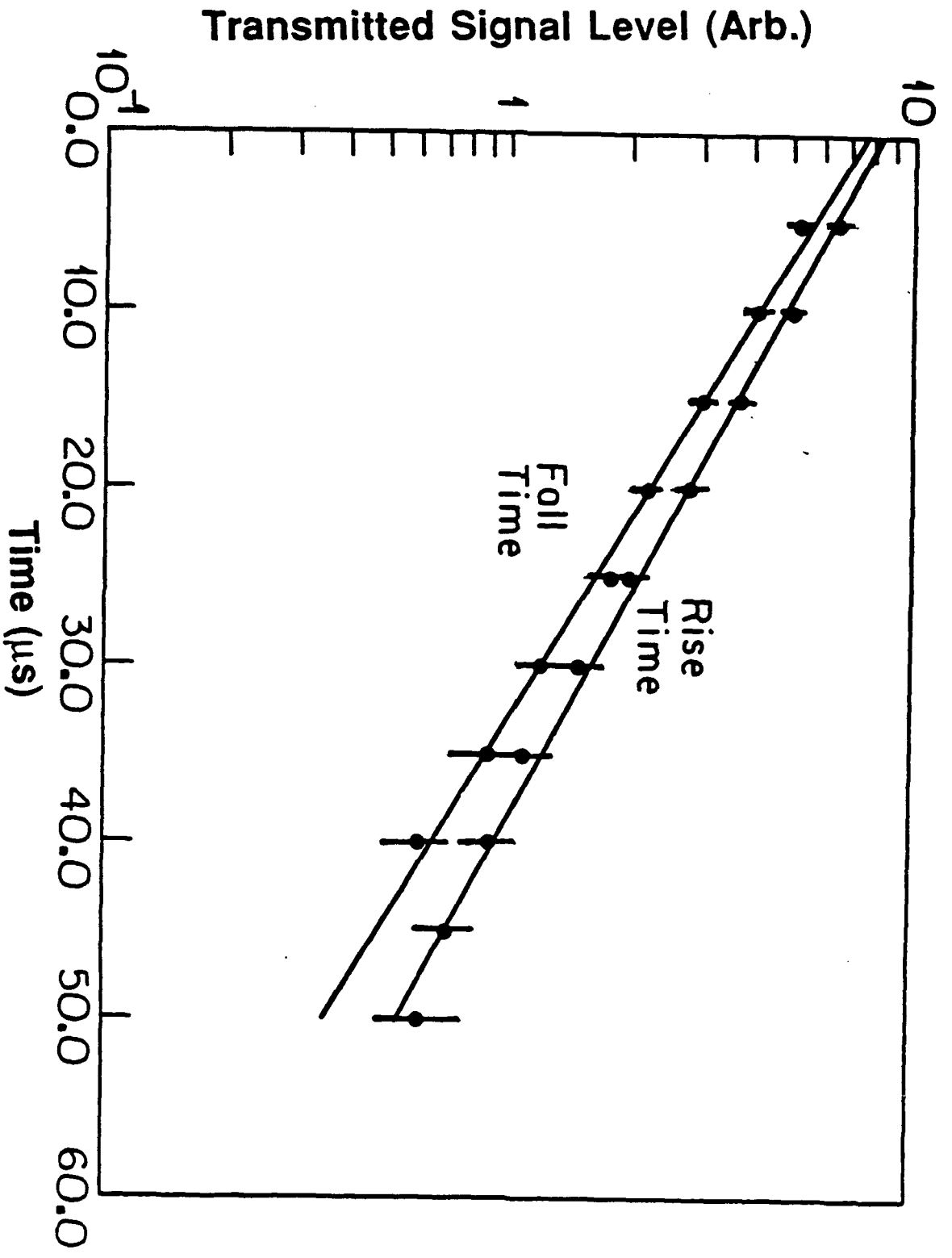
Transmitted Signal Level (Arb.)
10⁻¹
1
10
0.0
10.0
20.0
30.0
40.0
50.0
60.0
Time (μs)
Fall Time
Rise Time

Fig. 18

Evidence for Exciton Confinement in Crystalline Organic Multiple Quantum Wells

F. F. So and S. R. Forrest

Center for Photonic Technology, Departments of Electrical Engineering/Electrophysics and Materials Science, University of Southern California, Los Angeles, California 90089-0241

(Received 31 January 1991)

Multiple-quantum-well structures based on two crystalline organic semiconductors, namely, 3,4,9,10 perylenetetracarboxylic dianhydride and 3,4,7,8 naphthalenetetracarboxylic dianhydride, have been grown by organic molecular-beam deposition. Both optical-absorption and time-resolved photoluminescence measurements reveal a significant effect on the binding energy and the radiative recombination probability of excitons due to localization of carriers. Variational calculations of the ground-state exciton energy in quantum wells have been done, and the results agree with the experimental data. This provides evidence for exciton confinement in organic quantum-well structures.

PACS numbers: 72.80.Le

Inorganic semiconductor multiple-quantum-well (MQW) structures have been a subject of intense study in the past decade due to their interesting electronic and optical properties which have many promising applications in optoelectronic device technology.[1] However, epitaxial growth of semiconductor heterostructures is limited to materials with small lattice mismatch.[2] In contrast, organic crystals are bonded together by the relatively weak van der Waals force,[3] which allows for the layering of materials of widely differing crystal lattices whose strain energy is insufficient to create lattice defects. In principle, therefore, it is possible to grow defect-free heterostructures with a wide range of crystalline organic semiconductors. Recently, highly ordered organic MQW structures based on 3,4,9,10 perylenetetracarboxylic dianhydride (PTCDA) and 3,4,7,8 naphthalenetetracarboxylic dianhydride (NTCDA) have been grown by the ultrahigh-vacuum process of organic molecular-beam deposition (OMBD).[4,5] The so-called "quasiepitaxial" growth of organic thin films has also been demonstrated on a variety of substrate materials including inorganic semiconductors such as InP and Si. More surprisingly, highly ordered organic thin films can be grown on noncrystalline substrates such as fused quartz and glass. Thus, new opportunities for engineered heterostructures consisting of a wide range of organic material combinations layered without regard to lattice match provide exciting possibilities in the field of optoelectronics.

Both the optical and electronic properties of organic semiconductors are governed by the nature of excitons in the crystal. Excitons in most organic crystals are thought to be Frenkel-like,[3] although there are a few reports suggesting that excitons in anthracene crystals are Wannier[6,7] in nature. Therefore, it is important to determine the characteristics of excitons in the archetype compound PTCDA in order to understand its optical and electronic properties. Crystalline organic semiconductor heterojunctions (HJs) have been grown previous to this work, and their electrical and optical properties indicate that the HJ band offsets control the flow of charge between the contacting semiconductors in a manner similar to inorganic heterostructures.[8-10] Thus, MQW structures based on PTCDA and NTCDA provide the ideal tools for a study of the nature of excitons in crystalline organic semiconductors.

In this paper we report the measurement and analysis of optical-absorption spectra of organic multiple-quantum-well structures grown by OMBD. An increase of the singlet ground-state exciton energy in PTCDA with decreasing layer thickness has been observed, and the results can be understood in the context of a change in exciton binding energy due to quantum confinement in a potential well[11,12] formed by the energy-band offsets between the contacting materials. The results of our variational calculations on the well-width dependence of exciton binding energy are in good agreement with experimental data. Time-resolved photoluminescence measurements were also done for organic MQW structures, and the exciton lifetimes were found to decrease with decreasing PTCDA/NTCDA layer thickness. The decrease in exciton lifetime is explained in terms of a shrinkage in exciton volume in the MQW's,[13] and is also a result of quantum confinement of charge carriers.

The organic MQW structures investigated in this work consist of ultrathin, alternating layers of PTCDA and NTCDA of equal thickness, with layer thicknesses in the several samples ranging from 10 to 200 Å. Layer thicknesses are estimated to be uniform to within about two molecular layers (i.e., ≈ 6–7 Å). Organic MQW structures reported in this paper were grown on glass substrates by organic molecular-beam deposition[4]—a process analogous to conventional molecular-beam epitaxy used to grow inorganic semiconductor heterostructures. The key to achieving good surface morphology and sharp interfaces was to keep the substrates at about 90 K during growth. Low-temperature quasiepitaxial growth of crystalline organic thin films on inorganic substrates has been demonstrated for a number of crystalline organic materials.[4,14,15] Under such conditions, highly ordered molecular stacks are observed for our PTCDA/NTCDA MQWs using both birefringence and

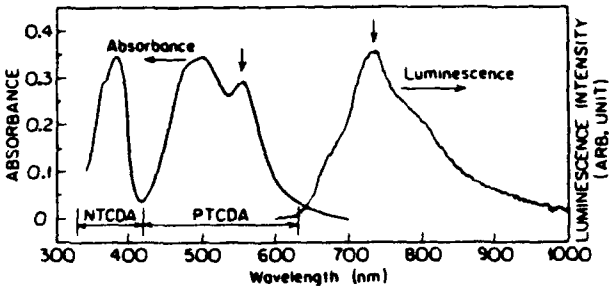

FIG. 1. Typical room-temperature optical-absorption and low-temperature (20 K) photoluminescence spectra of a PTCDA/NTCDA multiple-quantum-well sample.

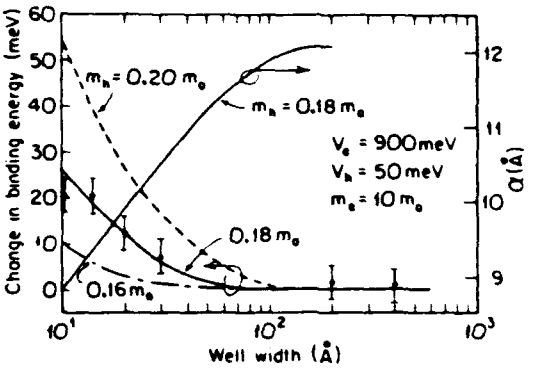

FIG. 2. Exciton line shift as a function of well width. The solid line is the result of variational calculations. The variational parameter α is also shown.

x-ray measurements in the multilayer structure consisting of PTCDA and NTCDA.[4,16]

Optical-absorption measurements were done at room temperature using a spectrophotometer. Time-resolved photoluminescence measurements of organic quantum-well samples were done at 20 K using a multiline cw Ar-ion laser with an output of 400 mW. At this energy, excitons were generated only in the PTCDA layers since the NTCDA layers are transparent to the incident light. Laser pulses were generated using an acousto-optic modulator with a rise and fall time of less than 4 ns. The laser-pulse width was 10 ns. The time decay of the monochromatic luminescence signal was measured using a double-pass 0.75-m Spex monochromator in conjunction with a multichannel photon counting averager. Deconvolution of the measured luminescence signal from the instrumental temporal response at the shortest times measured ($\sim$5 ns) has been carried out in all data analysis.

The room-temperature optical-absorption and low-temperature (20 K) photoluminescence spectra of a five-period symmetric PTCDA/NTCDA organic MQW sample with an individual layer thickness of 40 Å is shown in Fig. 1. The characteristic absorption spectra of both PTCDA and NTCDA are present, and the absorption bands are due to exciton generation in the corresponding crystalline layers. The absorption bands are relatively broad because of the strong exciton-phonon interaction characteristic of organic crystals.[7] From the lowest-energy cutoffs of the spectra, the "energy gaps" are determined to be 2.2 and 3.1 eV for PTCDA and NTCDA, respectively. We have found that the lowest-energy (0-0) singlet-exciton absorption peak in PTCDA (indicated by the arrow) shifts to higher energy as the layer thickness is decreased. No apparent shifts in the higher-energy exciton lines were observed, possibly as a result of the broad nature of these lines. The dependence of the ground-state-exciton energy shift with well width is shown by the data points in Fig. 2.

The blueshift in the exciton energy in PTCDA can be due to molecular polarization in the presence of an exciton which extends into the NTCDA in the multilayer structure.[4] It has been shown that the first-order exciton energy correction due to polarization arising from the multilayer structures decreases the total exciton energy by a quadratic function of increasing layer thickness. However, the observed dependence on layer thickness is much weaker than that predicted from the polarization model.

Alternatively, the exciton energy shift can be due to the change in exciton binding energy as a result of quantum confinement. As the layer thickness decreases, the exciton motion becomes two dimensional. The exciton is "squeezed" in the potential well formed in the PTCDA layer, resulting in an increase in exciton binding energy. In this model, the small-band-gap PTCDA layer is treated as a potential well bounded by the large-band-gap NTCDA layers in a type-I superlattice configuration. This picture is consistent with observations made for single PTCDA/NTCDA heterojunctions using current-voltage measurements similar to those used to determine the properties of other PTCDA-based heterojunctions.[8] Thus, electrons and holes are confined in PTCDA layers of width L_z. The total Hamiltonian[11] for an exciton in a quantum well is

$$H_{\rm tot} = H_e + H_h + H_{xy}, \qquad (1)$$

where H_e and H_h describe the motion of electrons and holes along the z axis in the quantum well, and H_{xy} describes the two-dimensional motion of excitons in the x-y plane (parallel to the heterointerfaces). The relative dielectric constant of PTCDA used in this calculation is 3.6,[16] assuming the crystal is an isotropic dielectric continuum. While it is known that dielectric anisotropies in such films are large, the isotropic continuum model nevertheless has been found to provide a very accurate description of charge-transfer exciton dynamics in similar organic crystals such as anthracene.[6]

The Schrödinger equation can then be solved by the variational principle using the following trial wave function:

$$\Psi_{\rm tot} = \Psi_e \Psi_h \exp[-(r^2/\alpha^2 + z^2/\beta^2)^{1/2}]. \qquad (2)$$

Here, $z = z_e - z_h$ and $r = r_e - r_h$, where z_e, r_e, z_h, r_h are the positions for electrons (e) and holes (h) in the z direction and the x-y plane. In Eq. (2), the total wave function Ψ_{tot} consists of the hydrogen 1s-like wave function (Ψ_{1s}), modulated by the harmonic part of the wave function, i.e., the electron (Ψ_e) and hole (Ψ_h) wave functions. Also, α is a variational parameter in the trial solution, and β is set equal to a_0, where a_0 is the exciton Bohr radius in the bulk crystal.

It should be noted that the trial wave function used is assumed to be ellipsoidal with $\beta = a_0$. Such an ellipsoidal trial wave function is consistent with the results of the theoretical calculations done by Shinozuka and Matsuura.[12] For very small well widths, the harmonic part of Eq. (2) dominates the exciton z dimension.

To solve the Schrödinger equation, the binding energy is minimized as a function of α. The results of the calculation are shown by the solid line in Fig. 2. The parameters used in this model are listed in Table I. Here, the sum of the electron potential (V_e) and the hole potential (V_h) is equal to the difference in energy gaps of PTCDA and NTCDA. Of all the parameters used in the calculation, the results are only sensitive to the choice of the effective hole mass m_h. Using these parameters, a good fit to the experimental data is obtained for $m_h = 0.18 m_0$, where m_0 is the electron rest mass. Note that a small value of m_h and a relatively large value of effective electron mass m_e were chosen in the calculation. A large difference in electron and hole effective masses is common in organic crystals such as naphthalene and anthracene.[17] Indeed, in previous work, it has been shown that PTCDA is a preferentially hole-transporting material, indicating that m_h is substantially less than m_e.[4] The effect of different values of m_h are shown for comparison in Fig. 2. Note that the fit to the data is good except for the 10-Å sample. This can have several causes, including nonuniform layer thickness and penetration of the exciton wave function into adjacent PTCDA layers.

The calculated values of α, as shown in Fig. 2, increase monotonically with increasing well width, and asymptotically approach the free-exciton Bohr radius of 12 Å, indicating that the exciton is confined in the quantum wells. The dependence of α on L_z for the ellipsoidal exciton can be understood as follows: As well width decreases, Ψ_{1s} becomes a 2D wave function resulting in a decrease in its extent in the z direction. At the same time, the effective Bohr radius (α) in the x-y direction also decreases with decreasing L_z in order for the wave function to retain spherical symmetry. In the case of an extremely narrow well, the exciton is squeezed to the extent that its wave function is forced to deviate from spherical symmetry.

TABLE I. Parameters used in the variational calculations.

Parameters	Symbol	Unit	Value
Hole mass	m_h	m_0	0.18
Electron mass	m_e	m_0	10.0
Electron potential	V_e	meV	900
Hole potential	V_h	meV	50
Relative dielectric constant of PTCDA	ε_p		3.6

To test this conclusion of quantum confinement, photoluminescence (PL) measurements were carried out by optically pumping the MQW's with an Ar-ion laser. From the absorption spectrum in Fig. 1, it is apparent that NTCDA is transparent to the excitation from the Ar-ion laser, and therefore the PL spectrum for a MQW sample shown in the figure is due to PTCDA alone. Also, no PL signal is obtained when NTCDA is optically pumped by the Ar-ion laser. From the PL spectrum, we can identify two major emission bands at 720 and 800 nm, and a shoulder at about 680 nm. From the energy difference between the absorption and luminescence spectra (indicated by arrows), we obtain a Franck-Condon shift of 4050 cm^{-1}. Indeed, such a large Franck-Condon shift in PTCDA is observed in MQW samples as well as in the bulk PTCDA crystal. To our knowledge, this is the largest value reported for a Franck-Condon shift in organic crystals, and is indicative of an extremely strong exciton-phonon coupling along the tightly packed PTCDA molecular stacks.

Time-resolved PL measurements were made by monitoring the time decay of the luminescence signal at 720 nm (the 1-0 singlet transition). The PL-signal decay transients for two MQW samples obtained at 20 K are shown in the inset of Fig. 3. The inset shows the response for the two samples under equal excitation intensity. Here, the exponential decay over several decades in intensity of the transient is apparent. In addition, the PL decay time is found to decrease as the layer thickness decreases. The dependence of the exciton lifetime on well width is shown in Fig. 3. The exciton lifetime τ_{ex} is found to be 10.8 ± 0.5 ns for $L_z = 20$ nm, decreasing to 5.7 ± 0.5 ns for $L_z = 1$ nm. The change in exciton lifetime in the MQW samples could be due to traps at the interface. The overall recombination rate can be written as $\tau^{-1} = \tau_r^{-1} + \tau_{nr}^{-1}$, where τ_r is the exciton radiative lifetime and τ_{nr} is the trapping time. If the nonradiative recombination rate is such that $\tau_{nr} \leq \tau_r$, the observed lifetime should decrease due to traps. The results of our PL measurements show that the time-integrated luminescence intensity was found to be constant with sample layer thickness, indicating that nonradiative recombination is not important. Further, if the exciton lifetime in molecular crystals is dominated by traps, it should decrease with increasing temperature.[18] However, our time-resolved measurements show that the radiative decay time is independent of temperature from 20 to 295 K, indicating again that the PL signal here is not due traps.

The decrease of τ_{ex} with decreasing L_z, therefore, can result from an increase in the spontaneous recombination

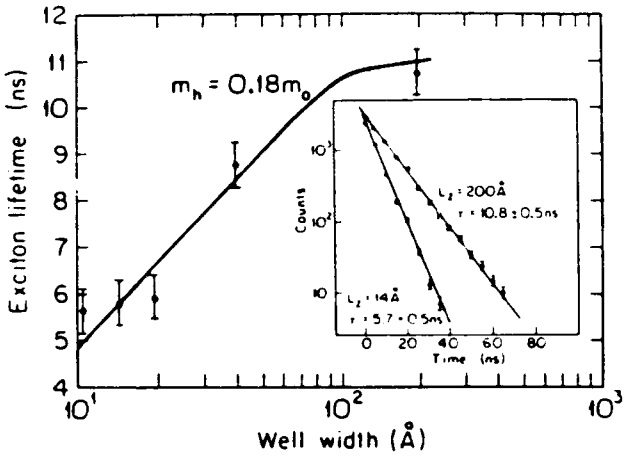

FIG. 3. Exciton lifetime τ_{ex} as a function of well width. The solid line is the fit to the data based on the theory described in the text. Inset: PL-signal time-decay transients for two MQW samples. Note that the transient for the $L_z = 200$ Å sample has been shifted upward by 10% of a decade in this plot.

rate due to an increase in the overlap of the electron and hole wave functions in the PTCDA potential wells. A similar explanation of the observed dependence of the exciton lifetime on well width has been observed in GaAs/GaAlAs quantum wells.[13] For the hydrogenic $1s$ state, R_{sp} can be shown to be proportional to the exciton volume[19] (given by $\int|\Psi_{tot}|^2 d^3r$, which differs significantly from $a_0^2 L_z$ used in previous work[13]). Using the results of the calculation of α discussed above (Fig. 2), the exciton volume in a MQW is observed to decrease with decreasing well width. The shrinkage of the exciton due to quantum confinement can thus account for the decrease in exciton lifetime. Based on the above analysis and using the parameters given in Table I, the dependence of exciton volume, and hence τ_{ex}, on well width is shown by the solid line in Fig. 3. The results of the calculation are in good agreement with the exciton lifetime data, indicating the exciton quantum-confinement model can quantitatively account for the change in both exciton binding energy and exciton lifetime using the model given above and the parameters in Table I.

In summary, we have characterized PTCDA/NTCDA organic quantum-well structures by both optical-absorption and time-resolved photoluminescence measurements. The exciton binding energy was found to increase with decreasing well width, whereas its lifetime decreased with decreasing well width. The dependence of exciton binding energy and lifetime on L_z can both be understood in terms of confinement of Wannier-like molecular excitons in quantum wells. To our knowledge, these results provide the first evidence for exciton quantum confinement in organic MQW structures. From the results of our calculation, the effective exciton Bohr radius is 12 Å, indicating that the exciton wave function extends to three or four molecular layers in PTCDA.

The authors would like to thank the Air Force Office of Scientific Research for the support of this work.

[1] *Semiconductors and Semimetals*, edited by R. Dingle (Academic, New York, 1987), Vol. 24.

[2] J. W. Matthews and A. E. Blakeslee, J. Cryst. Growth **27**, 118 (1974).

[3] M. Pope and C. E. Swenberg *Electronic Processes in Organic Crystals* (Oxford Univ. Press, New York, 1982).

[4] F. F. So, S. R. Forrest, Y. Q. Shi, and W. H. Steier, Appl. Phys. Lett. **56**, 674 (1990).

D.-Y. Zang, Y. Q. Shi, F. F. So, S. R. Forrest, and W. H. Steier, Appl. Phys. Lett. **58**, 562 (1991).

[6] P. J. Bounds and W. Siebrand, Chem. Phys. Lett. **75**, 414 (1980).

[7] E. A. Silinsh, *Organic Molecular Crystals* (Springer-Verlag, Heidelberg, 1980).

[8] S. R. Forrest, L. Y. Leu, F. F. So, and W. Y. Yoon, J Appl. Phys. **66**, 5908 (1989).

[9] C. W. Tang, Appl. Phys. Lett. **48**, 183 (1986).

[10] C. Adachi, S. Tokito, T. Tsutsui, and S. Saito, Jpn. J. Appl. Phys. **27**, L713 (1988).

[11] G. Bastard, E. E. Mendez, L. L. Chang, and L. Esaki, Phys. Rev. B **26**, 1974 (1982).

[12] Y. Shinozuka and M. Matsuura, Phys. Rev. B **28**, 4878 (1983).

[13] E. O. Gobel, H. Jung, J. Kuhl, and K. Ploog, Phys. Rev. Lett. **51**, 1588 (1983).

[14] A. J. Dann, H. Hoshi, and Y. Maruyama, J. Appl. Phys. **67**, 1371 (1990).

[15] M. K. Debe, K. K. Kam, J. C. Liu, and R. J. Poirier, J. Vac. Sci. Technol. A **5**, 1914 (1987).

[16] S. R. Forrest, M. L. Kaplan, and P. H. Schmidt, J. Appl. Phys. **55**, 1492 (1984).

[17] W. Warta and N. Karl, Phys. Rev. B **32**, 1172 (1985).

[18] A. Matsui and K. Mizuno, Chem. Phys. **113**, 111 (1987).

[19] H. Barry Bebb and E. W. Williams, in *Semiconductors and Semimetals*, edited by R. K. Willardson and A. C. Beer (Academic, New York, 1972), Vol. 8.

All-optical modulation in crystalline organic semiconductor waveguides

D. Y. Zang and S. R. Forrest
National Center for Integrated Photonic Technology, Departments of Electrical Engineering and Materials Science, University of Southern California, Los Angeles, California 90089-0241

(Received 29 July 1991; accepted for publication 4 November 1991)

We demonstrate all-optical modulation in crystalline organic semiconductor waveguides grown by the ultrahigh vacuum process of organic molecular-beam deposition. Two light beams with wavelengths of 1.06 and 0.514 μm were used as the guided and the pump light sources, respectively. A refractive index change of 5.4×10^{-5} at 1.06 μm was observed at a pump intensity of 1.0 W/cm^2. This large nonlinear effect is attributed to free electron-hole pairs produced by the dissociation of excitons generated by the short wavelength beam. A carrier lifetime of (17 ± 1) μs which determines the modulator switching time is in good agreement with theoretical predictions. To our knowledge, this is the first observation of free-carrier-induced index modulation in crystalline organic waveguides.

For more than two decades, organic materials have been investigated for their potential usefulness to nonlinear optics (NLO).[1] Most research has been focused on nonresonant nonlinear effects since the losses are smaller and the response times are shorter than at resonance. Resonant NLO effects, however, are interesting because they can be induced at very small optical powers.[2] Resonant NLO effects also clarify the nature of optical transitions and dynamic processes which are not yet completely understood for organic materials. In previous work,[3] the linear dielectric properties of the crystalline organic compound, 3, 4, 9, 10 perylenetetracarboxylic dianhydride (PTCDA) were reported. In this letter, we report on the demonstration of resonant NLO effects associated with free carriers (plasma) generated by dissociated excitons in PTCDA rib waveguides. To our knowledge, this is the first observation of light-generated plasma effects in organic crystals.

Charge transport in molecular semiconductors is thought to be initiated via excitonic transitions.[4] Here, free electron-hole pairs are generated in a second-order process via dissociation of photogenerated excitons at surfaces or bulk material impurities. That is, given a molecule in ground state S_0, a dominant channel for free-carrier production due to absorption of light of energy $\hbar\omega$, is $S_0+\hbar\omega\rightarrow S^*$, followed by $S^*+M\rightarrow e^-+h^+$. Here S^* is the excited singlet exciton state of the molecule, M represents an impurity or interface, and e^- and h^+ are the free electron and hole, respectively. The absorbed light must have a photon energy greater than the exciton transition energy (typically 1.5–3 eV). Since the process is second order, the quantum efficiency (η) for electron-hole generation is usually $<1\%$. Assuming that there is a refractive index change (Δn) associated with the optical generation of free carriers (via excitons), the Drude model gives

$$\Delta n=\frac{-e^2N}{2nm^*\epsilon_0\omega^2}, \tag{1}$$

where e is the electronic charge, N is the free-carrier density induced by the optical beam, n is the refractive index in the dark, m^* is the carrier effective mass, ϵ_0 is the permittivity in vacuum, and ω is the light frequency. A steady-state solution of the continuity equation for N gives

$$\Delta n=n_2I=\frac{-e^2\alpha\tau\eta I}{2nm^*\epsilon_0\hbar\omega^3}. \tag{2}$$

Here, α is the absorption coefficient, I is the optical intensity, τ is the free-carrier lifetime, and $\hbar$ is Planck's constant divided by 2π. Note that the NLO coefficient, n_2, given by Eq. (2), is only due to the free-carrier concentration (not the exciton population), and is intensity dependent.

To fabricate the waveguide devices in which n_2 was measured, a 1-μm-thick, AZ 1400 photoresist layer (with $n_p=1.61$) was first spun onto the surface of a cleaned and polished (100) InP substrate. Next, a series of 2-μm-wide strips were patterned onto the photoresist along the (110) direction by standard photolithographic techniques. A 1-μm-thick crystalline PTCDA layer was then deposited onto both the InP substrate and the photoresist ridges using the ultrahigh vacuum ($\sim10^{-9}$ Torr) process of organic molecular-beam deposition.[5] Deposition proceeds by heating a prepurified source of PTCDA to 450 °C to achieve a deposition rate of approximately 3 Å/s, while the substrate temperature is maintained at 90 K. It has previously been found that thin-film deposition under these conditions results in single-crystalline growth of PTCDA on the photoresist strips into low-loss (<2.5 dB), TE-mode waveguides.[3] To form waveguide facets, the InP substrate was cleaved along the $(\bar{1}10)$ direction. The facet surfaces are sufficiently smooth to allow for observation of Fabry–Perot resonances as the index of the guide is thermally or optically varied.

In the experiments, 1.06-μm wavelength light from a YAG laser was coupled into and out of the waveguide using two microscope objective lenses (see inset, Fig. 1). A high-speed $In_{0.53}Ga_{0.47}As$ avalanche photodetector (APD) was used to detect the light signal. To ensure a constant coupling efficiency, a TV camera monitored the beam spot position using a beam splitter placed in front of the APD. The waveguide was placed on a copper block mounted on a thermoelectric cooler. Using a thermocouple and a temperature controller, the temperature of the waveguide device was controlled to within ±0.05 °C.

The 2-μm-wide PTCDA rib waveguide allowed for propagation of a single TE_{00} mode. The waveguide, with its

 0003-6951/92/020189-03$03.00

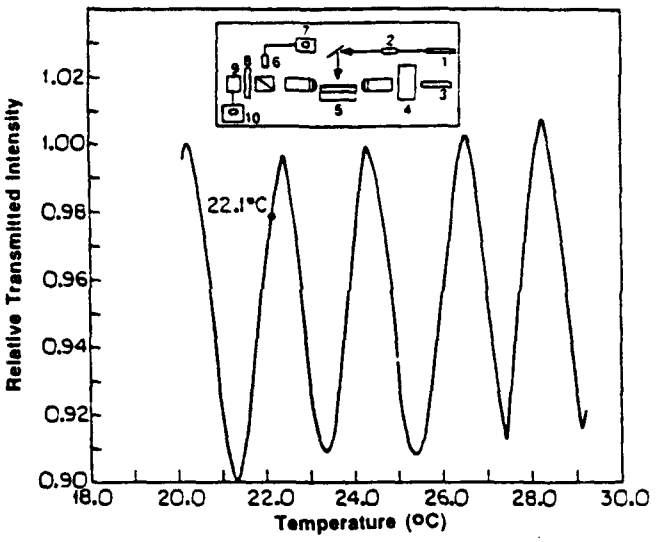

FIG. 1. Temperature-dependent intensity measured in a PTCDA Fabry–Perot waveguide resonator at $\lambda = 1.06\ \mu m$ with a length of 1.62 mm and a width of 2 μm. Inset: The experimental setup. 1: argon laser ($\lambda = 0.514\ \mu m$); 2: AO modulator; 3: ring YAG laser ($\lambda = 1.06\ \mu m$); 4: Glan–Thompson polarizer; 5: thermoelectric cooler and thermocouple; 6: TV camera; 7: monitor; 8: iris; 9: APD; 10: oscilloscope.

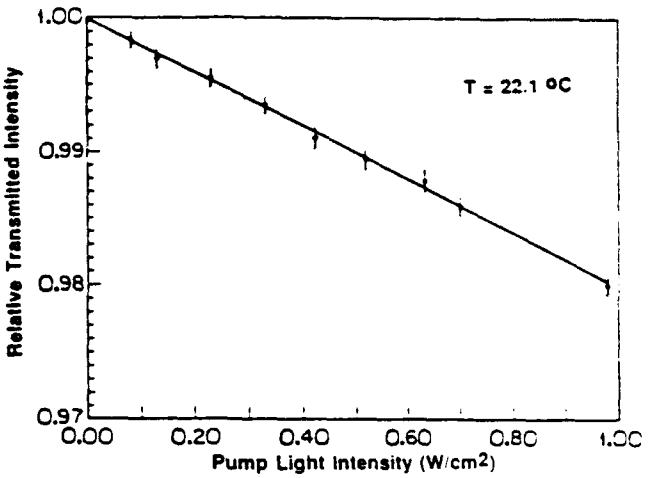

FIG. 2. Intensity of guided light ($\lambda = 1.06\ \mu m$) vs pump light intensity ($\lambda = 0.514\ \mu m$) in a PTCDA waveguide with the same parameters in Fig. 1.

cleaved facets, acts as a lossy Fabry–Perot resonator with a transmission function of

$$P(\delta) = \frac{(1-R)^2 e^{-\alpha L}}{(1-Re^{-\alpha L})^2 + 4Re^{-\alpha L}\sin^2(\delta/2)}, \qquad (3)$$

where α is the absorption coefficient, L is the device length (1.62 mm), R is the reflection coefficient at the waveguide facets which is calculated to equal 0.11 considering only Fresnel reflections, and δ is the phase shift defined as $\delta = \delta_0 + \Delta\delta = (4\pi L/\lambda)(n + \Delta n)$. When the temperature T is varied, the transmitted intensity varied periodically (see Fig. 1) as is characteristic of a Fabry–Perot resonator. A complete fringe (two adjacent maxima) corresponding to a phase difference of $\Delta\delta = 2\pi$ was observed for a temperature change of 2 °C, from which we obtain $(1/n)\Delta n/\Delta T = (8.1 \pm 0.5) \times 10^{-5}\ K^{-1}$. Using Eq. (3), however, a maximum transmission modulation of ~50% was expected, compared to an observed modulation of only 10%. This smaller-than-expected modulation is possibly due to imperfect waveguide facets which lower the finesse of the resonator.

To measure the all-optical modulation characteristics of the guide, a pump light beam of 0.514-μm wavelength with a diameter $L' = 1$ mm directly illuminated the surface of the PTCDA waveguide, while the 1.06-μm beam was end-fire coupled into the waveguide, as in the case of the $\Delta n/\Delta T$ measurements. In order to avoid thermally induced intensity changes from the pump, the device temperature was precisely maintained at 22.1 °C using the thermoelectric cooler. The pump-induced intensity changes are shown in Fig. 2. Here, the transmitted intensity is *decreased* nearly linearly proportional to the pump intensity at a temperature of 22.1 °C. In contrast, the transmitted intensity due to a temperature rise at 22.1 °C is *increased* (Fig. 1).

While we suggest that the pump power dependence of $P(\delta)$ is due to an optically induced index change, it is nevertheless important to consider other competing processes. The most significant contributions to Δn are thermally induced index changes and optically induced absorption effects. To differentiate between these various mechanisms, we have investigated the modulation behavior at very low pump light intensities ($< 1\ W/cm^2$) over a wide temperature range (16–37 °C). Three observations exclude the possibility of thermal effects: First, the changes in transmitted intensity under a constant pump power could either be increased or decreased, depending on temperature. However, the sign of the optically induced change of transmitted intensity was always *opposite* to the thermally induced changes over the entire temperature range explored. For instance, at a certain temperature, if the transmitted intensity was *decreased* due to pump light illumination, it was *increased* due to a temperature rise. This is similar to observations for inorganic semiconductors[6] in which nonlinear effects were attributed to index changes due to excitons.

A further observation ruling out thermal effects is that the temperature increase is calculated to be ~0.03 °C under a maximum pump light intensity of 1 W/cm^2. This calculation assumes a steady-state thermal conductivity of 0.1, 0.007, and 0.8 W/cm K for PTCDA, AZ1400, and InP, respectively. Such a small temperature rise does not significantly contribute to the intensity modulation, as inferred from Fig. 1. Finally, the transient thermal relaxation time was calculated to be > 13 ms, which is three orders of magnitude larger than the measured modulation time of 17 μs, as shown below. A very low amplitude "tail" in the modulation response with a time constant of ~6 ms was observed at the highest pump intensities. We attribute this latter time constant to be characteristic of very small thermal effects, whereas the shorter time constant results from significantly larger carrier lifetime effects.

The second "parasitic" effect to be considered is pump induced absorption changes, $\Delta\alpha$. Using Eq. (3), it can be

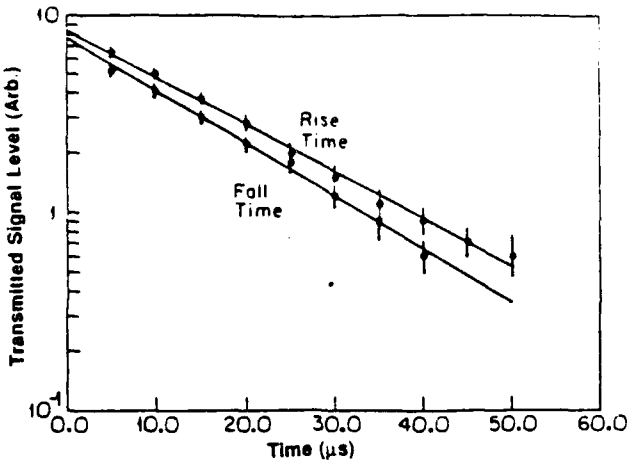

FIG. 3. Rise and fall times of the 1.06-μm wavelength beam due to modulation of the $\lambda = 0.514$-μm beam.

show. that the change of transmitted light intensity, ΔP, in the limit of $\alpha L \ll 1$, is given by $\Delta P = -A\Delta\alpha$, where A is a constant. Since the waveguide used in our experiment had $\alpha L = 0.092$, this expression is valid. Thus, if the optically induced intensity change is due to $\Delta\alpha$, we should see a constant decrease of the transmitted intensity under a constant pump light illumination, *independent* of temperature. However, as noted above, the sign of the observed change varied, dependent on temperature. In addition, the absorption change due to the optically induced plasma is given by $\Delta\alpha/\Delta n = 2/c\tau$, where τ is the carrier lifetime and c is the velocity of light. For PTCDA, $\Delta\alpha/\Delta n = 4.2\times10^{-6}$ cm^{-1}, and absorption changes are insignificant. We conclude, therefore, that the modulation is due to an intensity dependent refractive index, rather than a change in the absorption coefficient.

Since both the optically and the thermally induced modulation is caused by the changes in refractive index, the thermal measurements can be used to determine $\Delta n = n_2 I$.[6] That is, since the thermal measurements indicated that an output intensity change of 10% corresponds to a π-phase change (Fig. 1), then the 2% decrease in transmitted intensity induced by a pump power of $I = 0.98$ W/cm^2 corresponds to $\Delta\delta = \pi/5$. Using the relationship $\Delta\delta = 4\pi(n_2 I)L'/\lambda$, we get $n_2 = 5.4\times10^{-5}$ cm^2/W, where $L' = 1$ mm is the interaction length. Here, 22.1 °C was chosen as the measurement temperature since the optically induced intensity change is nearly linear over a small range of pump intensity (< 1 W/cm^2). Of course, the measurement can be made equally well at other temperatures.

By comparing the measured carrier lifetime to theoretical predictions, we verified that n_2 is indeed due to an optically generated plasma. Here, τ was directly measured from the transient response time of the 1.06-μm wavelength beam due to a pulsed 0.514-μm pump beam. Using a measurement system with a response time of < 1 μs, the rise and fall times of the 1.06-μm beam were found to be 18 and 16 μs, respectively (Fig. 3). For comparison, from the steady-state measurements of n_2, using Eq. (2), we obtain $\tau = (14\pm1)$ μs, which is very close to the measurement.

TABLE I. Resonant nonlinear properties of some typical materials

Material	Energy gap (eV)	λ (μm)	Response time	Temp (K)	n_2 (cm^2/W)	Refs.
InSb	0.18	5.5	0.3 μs	80	10^{-1}	9
InAs	0.40	3.1	0.2 μs	80	2×10^{-4}	10
Si	1.12	1.06	···	300	1.2×10^{-10}	11
GaAs	1.42	0.81	30 ps	80	8.6×10^{-10}	12
SINC[a]		0.81	···	300	10^{-7}	2
PTCDA	2.2	0.514	16 μs	295	5.4×10^{-5}	This work

[a]SINC is silicon naphthalocyanine oligomer, which is a random glassy polymer.

The constants used in the calculation for PTCDA are $\alpha = 4.6\times10^5$ cm^{-1} at $\lambda = 0.514$ μm as obtained from absorbance measurements, a hole effective mass for PTCDA of $m^* = 0.18m_0$ (where m_0 is the electron rest mass),[5] and a quantum efficiency of $\eta = 0.01$.[8] The presence of electrons was ignored since their effective mass is at least an order of magnitude larger than that of holes.[5] In this case, Eq. (2) implies that their effect on Δn is negligible.

In Table I we list the resonant nonlinear properties of some typical inorganic semiconductors, along with one organic polymer, and PTCDA. From this Table, n_2 of PTCDA is one of the highest observed to date. However, the response time (τ) is comparatively long. To reduce the carrier lifetime for high-speed applications, organic multiple-quantum-well structures[5] are potentially useful. However, decreasing the carrier lifetime might also reduce η, thereby ultimately decreasing n_2. Alternatively, one can reduce τ by electrically injecting holes from contacts, and then sweep them out using an applied electric field.

In the conclusion, we report the apparently first observation of free-carrier-induced nonlinear effects in crystalline organic semiconductors. An intensity-dependent refractive index of $n_2 = 5.4\times10^{-5}$ cm^{-2}/W has been measured, and is among the highest values reported for practical optical device materials.

The authors thank the Rome Air Development Center (Hanscom AFB), DARPA, and 3M Corp. for support of this work. We also thank F. F. So for many helpful discussions.

[1] D. S. Chemla and J. Zyss, *Nonlinear Optical Properties of Organic Molecules and Crystals* (Academic, New York, 1987), Vols. 1 and 2.
[2] A. F. Garito and J. W. Wu, Proc. SPIE **1147**, 2 (1989).
[3] D. Y. Zang, Q. Shi, F. F. So, S. R. Forrest, and W. H. Steier, Appl. Phys. Lett. **58**, 562 (1991).
[4] R. F. Chaiken and D. R. Kearns, J. Chem. Phys. **45**, 3966 (1966).
[5] H. M. Gibbs, S. L. McCall, T. N. C. Venkatesan, A. C. Gossard, A. P. Passner, and W. Wiegman, Appl. Phys. Lett. **35**, 451 (1979).
[6] M. C. Gabriel, H. A. Haus, and E. P. Ippen, J. Lightwave Technol. **LT-4**, 1482 (1986).
[7] F. F. So and S. R. Forrest, Phys. Rev. Lett. **66**, 2649 (1991).
[8] C. Arbour, N. R. Armstrong, R. Brina, G. Collins, J. Danziger, J.-P. Dodelet, P. Lee, K. W. Nebesney, J. Pankow, and S. Waite, Mol. Cryst. Liq. Cryst. **183**, 307 (1990).
[9] D. A. B. Miller, C. T. Seaton, M. E. Prise, and C. D. Smith, Phys. Rev. Lett. **47**, 197 (1981).
[10] C. D. Poole and E. Garmire, Appl. Phys. Lett. **44**, 363 (1984).
[11] R. A. Fisher, in *Optical Phase Conjugation*, edited by R. K. Jain and M. B. Klein (Academic, New York, 1983), Chap. 10, p. 369.
[12] J. L. Oudar, I. Abram, and C. Minot, Appl. Phys. Lett. **44**, 689 (1984).

Observation and modeling of quasiepitaxial growth of a crystalline organic thin film

P. E. Burrows,[a] Y. Zhang,[a] E. I. Haskal,[a] and S. R. Forrest[a]
Department of Electrical Engineering/Electrophysics and Materials Science, University of Southern California, Los Angeles, California 90089-0241

(Received 9 June 1992; accepted for publication 16 September 1992)

We directly observe, using the scanning tunneling microscope, a two-dimensional crystal of the organic compound 3, 4, 9, 10-perylenetetracarboxylic dianhydride (PTCDA). The surface unit cell dimension is found to be 21.6±2.2 Å by 15.2±1.6 Å, or approximately 20% larger than the bulk unit cell. Furthermore, the organic lattice is oriented with respect to the graphite substrate even though the two lattices are incommensurate. These observations are consistent with reflection high energy electron diffraction measurements, and energy minimization calculations, assuming that the van der Waals bond is the predominant intermolecular force which determines the equilibrium crystal structure. The combination of measurement and theory provides the first step in developing tools for predicting the conditions which lead to quasiepitaxial growth of these technologically important van der Waals solids.

The archetype crystalline organic semiconductor 3, 4, 9, 10-perylenetetracarboxylic dianhydride (PTCDA or $C_{24}O_6H_8$), has many practical device applications such as waveguides,[1] couplers,[2] and organic/inorganic semiconductor heterojunction devices.[3] Since the organic crystal is bonded by weak van der Waals (vdW) forces, single-crystal thin films can be deposited on inorganic substrates without regard for lattice matching; a process known variously as "van der Waals epitaxy" or "quasiepitaxy". Understanding this new growth process is crucial if we are to fully exploit its potential for use in a wide range of device structures.

In this work we use the scanning tunneling microscope (STM) to study the crystal structure at the onset of film growth by examining the first monolayer of PTCDA deposited by the ultrahigh vacuum process of organic molecular beam deposition (OMBD) on highly oriented pyrolytic graphite (HOPG) substrates held at low temperature (90 K). We show that the surface unit cell is expanded from that found in the bulk, and is also distorted by rotations of individual molecules with respect to the unit cell. Furthermore, we determine an orientational relationship between the PTCDA layer and the graphite substrate. This is supported by calculations which minimize total crystal energy to determine the equilibrium positions of molecules within the two-dimensional unit cell of PTCDA, and is consistent with recent observations obtained using reflection high energy electron diffraction (RHEED).[4]

A perspective view along the *c*-axis of the monoclinic bulk structure of PTCDA is shown in Fig. 1. The material forms planar stacks with molecular spacing of 3.21 Å, and has lattice constants of $a=3.72$ Å, $b=11.96$ Å, and $c=17.34$ Å, and a lattice angle $\beta=98.8°$. Thick films (ca. 1000 Å) of PTCDA have long range crystalline order when deposited at high rates,[5] or on substrates held at low temperature.[1] Scanning tunneling microscopy has been shown to be capable of molecular resolution of organic molecules.[6,7] Ludwig *et al.*[8] recently presented molecular resolution images of PTCDA deposited on HOPG held at 340–400 K. They explained their results in terms of a surface unit cell similar to the bulk unit cell, but 5%–10% larger. However, their films were deposited under conditions far from those shown to produce single crystalline layers of PTCDA.[1,5,9]

The OMBD vacuum system used to prepare our samples is described elsewhere.[9] A 1.4 cm^2 HOPG substrate was cleaved in air and immediately loaded into the deposition chamber via a vacuum load lock. The PTCDA, prepurified by repeated temperature gradient sublimation, was loaded into a Knudsen cell and thoroughly degassed at 200 °C prior to film deposition. Approximately 4 Å (1 monolayer) of PTCDA was deposited at a rate of 0.1–0.2 Å/s, measured by a quartz crystal thickness monitor. Such a measured thickness is consistent with the disappearance of the substrate streaks in the RHEED experiments.[4]

The deposited film was imaged in air using a commercially available STM[10] with controlled geometry, Pt/Ir tips[11] within about 24 h of growth. Current images (constant height mode) apparently showing single molecules of PTCDA were readily obtained on several samples at tun-

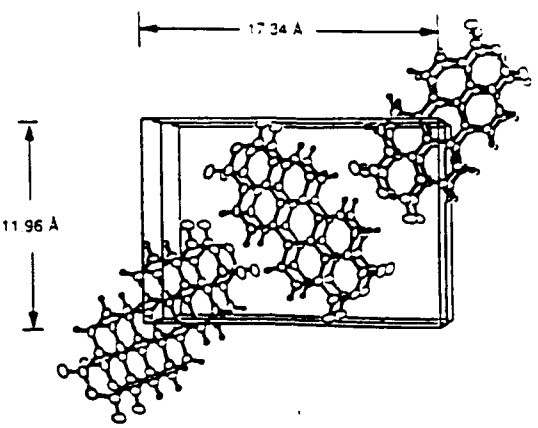

FIG. 1. The PTCDA bulk unit cell viewed along the *c*-axis.

[a]Current address: Department of Electrical Engineering, Princeton University, Princeton, NJ 08544.

 0003-6951/92/452417-03$03.00

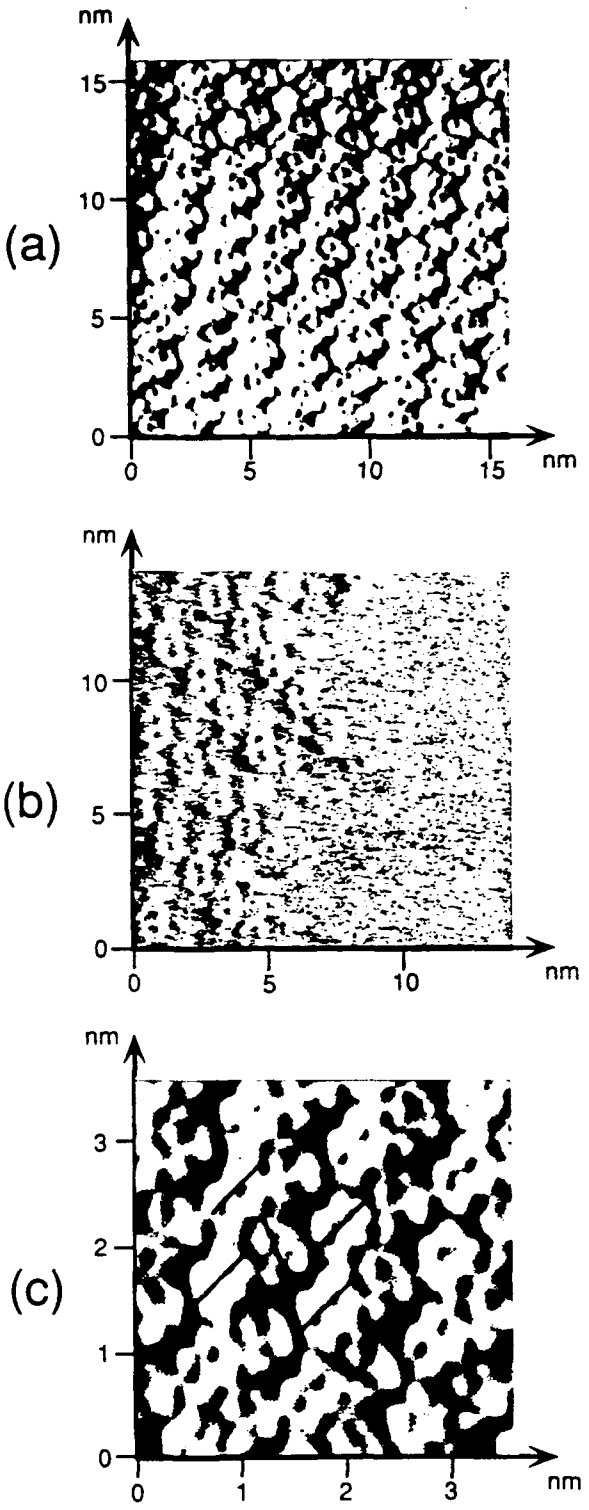

FIG. 2. (a) False color filtered STM image of crystalline PTCDA on HOPG. Tip operating parameters: 402.1 mV, 0.10 nA tip positive. (b) Unfiltered STM image of the edge of an island of PTCDA on HOPG. Tip operating parameters: 403.7 mV, 0.10 nA tip positive. (c) Detail of (a), showing the unit cell of PTCDA on HOPG. Superimposed lines are a guide to the eye.

neling currents of ~ 0.1 nA and a tip voltage of $\sim +400$ mV with respect to the substrate. No images were obtained with the tip biased negative with respect to the substrate. A typical image, filtered to reduce noise, is shown in Fig. 2(a). Such images were stable for ~ 10–20 scans before being replaced by an image of the underlying graphite lattice. Since higher tunneling currents result in a higher rate of image degradation, this is attributed to the weakly bound organic molecules being swept away by the tip.

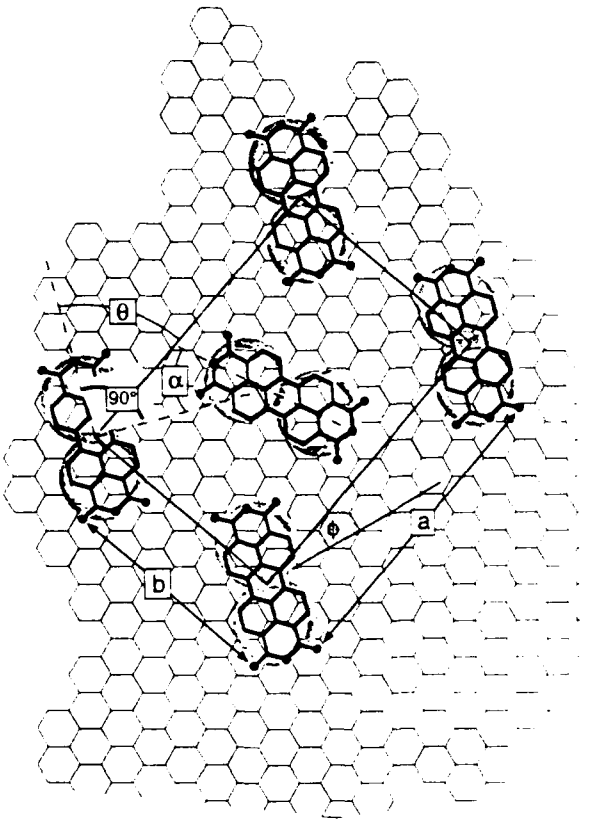

FIG. 3. Proposed structure for the two-dimensional unit cell of PTCDA on HOPG, showing the parameters measured and displayed in Table I.

Figure 2(b) shows an example unfiltered image of the edge of an island of PTCDA; the individual molecules appearing as broken double circles. Coupled with the high reproducibility of the images between numerous different samples and using different tips, the observation of island edges provides evidence that the images presented are, in fact, of a monolayer of the organic thin film on graphite.

Based on the STM images, we propose a model for the two-dimensional unit cell of PTCDA on HOPG shown in Fig. 3, with the measured dimensions and angles between the molecules listed in Table I. The linear dimensions, a and b, are measured and calibrated relative to an image of the HOPG lattice. The angle θ is measured directly from the images taken from several samples studied, whereas the angle α is measured using Fig. 2(c). This is a magnified detail of the unit cells in Fig. 2(a) showing the fifth, central, molecule of the unit cell, which is faintly apparent in

TABLE I. PTCDA crystal dimensions and angles.

	a(Å)	b(Å)	θ	α	ϕ
STM	21.6 ± 2.2	15.2 ± 1.6	55 ± 2°	35 ± 10°	17 ± 4°
RHEED	22.4 ± 1.0	16.0 ± 1.0	...	...	...
Theory	20.0 ± 1	15.7 ± 1	49.3 ± 1°	27.5 ± 1°	11 ± 4°
Bulk	17.34	11.96	47°	7.5°	...

the low magnification image as well. The positions of the long molecular axes are indicated by the line segments shown in the figure.

Lattice dimensions and angles measured from images of different samples with different tips are reproducible within the limits quoted in Table I. Two PTCDA molecules define a rectangular unit cell with dimensions $a = 21.6 \pm 2.2$ Å and $b = 15.2 \pm 1.6$ Å, in contrast to the bulk unit cell with dimensions $a = 17.34$ Å and $b = 11.96$ Å. The angles θ and α are $55 \pm 2°$ and $35 \pm 8°$, respectively. These parameters agree with those recently reported using RHEED (Table I).

The apparent removal of the organic molecules by the tip allows us to examine the orientational relationship between the organic film and the graphite substrate. From these images we find the angle between the graphite and PTCDA lattices, shown as ϕ in Fig. 3, to be $17 \pm 4°$.

Some larger area scans show adjacent islands of PTCDA. The angle between equivalent PTCDA molecules in different islands is always an integer multiple of 60°. Since the graphite substrate has sixfold rotational symmetry, nucleating islands of PTCDA are energetically identical at rotations of 60° with respect to the substrate. The absence of any other angles in the observed STM images strongly suggests that even though the two lattices are highly incommensurate, they align in a consistent fashion with respect to each other; striking evidence for quasiepitaxial growth. This represents a fundamental limitation of quasiepitaxy: if the symmetries of the two lattices are not identical, the deposited layer must contain high angle grain boundaries between islands which have separately nucleated at different lattice sites.

To interpret the STM images, we have calculated the crystal energy of a monolayer of PTCDA by assuming that the dominant intermolecular and substrate-molecule bond is due to the vdW interaction (true for nonpolar molecules such as PTCDA which lie flat on the substrate.[12] Thus, the interaction potential, u_{ij}, between the ith atom in one molecule and the jth atom in its neighbor is derived from the Buckingham potential, i.e.:

$$u_{ij} = -\frac{\alpha_{ij}}{r_{ij}^6} + \beta_{ij} \exp(-\gamma_{ij} r_{ij}),$$

where r_{ij} is the distance between the ith and jth atoms, and α_{ij}, β_{ij}, γ_{ij} are the vdW coefficients between atom pairs involved in bonding PTCDA to its neighbors and to the substrate.[13,14] Periodic boundary conditions are assumed so that only potentials within the unit cell are considered. The total interaction potential is U_T, obtained by summing u_{ij} over all atoms in the unit cell and substrate. The favored crystal configuration is then given by

$$\frac{\partial}{\partial x_k} [U_T(x_k)] = 0,$$

where x_k ranges over the independent parameters, a, b, θ, and ϕ (Fig. 3). Because of the short range of the van der Waals potential ($\sim 1/r^6$), distant molecular interactions are negligible and the model is rapidly tractable.

Unit cell parameters of the bulk crystal calculated using this model agree with those measured by X-ray diffraction to within 2%. In addition, the calculated crystal sublimation energy of ~ 30 kcal/mol is consistent with observations for PTCDA and other anthracene-like crystals. Therefore, application of the model to two-dimensional surface cells appears to be justified.

Results of the calculations applied to the PTCDA surface unit cell are also given in Table I. The calculated equilibrium distance of the PTCDA layer to the graphite substrate is 3.21 Å; a value equal to the intermolecular spacing in bulk PTCDA. The close agreement between a, b, θ, and α predicted by the model and those measured using STM and RHEED clearly supports the structure shown in Fig. 3. For example, the calculated rotational orientation of $\phi = 11°$ is energetically favored by ~ 100 meV over other angles.

From these model calculations, we infer that the enlarged reconstructed surface unit cell is a direct result of the lack of vdW bonds extending above the top layer, allowing the cell to expand slightly to minimize the repulsive core energy between adjacent atoms. We note, however that this surface reconstruction does *not* depend strongly on the substrate, but rather is a result of the comparatively strong *intermolecular* forces within the cell itself. A more detailed discussion of these results will be presented elsewhere.

In summary, the STM images of the surface unit cell are in close agreement both with *in situ* RHEED data taken for films grown under similar conditions and with crystal energy minimization calculations. Such close agreement implies that the calculations should be predictive of the optimal conditions under which quasiepitaxial growth can be obtained for a wide range of van der Waals-bonded materials with a broad range of applications to optoelectronics.

The authors gratefully acknowledge AFOSR (Gernot Pomrenke and Charles Lee) and RADC (Joe Lorenzo) for support of this project, and Rockwell International through USC for a fellowship (to E.I.H.).

[1] D. Y. Zang, Y. Q. Shi, F. F. Shi, F. F. So, S. R. Forrest, and W. H. Steier, Appl. Phys. Lett. **58**, 562 (1991).
[2] D. Y. Zang and S. R. Forrest, Photon. Technol. Lett. **4**, 365 (1992).
[3] S. R. Forrest, IEEE Circuits Devices Mag. **5**, 33 (1989).
[4] E. I. Haskal, F. F. So, P. E. Burrows, and S. R. Forrest, Appl. Phys. Lett. **60**, 3223 (1992).
[5] S. R. Forrest, M. L. Kaplan, and P. H. Schmidt, Appl. Phys. Lett. **56**, 543 (1984).
[6] M. Hara, I. Iwakabe, H. Sasabe, A. Yamada, and A. F. Garito, Nature **344**, 228 (1990).
[7] P. H. Lippel, R. J. Wilson, M. D. Miller, Ch. Woll, and S. Chiang, Phys. Rev. Lett. **62**, 171 (1989).
[8] C. Ludwig, B. Gompf, W. Glatz, J. Petersen, W. Eisenmenger, M. Mobus, U. Zimmermann, and N. Karl, Z. Physik B-Condensed Matter **86**, 397 (1992).
[9] F. F. So, Ph.D. thesis, University of Southern California, 1991.
[10] Nanoscope II, Digital Instruments Inc., Santa Barbara, CA 93110
[11] Controlled Geometry Pt/Ir STM tips, Materials Analytical Services, Raleigh, NC 27607.
[12] Y. Saito and M. Shiojiri, J. Cryst. Growth **67**, 91 (1984).
[13] R. A. Scott and H. A. Scheraga, J. Chem. Phys. **42**, 2209 (1965).
[14] A. Abe, R. L. Jernigan, and P. J. Flory, J. Am. Chem. Soc. **88**, 631 (1966).

Mol. Cryst. Liq. Cryst. Sci. Technol. – Sec B: Nonlinear Optics, 1992, Vol. 2, pp. 205–222
Reprints available directly from the publisher
Photocopying permitted by license only

Quasi-Epitaxially Grown Crystalline Organic Semiconductors: Structural, Electrical and Optical Properties

F. F. SO AND S. R. FORREST
Departments of Electrical Engineering and Materials Science, Center for Photonic Technology, University of Southern California, Los Angeles, CA 90089-0241, USA

Received 12 Aug 1991; accepted 30 Aug 1991

A new class of engineered materials based on crystalline organic semiconductors grown by the ultra-high vacuum process of organic molecular beam deposition is described. We discuss the conditions which lead to ordered growth between highly lattice-mismatched van der Waals crystals into novel 'quasi-epitaxial' structures. Furthermore, a model is presented which describes the physical mechanisms underlying quasi-epitaxy. The electrical and optical properties of both single and multiple heterojunction structures grown using alternating layers of two different, lattice-mismatched organic molecules are considered in detail. It is found that the layers can be grown sufficiently thin (10 Å) to result in exciton confinement in organic multiple quantum wells. These and other quasi-epitaxially grown structures can lead to an entirely new family of optoelectronic devices.

Keywords: molecular beam epitaxy, nonlinear optics, quantum well

INTRODUCTION

Recent work in many laboratories worldwide[1-7] has demonstrated a new class of engineered materials with application to photonic devices. These materials are variously known as 'van der Waals solids', 'layered materials' or 'quasi-epitaxial materials'. The property these materials have in common is that the cohesive force which bonds the various material layers together is the relatively weak van der Waals force. This results in an ability to layer materials which are highly lattice-mismatched without inducing defects in the crystal structure. One particularly interesting class of van der Waals solids with applications to a very broad range of optical and electronic devices is based on multilayered structures consisting of crystalline organic semiconductors.[1] These materials have been found to have excellent electrical and optical characteristics when grown by the ultra-high vacuum process of organic molecular beam deposition (OMBD) onto other organic semiconductors, or even onto the surfaces of inorganic semiconductors such as Si, GaAs or InP.[8,9] For example, high bandwidth photodetectors consisting of layers of perylene-based compounds deposited on Si substrates have been demonstrated,[8] as have field-effect transistors based on organic/InP heterojunctions.[10] Furthermore, waveguides and other optical devices have been demonstrated using these quasi-epitaxially grown layers.[11]

In this work, we discuss the structural, dielectric, conductive, and optical properties of this new and exciting class of engineered materials. In particular, we have

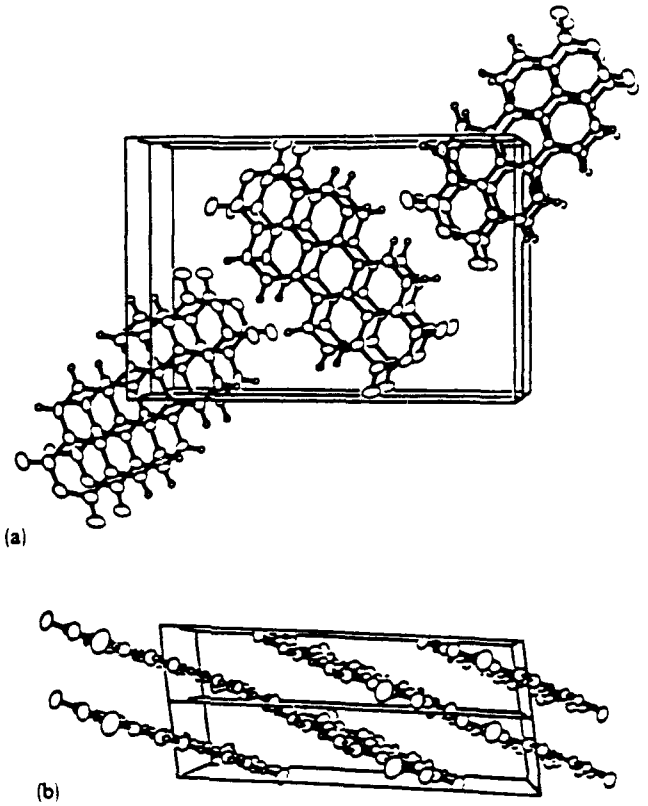

FIGURE 1 Two views of a unit cell of PTCDA.

grown which extended several centimetres across the substrate surface. Following that initial work, Debe *et al.*[13] demonstrated that other perylene derivatives similar to PTCDA could attain single crystallinity when deposited more slowly onto substrates held well below room temperature. More recently, we have found that PTCDA, and an analogous compound, 3,4,7,8 naphthalenetetracarboxylic dianhydride (NTCDA), or $C_{14}O_6H_8$, can both be grown quasi-epitaxially at a rate of 1–3 Å/s when deposited onto glass substrates held at approximately 90 K.[1] Low substrate temperature during growth is required since the thermal energy of the molecules on the surface needs to be brought well below the intermolecular bond energy for ordered growth to be established.

Multilayer stacks of alternating layers of PTCDA and NTCDA also have recently been found to form ordered crystalline structures. This order is achieved even though the crystal structures of PTCDA and NTCDA are highly mismatched. In Figure 2 we show a unit cell of NTCDA (cf. Figure 1). Here, it is seen that rather than forming planar stacks as in the case of PTCDA, NTCDA molecules stack in a herringbone manner, with an intermolecular spacing of 3.5 Å. In the herringbone structure, adjacent stacking axes are positioned at 90° with respect to each other, once again leading to anisotropies in the conductive and dielectric properties of these crystals. However, the asymmetries are much less pronounced than those found in PTCDA.

In growing the multilayer stacks of PTCDA and NTCDA onto glass substrates, pre-purified powder samples of the materials were loaded into separate sublimation cells in the OMBD growth chamber which had a base pressure of 10^{-10} torr. The

focused beam, this birefringence measurement determines the local orientation of the optic axis of PTCDA (NTCDA has only very weak birefringence and hence the probe is not sensitive to its presence in the stacks). This technique, therefore, is sensitive to the degree of crystalline order over the region covered by the beam diameter. The finding that the optic axis of PTCDA is orientated in the same direction across the wafer surface, and that the birefringence of a multilayer stack is equal in magnitude to a single PTCDA film of equal total thickness, indicates that the crystalline orientation of one PTCDA layer is the same as all other PTCDA layers in a multilayer structure. By inference, the NTCDA layers must be likewise aligned. This ordering, both across wafer surfaces as well as between layers in the stacks, is evidence for quasi-epitaxy in the multilayer samples.

The process of q-e can be quantitatively understood if we require that a monolayer of one material must find a minimum energy configuration with the underlying crystal during growth. That is, when growth of material B is initiated on the surface of material A, the first few molecules B align themselves to A to minimize their individual molecular interaction energies. As the growth of layer B approaches a full monolayer, different islands of material B arising from nucleation at random sites across the surface of A will be out of register with each other, although they may all be approximately aligned. As the spacing between islands is filled in with additional deposition of material B, the islands must shift slightly (but in a rigid manner) to accommodate these last, interstitial molecules. This process must occur without increasing the overall energy of the layer to the extent that a dislocation is generated. Note that this picture requires that the substrate temperature be high enough to allow for some surface mobility of the islands and molecules, yet not so high that the individual molecules are only very loosely bound to the surface. For this reason, deposition of q-e grown materials occurs on substrates cooled below room temperature.

One condition which must be fulfilled for the above scenario to occur is that the binding energy minimum between molecules A and B must be very broad – i.e. there is a range of positions which molecule B can have when aligned to molecule A which does not significantly change the total energy of the system. In this way, small shifts in position can be accommodated without significantly increasing the total crystal energy. We have tested this hypothesis by calculating the vdW bond energy between PTCDA (molecule A) and NTCDA (molecule B). These calculations are done using the atom-atom potential method.[14] In this method, we calculate (and minimize) the vdW energy between each pair of atoms in both the PTCDA and NTCDA molecules. The total bond energy is simply:

$$\Phi = \sum \phi_{ij} \tag{1}$$

where ϕ_{ij} is the atom-atom potential between the ith and jth *atoms* in molecules A and B, respectively. This, in turn, is calculated using the Buckingham potential:

$$\phi_{ij} = \alpha / r_{ij}^6 + \beta \exp(-\gamma r_{ij}) \tag{2}$$

Here, r_{ij} is the distance between atoms i in molecule A and j in molecule B, and α, β and γ are vdW atom-atom potential constants for the constituent atoms in the two molecules (C, O and H for PTCDA and NTCDA, for example). The constants used in the case of PTCDA and NTCDA are given in Table 1.

The accuracy of this method has been tested by calculating the minimum energy configuration of *bulk* PTCDA, and comparing the results to the measured crystal structure. Under this test, the model works surprisingly well. For example, the calculated intermolecular stacking distance is 3.26 Å as compared with the actual value of 3.21 Å. Furthermore, the model predicts that two molecules stack with

From the energy contour plot, we see that the energy minimum between PTCDA and NTCDA is indeed broad, allowing for nearly a 2 Å translation of one molecule with respect to another without any significant increase in Φ. Thus, we can conclude from this first order, somewhat simplified, calculation that our 'picture' of the process of q-e is plausible. That is, we expect that once the islands are nucleated around the surface of the substrate, they are still free to translate rigidly to accommodate the arrival of the final molecules which fill in the interstices between neighbouring islands. This shift occurs without inducing strain or polycrystalline growth.

While this model is still unsophisticated in many ways, it suggests the properties which molecules must possess before they can be grown into q-e structures. From these initial results, we infer that the process is, in fact, a very general property of vdW solid growth.

One consequence of being able to reproduce the anisotropic crystal structure in a thin film is that the films exhibit enormous anisotropies in both their conductive and dielectric properties. For example, the in-plane conductivity of PTCDA films is found to be at least six orders of magnitude lower than the conductivity perpendicular to the film plane.[15] It is also expected that the dielectric properties of highly ordered films would have a considerable degree of anisotropy along different crystalline directions. The off-resonance dielectric constant of a material at frequency, ω, is given by:

$$\epsilon - 1 = \frac{4\pi N q^2 f_j}{m^*(\omega_j^2 - \omega^2)} \tag{3}$$

where N is the molecular number density, ω_j is the dipole transition frequency, q is the electronic charge, and m^* is the electron effective mass. The oscillator strength of the dipole transition from level o to j is given by $f_j = 2m^*\hbar\omega|x_{oj}|^2/\hbar^2$, where x_{oj} is the electron position expectation value, and $\hbar$ is Planck's constant divided by 2π. Assuming that the largest contribution to the dipole moment of the molecule is due to the π-orbitals, and that the electron within a given orbital is completely delocalized, then we can make the approximation that $f_{j\perp}/f_{j\parallel} \approx |x_{oj\perp}|^2/|x_{oj\parallel}|^2 \approx d^2/L^2$. For the case of PTCDA, $d \cong 3.2$ Å is the extent of the π-orbital system perpendicular to the molecular plane, and L is its extent in the plane, which is approximately equal to the length of the perylene molecular core of PTCDA (i.e. $L \cong 6.9$ Å). Hence, provided that there is perfect crystalline alignment throughout the q-e film, we can expect an anisotropy in ϵ between directions perpendicular and parallel to the thin film plane (and hence approximately perpendicular and parallel to the molecular stacking axis) of $(\epsilon_\perp - 1)/(\epsilon_\parallel - 1) \approx d^2/L^2 \approx 0.22$. This value is only an approximation, since we are assuming that m^* is isotropic,[16] and that the dipole moment is due to a completely delocallized electron in the extended π-system. Nevertheless, it has been found[3] that the measured value of $(\epsilon_\perp - 1)/(\epsilon_\parallel - 1)$ for PTCDA is 0.26, which is quite close to the value 'predicted' by the above model. Furthermore, the index of refraction measured at a wavelength of $\lambda = 1.064\,\mu$m in the direction perpendicular to the substrate plane is $n_\perp = 1.36 \pm 0.01$, whereas parallel to the plane, $n_\parallel = 2.017 \pm 0.005$, resulting in an index difference of $\Delta n = 0.66$. To our knowledge, these are the largest index anisotropies ever measured for thin films, giving further evidence for the nearly perfect crystalline order achieved in q-e growth.

ORGANIC HETEROJUNCTIONS

It is well known that multiple quantum wells can be fabricated by alternately layering two inorganic semiconductors with different bandgaps. Thus, the question arises:

the hole mobility was found to increase linearly at low electric fields, and saturates at high fields. The high field carrier velocity saturation is due to phonon emission, consistent with band theory. Further, the long carrier mean free path (as compared with the intermolecular stacking distance) in these crystalline organic materials estimated from the low temperature mobility data also supports the band description. Provided that we can use this model to describe the charge transport in PTCDA and CuPc, the transport theory for inorganic semiconductor heterojunctions can also be applied (with caution) to organic heterojunctions.

Using the treatment of Chang for isotype heterojunctions,[21] the saturation current density for an HJ is given by:

$$J_s = BT^{1/2} \exp[-qV_{D2}/kT] \tag{4}$$

where B is a pre-factor which depends on the density of acceptors and the hole effective mass in CuPc, kT is the Boltzmann energy at temperature T, V_{D2} is the diffusion potential on the depleted, CuPc side of the heterojunction, and q is the electron charge. The valence band discontinuity energy, ΔE_v, is then given by:

$$\Delta E_v = qV_{D1} + qV_{D2} \tag{5}$$

In the above equation, V_{D1} is the diffusion potential on the PTCDA side of the heterojunction. For simplicity, we assume that there is no significant difference in the effective hole densities of states and in the acceptor concentrations between CuPc and PTCDA.

From Equation 4, it can be seen that J_s is thermally activated with energy qV_{D2}. In Figure 5, we show the dependence of log (J_s) on $1/T$ for a CuPc/PTCDA heterojunction. Here, J_s is obtained by extrapolating both the forward and reverse bias currents to an applied voltage of $V = 0$. The activation energies for both the forward and reverse bias are the same, yielding $V_{D2} = 0.51 \pm 0.05$ V. This value is consistent with that obtained from capacitance-voltage (C-V) measurements, where we find that $V_{D2} = 0.45 \pm 0.15$ V. Following the treatment of Chang, we obtain $V_{D1} = 0.01$ V, and hence the valence-band discontinuity energy for CuPc/PTCDA heterojunctions is $\Delta E_v = V_{D1} + V_{D2} = 0.52 \pm 0.05$ V.

Based on the electrical characteristics of the CuPc/PTCDA heterojunctions, a

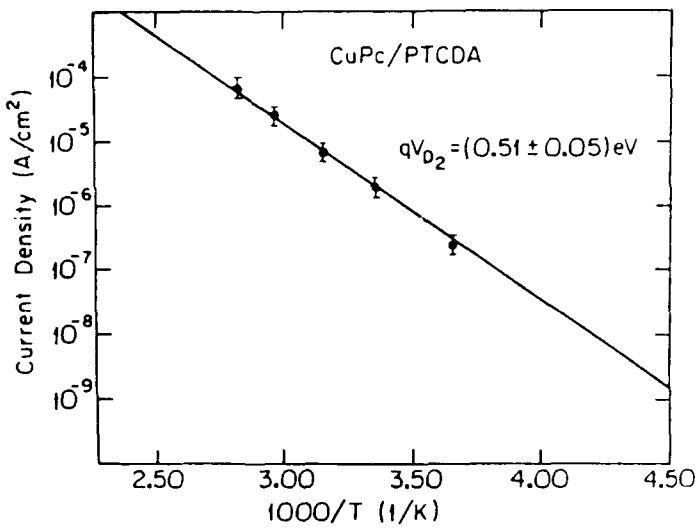

FIGURE 5 Saturation current versus temperature for a CuPc/PTCDA heterojunction.

to quantum confinement of excitons in a quantum well structure. We now discuss both models in detail.

The change of polarization energy of PTCDA due to the proximity of NTCDA molecules in closely spaced layers can be calculated using perturbation theory. A derivation of the perturbation of the exciton energy due to polarization effects is given in the Appendix. The results of the calculation show that the first order energy shift of the polarization energy *increases* linearly with the layer thickness, t. This effect, while being very short range, can actually increase the exciton energy with increasing well width, contrary to our observations. Hence, we can rule out this first order 'energy offset' effect. On the other hand, the second order polarization energy correction is proportional to t^{-4}. As shown in Figure 10, the data are not consistent with the results of the calculation since their energy dependence is considerably smaller than even t^{-2}. Hence, we conclude that the polarization model does not adequately explain the observed blue shift in the exciton line.

Quantum confinement provides an alternative explanation for the observed blue shift in the absorption spectrum.[1,2] Here, we use the variational method to evaluate the binding energy of an exciton in a quantum well. The Schrödinger equation for an exciton can be solved using the trial wavefunction:

$$\psi_{tot} = \psi_e(Z_e)\psi_h(Z_h)\psi_{1s}(\rho, z) \tag{6}$$

where $\psi_{1s}(\rho, z)$ is the hydrogenic 1s wavefunction, $\rho = x^2 + y^2$, z_e and z_h are coordinates in the z-direction for the electron and hole, respectively, $\psi_e(z_e)$ and $\psi_h(z_h)$ are the exact solutions to the finite square well problem, and $z = z_e - z_h$. In Equation 6, the hydrogenic state has the form:

$$\psi_{1s} = \exp\left[-(\rho^2/\alpha^2 + z^2/\beta^2)^{1/2}\right] \tag{7}$$

Here, α is a variational parameter in the trial solution, and β is set equal to a_o, where a_0 is the exciton Bohr radius in the bulk crystal. For crystalline organic MQW structures, typically $a_o \ll L_z$, where L_z is the quantum well width. In this case, therefore, it is reasonable to assume $\beta = a_o$, with α being the only variation parameter.

The parameters used in this model to fit the data in Figure 10 are listed in Table 2. Here, the sum of V_e and V_h is equal to the difference in energy gaps of PTCDA and NTCDA. Of all the parameters used in the calculation, the results are most sensitive to the choice of m_h and the ratio, V_e/V_h. Using these parameters, a good fit to the experimental data is obtained for $m_h = 0.18m_o$, where m_o is the electron rest mass. A small value of m_h and a relatively large value of m_e were chosen in the calculation since PTCDA is predominantly a hole-transporting material. The effect of using different values of m_h are also shown for comparison in Figure 10 indicating the sensitivity of the fit to this parameter. Note that our calculation implies that $V_e \gg V_h$. This is consistent with electrical measurements made for PTCDA/NTCDA heterojunctions which do not exhibit significant rectification of the hole current at temperatures ranging from room temperature to about 90 K. This

TABLE 2
Variational calculation parameters

Parameter	Symbol	Unit	Value
Hole mass	m_h	m_o	0.18
Electron mass	m_e	m_o	10.0
Electron potential	V_e	meV	900
Hole potential	V_h	meV	50
Relative dielectric constant of PTCDA	ϵ_p		3.6

exhibit electrical and optical properties analogous in many ways to fully inorganic heterojunctions.

5. Evidence for quantum confinement in very thin layer organic multiple quantum well structures has furthered our understanding of the nature of excitons in crystalline organic materials. Given that excitons in these materials have been the focus of study for over 40 years,[22,23] in many ways they are the key to our understanding the physics of vdW solids in general. In addition, the observation of quantum confinement suggests that many devices based on organic MQWs are becoming a realistic possibility. One example of such a device would be an organic MQW optical modulator which could be made to cover all regions of the ultra-violet, visible or near infra-red spectral regions, depending on the choice of organic compounds employed.
6. The large exciton-phonon coupling strength characteristic of organic semiconductors can lead to exciting, very large nonlinear optical effects. For example, Lam and co-workers[24] predicted that organic MQWs have large $\chi^{(3)}$ effects, and are therefore potentially useful for a broad range of applications which are unattainable using the polymers and photorefractive materials studied today. They have shown that quasi-epitaxially grown crystalline organic thin films and MQWs with large Franck-Condon (FC) shift energies exhibit an intensity-dependent absorption and index of refraction at relatively low input powers. Here, the FC shift is the energy difference between the lowest energy absorption and the highest energy luminescence spectral peaks, and is proportional to the square of the exciton-phonon coupling strength. As shown by the arrows in Figure 10, the PTCDA/NTCDA MQW structure with 40 Å layer thickness has FC = 4050 cm^{-1}, which to our knowledge is the largest yet observed for organic semiconductors.

To understand the nonlinear optical properties of organic MQWs, the Hamiltonian for organic MQWs under illumination can be written[24]:

$$\mathcal{H} = \hbar(\omega_x - \omega_l)a^+a - \hbar\lambda Qa^+a + \hbar\omega_o b^+b - \mu a^+E - \mu aE^* \tag{8}$$

where ω_x, ω_l, and ω_o are the exciton, incident light and phonon frequencies, respectively, and λ is the exciton-phonon coupling constant, $\mu = qa_o$ is the exciton dipole moment, E is the external electrical field, and a^+a and b^+b are the exciton and phonon populations, respectively. Also, $Q = b^+ + b$ is the phonon amplitude.

The origin of the optical nonlinearities in organic MQWs lies in the second term of Equation 8, which is proportional to the exciton-phonon coupling strength, λ, given by:

$$\lambda = [\omega_o(FC)]^{1/2} \tag{9}$$

The second term in Equation 8 'renormalizes' the exciton energy, ω_x, by $-\hbar\lambda Q$. As the incident optical field intensity increases, the exciton population increases, resulting in a decrease in the energy of the exciton absorption peak. Such an effect leads to an intensity dependent absorption, and hence an intensity dependent index of refraction through the Kramers-Kroenig effect. Note that if the incident light beam is detuned from the exciton peak on the low side of ω_x by a factor of $\omega_l - \omega_x$, then the absorption peak energy is shifted toward the pump light energy, which decreases the detuning. This increases the absorption with increasing incident light intensity, leading to optical bistability.

The two-wave mixing gain for a weak probe beam interacting with a strong pump beam for PTCDA/NTCDA MQW structures, predicted by the time dependent solution of Schrödinger's Equation and using Equation 8, is shown in Figure 11. The horizontal axis corresponds to the (Rabi frequency)^2 which is proportional to

2. F. F. So and S. R. Forrest, Evidence for exciton confinement in crystalline organic multiple quantum wells, *Phys. Rev. Lett.*, **66**, 2649 (1991).
3. D. Y. Zang, F. F. So and S. R. Forrest, Giant anisotropies in the dielectric properties of quasi-epitaxial crystalline organic semiconductor thin films, *Appl. Phys. Lett.* (Aug. 12, 1991).
4. A. J. Dann, H. Hoshi and Y. Maruyama, The structure and properties of phthalocyanine films grown by the molecular beam epitaxy technique. I. Preparation and characterization, *J. Appl. Phys.*, **67**, 1371 (1990).
5. M. Hara, H. Sasabe, A. Yamada, and A. F. Garito, Epitaxial growth of organic thin films by organic molecular beam epitaxy, *Jpn. J. Appl. Phys.*, **28**. L306 (1989).
6. K. Ueno, K. Saiki, T. Shimada and A. Koma, Epitaxial growth of transition metal dichalcogenides on cleaved faces of mica, *J. Vac. Sci. Technol.*, **A8**, 68 (1990).
7. A. Koma, K. Saiki and Y. Sato, Heteroepitaxy of a two dimensional material on a three dimensional material, *Appl. Surf. Sci.* **41/42**, 451 (1989).
8. F. F. So and S. R. Forrest, Organic-on-inorganic semiconductor photodetector, *IEEE Trans. Electron. Dev.*, **36**, 66 (1988).
9. S. R. Forrest, M. L. Kaplan and P. H. Schmidt, Organic thin-film techniques for semiconductor wafer diagnostics, *Ann. Rev. Mat. Sci.*, **17**, 189 (1987).
10. C.L. Cheng, S. R. Forrest, M. L. Kaplan, P. H. Schmidt and B. Tell, Novel organic-on-InP field-effect transistor, *Appl. Phys. Lett.*, **47**, 1217 (1985).
11. D. Y. Zang, Y. Q. Shi, F. F. So, S. R. Forrest and W. H. Steier, Optical waveguides in crystalline organic semiconductor thin films, *Appl. Phys. Lett.* **58**, 562 (1990).
12. S. R. Forrest, M. L. Kaplan and P. H. Schmidt, Organic-on-inorganic semiconductor contact barrier diodes. II. dependence on organic film and metal contact properties, *J. Appl. Phys.*, **56**, 543 (1984).
13. M. K. Debe, K. K. Lam, J. C. Liu and R. J. Poirer, Vacuum vapor deposited thin films of a perylene dicarboximide derivative: Microstructure versus deposition parameters, *J. Vac. Sci. Technol.*, **A6**, 1907 (1988).
14. A. I. Kitaigorodsky, *Molecular Crystals and Molecules*, Academic Press, NY (1973).
15. S. R. Forest, M. L. Kaplan and P. H. Schmidt, Organic-on-inorganic semiconductor contact barrier diodes. I. theory with applications to organic thin films and prototype devices, *J. Appl. Phys.*, **55**, 1492 (1984).
16. P. J. Bounds and W. Siebrand, Charge-transfer excitons in anthracene crystals and their role in optical charge carrier generation, *Chem. Phys. Lett.*, **75**, 414 (1980).
17. C. Adachi, T. Tsutsui and S. Saito, Organic electroluminescent device having a hole conductor as an emitting layer, *Appl. Phys. Lett.*, **55**, 1489 (1989).
18. C. W. Tang, Two-layer organic photovoltaic cell, *Appl. Phys. Lett.*, **48**, 183 (1986).
19. S. R. Forrest, L. Y. Leu, F. F. So and W. Y. Yoon, Optical and electrical properties of istotype crystalline molecular organic heterojunctions, *J. Appl. Phys.*, **66**, 5908 (1989).
20. W. Warta and N. Karl, Hot holes in naphthalene: High, electric-field-dependent mobilities, *Phys. Rev.*, **B32**, 1172 (1985).
21. L. L.Chang, The conduction properties of Ge-$GaAs_{1-x}P_x$ $n-n$ heterojunctions, *Solid State Electron.*, **8**, 721 (1965).
22. E. A. Silinsh, *Organic Molecular Crystals*, Springer, Berlin (1980).
23. N. Kari, Studies of organic semiconductors for 40 years-III, *Mol. Cryst. Liq. Cryst.*, **171**, 31 (1989).
24. J. F. Lam, S. R. Forrest ar G. L. Tangonan, Optical nonlinearities in crystalline organic semiconductors, *Phys. Rev. Lett.*, **66**, 1614 (1991).

APPENDIX: POLARIZATION EFFECTS IN ORGANIC MQWs

Consider an exciton with a Bohr radius a_0 generated at point P in a PTCDA layer of thickness t sandwiched between two NTCDA layers with the same thickness, as shown in Figure A1. The change in exciton potential due to the presence of an NTCDA molecule at point N on the NTCDA surface is:

$$\Delta\varphi = \Delta\mu \cos\theta' / \epsilon_p |\boldsymbol{R} - \mathbf{r}|^2 \qquad \text{(A-1)}$$

where $\Delta\mu = \mu_P - \mu_N$, with $\mu_P(\mu_N)$ the dipole moment per unit volume of PTCDA (NTCDA), ϵ_p is the dielectric constant of PTCDA, $\boldsymbol{R}$ is a vector between points P and N, θ' is the angle between $\boldsymbol{R}$ and the normal to the NTCDA plane, and the charge density of the exciton is described by the spherical coordinates: r, θ, and ϕ. Using

Optical Nonlinearities in Crystalline Organic Multiple Quantum Wells

Juan F. Lam,[1] Stephen R. Forrest,[2] and Gregory L. Tangonan[1]
[1]*Hughes Research Laboratories, Malibu, California 90265*
[2]*Center for Photonic Technology, Departments of Electrical Engineering and Materials Science, University of Southern California, Los Angeles, California 90089-0241*
(Received 2 November 1990)

A study of the linear and nonlinear optical behavior of recently realized crystalline organic semiconductor quantum wells is reported. Using the Davydov Hamiltonian, we find analytical solutions for the optical response function, and we predict the existence of intrinsic optical bistability and two-beam-coupling energy transfer in these materials.

PACS numbers: 72.80.Le, 78.20.−e

Current research in the optical properties of organic materials has been directed toward the elucidation of the dominant mechanism that gives rise to their nonlinear optical behavior.[1] In spite of the many experiments performed over the past decade,[2] little depth of understanding has been achieved. The complications arise from the competing effects between the delocalization of the photogenerated charge carriers,[3] and formation of the excitations or quasiparticles.[4] Recent nonlinear optical-absorption experiments[5] performed on the quasi-1D semiconductor polydiacetylene appeared to confirm the concept[6] that excitons are responsible for the nonlinear optical behavior of 1D organic materials.

In this work, we have extended the studies of semiconductor multiple quantum wells (MQWs) to the case of crystalline organic MQWs (CO-MQWs) (Ref. 7) and have found that the response of the quantum-confined charge-transfer (CT) excitons to external fields have novel nonlinear optical properties. CT excitons are known to exist in molecular crystals[8] and their electronic structure can be described by means of the Wannier picture[9] with an appropriate static dielectric constant. However, their interaction with the lattice is significantly different from the Wannier excitons found in inorganic semiconducting hosts. The CT exciton binding energy lies in the few-eV range, making them less susceptible to phonon-induced ionization as compared to Wannier excitons in inorganic semiconductors.

In previous work, the linear optical properties of CO-MQWs were measured in some detail.[7] It was found that the lowest-energy CT exciton absorption line was blueshifted with decreasing well width. This observation is consistent with quantum confinement of the CT exciton by energy wells formed in one of the two MQW layers (consisting of 3,4,9,10-perylenetetracarboxylic dianhydride or PTCDA), sandwiched between layers of a second material (3,4,7,8-naphthalene tetracarboxylic dianhydride or NTCDA) forming energy barriers. A variational study of the dependence of exciton energy on well width indicates that the exciton radius is approximately 15 Å. This number is significantly smaller than that found in III-V semiconducting compounds because of the smaller static dielectric constant of organic crystals. The strong Coulomb binding energy (as compared with the kinetic energy of each charge carrier) in the CO-MQW materials implies that the quantization due to the well thickness L is determined by the center-of-mass motion of the exciton. Hence the exciton binding energy is given by $\hbar\omega_x = \hbar\omega_B + (\hbar\pi n)^2/2ML^2$ for an infinitely deep potential well, where ω_B is the bulk exciton binding energy, n is an integer, and M is the total mass of the exciton. This expression provides a qualitative explanation of the observed blueshift that was reported in the linear absorption measurements. Since the CT exciton represents a correlated electron-hole pair between nearly adjacent molecules in a stack, we can consider this radius to be the spatial dimension in an electric dipole moment. Such a large dipole moment should, in turn, lead to large optical nonlinearities in these materials. These optical nonlinearities are the focus of this study.

The starting point of our analysis of the optical properties of CT excitons in crystalline organic materials is the Davydov Hamiltonian which describes the interaction of excitons with phonons and external radiation fields. Assuming the rotating-wave approximation, existence of one phonon mode, and keeping only the linear exciton-phonon interaction, the Hamiltonian is

$$H = \hbar(\omega_x - \omega)a^\dagger a + \hbar\omega_0 b^\dagger b - \hbar\lambda a^\dagger a Q - \tfrac{1}{2}\mu a^\dagger E - \tfrac{1}{2}\mu a E^*, \quad (1)$$

where $\hbar\omega_x$ and $\hbar\omega_0$ are the quantum-confined exciton binding and phonon energies, respectively. Also, λ is the exciton-phonon coupling constant, μ is the electric dipole moment of the exciton, $a^\dagger a$ and $b^\dagger b$ are the exciton and phonon populations, respectively. Further, $Q = b + b^\dagger$ is the phonon amplitude, E is the slowly varying envelope of the external field, and a and b are the exciton coherence and phonon annihilation operators, respectively.

Careful interpretation of the constants λ and μ must be considered. Current measurements appear to be inconclusive concerning the effects of quantization on these

constants. From a theoretical point of view, quantum confinement should play a role since the envelope wave functions are quantized and they enter in the computation of the matrix elements of the observables. That is, the quantum confinement modifies the bulk values by a factor that reflects the overlap of the spatial wave functions for the electrons and holes.

The temporal evolution of the exciton coherence a and phonon amplitude Q are determined by the Heisenberg equation of motion, and are given by

$$\frac{da}{dt}+[i(\omega_x-\omega)+\gamma]a=i\lambda Qa+i\frac{\mu E}{2\hbar}, \tag{2a}$$

$$\frac{d^2Q}{dt^2}+\Gamma\frac{dQ}{dt}+(\omega_0)^2Q=2\omega_0\lambda a^\dagger a, \tag{2b}$$

where γ and Γ are phenomenological exciton dephasing and phonon decay rates, respectively. Equations (2) provide insight into the nonlinear optical behavior of exciton-phonon-coupled systems. The term $i\lambda Qa$ in Eq. (2a) is a renormalization of the exciton frequency due to its coupling to the phonon structure of the material. Since it depends on the phonon amplitude Q, the renormalization factor can be seen to be proportional to the exciton density from the steady-state solution of Eq. (2b). This implies that the effective exciton frequency is a function of the population of photogenerated excitons, which is proportional to the light intensity. Hence, optical nonlinearities in these materials have their origin in an exciton-phonon–induced frequency shift,[5] in a manner similar to the dynamic Stark shift in polaritons.[10]

The nonlinear evolution of coupled waves is determined by the Maxwell equations. In the slowly varying envelope approximation, they are given as

$$2ik_a\frac{dE_a}{dz}=-\left(\frac{\omega}{c}\right)^2P_a, \tag{3a}$$

where the nonlinear polarization density P_a is defined by

$$P_a=N\mu\langle a\rangle. \tag{3b}$$

Here, N is the number density of CT excitons and $\langle a\rangle$ is the expectation value of a. The subscript a denotes the radiation field oscillating at frequency ω_a.

Equations (1)–(3) have exact, closed-form analytical solutions in the steady-state regime. We shall consider three important cases. The first involves the linear response of the medium to an optical radiation field. A comparison of the theoretical model to the available experimental data will provide an estimate of the coupling parameters. Second, we will explore the nonlinear response of the medium by obtaining an exact solution to the CT exciton population $\langle a^\dagger a\rangle$. Finally, we will use the results to understand the process of two-beam coupling[1] in these materials. The latter involves the nonlinear coupling of strong and weak radiation fields.

For the case of a single input optical wave, the analytical solution of Eq. (2) is obtained under the condition of factorization of the respective variables, a and Q. First, in the low-intensity regime, the population of photogenerated excitons is proportional to the intensity of the optical wave, and the polarization density is determined by the steady-state small-signal solution of Eqs. (2). That is,

$$P=\frac{N\mu^2}{2\hbar}Ee^{-i\omega t}\left\langle\left\langle\frac{1}{\omega_x-\omega+i\gamma}\right\rangle\right\rangle. \tag{4}$$

Figure 1 depicts the linear absorption (dark solid line) measurement and the theoretical fit (light solid line) which assumes the existence of two excitonic lines in the S_0 to S_1 electronic manifold.[8] The theoretical result is fitted against the experimental data in the following manner. The wavelengths of the two maxima located in the right-hand side of the experimental absorption profile are chosen to set the horizontal scale. The vertical scale is set by the ratio of the two peaks in the right-hand side of the data, assuming that the height of the largest peak is equal to unity. In order to obtain reasonably good quantitative agreement, the imaginary part of the polarization density was averaged over a Maxwellian distribution with two distinct widths, which are chosen from the experimental data. The use of the Maxwellian distribution is consistent with the fast phonon-induced relaxation processes that exist in these materials. The result shown in Fig. 1 indicates that the experimental data contain more than two excitonic lines, which is the source of discrepancy between the theoretical model and experimental data. In spite of the complexity, the theoretical model gives an adequate understanding of the origin of the linear absorption spectra of these materials.

Second, in the fully nonlinear regime, the solution for the population $\langle a^\dagger a\rangle$ of the CT exciton is given by the

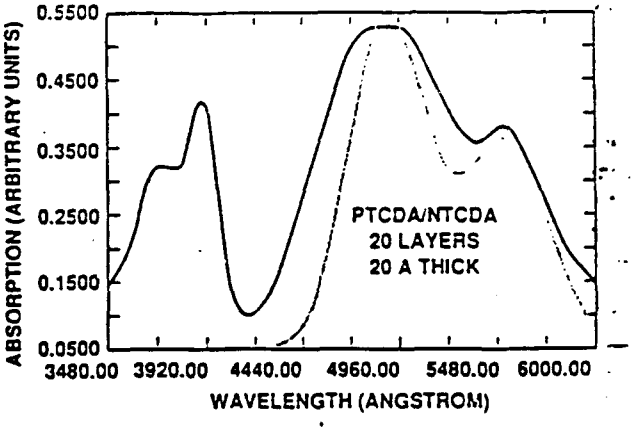

FIG. 1. Linear absorption coefficient of PTCDA/NTCDA MQWs. The experimental data (dark solid line) contain two additional sidebands on the left-hand side due to the presence of the NTCDA. The theoretical fit (light solid line) from the solution of the exciton-phonon equations is based on thermalization by phonons and the assumption of two exciton resonances.

cubic equation

$$\langle a^\dagger a\rangle = \frac{\Omega^2}{\gamma^2+[\Delta-(2\lambda^2/\omega_0)^2\langle a^\dagger a\rangle]^2}, \quad (5)$$

where $\Delta=\omega_x-\omega$ is the detuning from the exciton resonance and $\Omega=\mu E/2\hbar$ is the Rabi frequency. Figure 2 shows the solution of this cubic equation as a function of the Rabi frequency for different values of the detuning parameter Δ. In this plot, all physical variables have been normalized to $2\lambda^2/\omega_0$. A transition to multivalue behavior is observed for a sufficiently large value of the detuning parameter Δ. This behavior can be understood in the following manner. Multivalue behavior of Eq. (5) is achieved if the derivative of the Rabi frequency with respect to the exciton population changes sign. A simple calculation of this criterion asserts that bistability is present provided that

$$\Delta>\sqrt{3}\gamma. \quad (6)$$

This condition is valid even in the absence of an optical cavity. Hence, the coupled exciton-phonon system posseses the property of intrinsic bistable behavior which arises from the renormalization of the exciton frequency mediated by the exciton-phonon interaction.

Finally, we consider the interaction between a strong wave E_0, oscillating at frequency ω, and a weak wave E_1, oscillating at frequency $\omega+\delta$. Their nonlinear coupling yields a coherent traveling-wave excitation in the medium oscillating at frequency δ. The scattering of the strong wave from the coherent excitation changes the absorption coefficient and the index of refraction experienced by the weak wave. A calculation of the optical response function in the undepleted pump approximation gives the following expression for the spatial evolution of the weak wave:

$$\frac{1}{E_1}\frac{dE_1}{dz}=-\frac{\omega+\delta}{2n_1}\frac{N\mu^2\omega_0}{\epsilon_0\hbar 2\lambda^2}(\alpha+i\beta), \quad (7a)$$

where the dimensionless (all physical parameters are normalized to $2\lambda^2/\omega_0$) nonlinear absorption coefficient α is

$$\alpha=\frac{(\omega_\delta^2-\delta^2)C-\delta\Gamma D}{C^2+D^2} \quad (7b)$$

and the dimensionless nonlinear index of refraction is given by

$$\beta=\frac{(\omega_\delta^2-\delta^2)D+\delta\Gamma C}{C^2+D^2}, \quad (7c)$$

with the following expressions for C and D:

$$C=\gamma(\omega_\delta^2-\delta^2)+\delta\Gamma(\Delta-\delta)-\delta\Gamma\langle a^\dagger a\rangle,$$

$$D=(\omega_\delta^2-\delta^2)(\Delta-\delta)-\delta\Gamma\gamma-(2\omega_\delta^2-\delta^2)\langle a^\dagger a\rangle.$$

Figure 3 shows the behavior of the nonlinear absorption coefficient, $\alpha+i\beta$, of the weak wave as a function of the Rabi frequency induced by the strong wave for different values of the quantum-well dimension. A transition to bistable behavior, accompanied by gain (negative values of the nonlinear absorption coefficient) of the weak wave at the expense of the strong wave, is observed for a critical value of the normalized Rabi frequency and a small enough value of the quantum-well dimension. The dimension of the quantum well plays a key role in

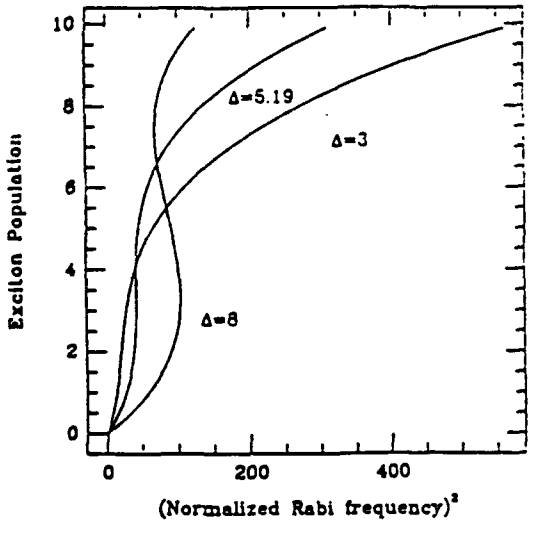

FIG. 2. Dependence of the exciton population on the normalized Rabi frequency to the second power. The linewidth and the detuning are also normalized to $2\lambda^2/\omega_0$, which has the unit of frequency. Curves are shown for normalized detuning $\Delta=3$, $\Delta=5.19$, which corresponds to the transition region for bistability to begin taking place, and $\Delta=8$.

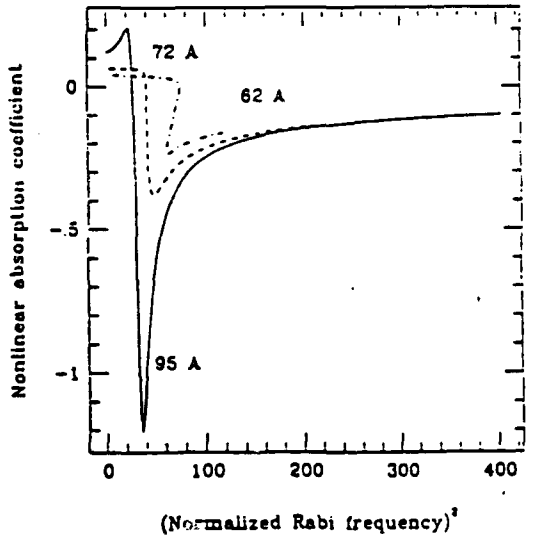

FIG. 3. Two-wave-mixing gain (negative value) and absorption (positive value) coefficient for three different values of the quantum-well size. Prediction of optical bistability and energy transfer is given for $L=62$ Å. The normalized probe-pump detuning parameter δ is set equal to -1.

the detuning parameter Δ. For large enough detuning or small enough well size, the value of the detuning parameter satisfies the bistability condition (6). Hence, a coherent energy transfer from the strong to the weak wave takes place with a threshold behavior. This phenomenon can be thought of as a coherent bistable optical switch. That is, the energy transfer takes place from the strong to the weak optical beams when a certain threshold is achieved. The bistable behavior is a reflection of the nonlinear functional dependence of the exciton population on the pump intensity.

The phenomena discussed in the previous paragraphs provide insight into subtle effects that appear in the Davidov Hamiltonian. Estimates of the physical parameters such as λ and ω_0 are crucial to the understanding of the materials growth conditions as well as to the future applications of these novel materials for optoelectronics. The beauty and simplicity of our results are contained in one single physical parameter, the Franck-Condon (FC) shift. This frequency shift is related to λ and ω_0 by the following expression:

$$FC = \lambda^2/\omega_0 ,$$

and is a measure of the degree of reduction of the potential energy of the material due to the exciton-phonon coupling. From measured values in aromatic molecules,[11] λ is approximately equal to ω_0. These numbers imply a FC shift of 700 cm^{-1} for the case of naphtalene compounds.

It is interesting to calculate the range of laser powers required to observe the onset of optical bistability and two-beam energy transfer. However, the nonlinear absorption coefficient is a sensitive function of the material parameters. For example, if one assumes a FC shift of approximately 1000 cm^{-1} expected for large molecules such as PTCDA,[12] an oscillator strength of unity (consistent with the observed large linear absorption coefficients of 10^5 cm^{-1}), a normalized exciton dephasing rate ranging from 10^{-3} to 1, one finds that the power density ranges from 100 to 10^6 W/cm^2 for $\Delta = 10^{-3}FC$. A more accurate value must wait for a detailed measurement of the FC shift, and the exciton dephasing rate.

In summary, we presented new results on the optical behavior of these newly discovered materials. We predict the existence of intrinsic bistability as well a coherent energy transfer from a strong wave to a weak wave. The energy exchange occurs under bistable conditions, leading to the possibility of novel optical devices using these materials.

This work is supported by the Air Force Office of Scientific Research (Dr. Howard Schlossberg and Major G. Pomrenke). One of us (J.F.L.) would like to thank Dr. R. N. Schwartz for enlightening discussion on organic materials.

[1]See *Nonlinear Optics of Organics and Semiconductors*, edited by T. Kobayashi (Springer-Verlag, Berlin, 1989).

[2]M. Sinclair, D. Moses, A. J. Heeger, K. Vilheimsson, B. Valk, and M. Salour, Solid State Commun. 61, 221 (1987).

[3]See *Nonlinear Optical Properties of Organic Molecules and Crystals*, edited by D. S. Chemla and J. Zyss (Academic, New York, 1987).

[4]W. P. Su, J. R. Schrieffer, and A. J. Heeger, Phys. Rev. Lett. 42, 1698 (1979); L. Rothberg, T. M. Jedju, S. Etemad, and G. L. Baker, Phys. Rev. Lett. 57, 3229 (1986).

[5]B. I. Greene, J. F. Mueller, J. Orenstein, D. H. Rapkine, S. Schmitt-Rink, and M. Thakur, Phys. Rev. Lett. 61, 325 (1988).

[6]S. A. Brazovskii and N. N. Kirova, Pis'ma Zh. Eksp. Teor. Fiz. 33, 6 (1981) [JETP Lett. 33, 4 (1981)].

[7]F. F. So, S. R. Forrest, Y. Q. Shi, and W. H. Steier, Appl. Phys. Lett. 56, 674 (1990).

[8]M. Pope and C. E. Swenberg, *Electronic Processes in Organic Crystals* (Oxford Univ. Press, New York, 1982).

[9]P. J. Bounds and W. Siebrand, Chem. Phys. Lett. 75, 414 (1980).

[10]A. L. Ivanov and L. V. Keldysh, Zh. Eksp. Teor. Fiz. 84, 404 (1983) [Sov. Phys. JETP 57, 234 (1983)].

[11]V. L. Broude, E. I. Rashba, and E. F. Sheka, *Spectroscopy of Molecular Excitons* (Springer-Verlag, Berlin, 1985).

[12]D. Haarer and N. Karl, Chem. Phys. Lett. 21, 49 (1973).

Giant anisotropies in the dielectric properties of quasi-epitaxial crystalline organic semiconductor thin films

D. Y. Zang, F. F. So, and S. R. Forrest
Center for Photonic Technology, Departments of Electrical Engineering and Materials Science, University of Southern California, Los Angeles, California 90089-0241

(Received 7 March 1991; accepted for publication 21 May 1991)

We have measured the indices of refraction and dielectric constants along different directions in thin films of the crystalline organic semiconductor compound 3, 4, 9, 10 perylenetetracarboxylic dianhydride (PTCDA). The films were deposited via organic molecular beam deposition, resulting in single-crystalline, "quasi-epitaxial" films. Due to inherent asymmetries in the molecular crystal structure, film ordering results in giant anisotropies in their dielectric properties. For example, the index of refraction measured at a wavelength of $\lambda = 1.064$ μm in the direction perpendicular to the substrate plane is $n_\perp = 1.36 \pm 0.01$, whereas parallel to the plane, $n_\parallel = 2.017 \pm 0.005$, resulting in an index difference of $\Delta n = 0.66$. Furthermore, the low-frequency dielectric constant of the films is $\epsilon_\perp = 1.9 \pm 0.1$ and $\epsilon_\parallel = 4.5 \pm 0.2$. To our knowledge, these are the largest anisotropies ever measured for thin films. We discuss a guided wave polarization-selective device which takes advantage of the large dielectric anisotropies characteristic of the thin organic films.

Crystalline organic semiconductors exhibit a diversity of optical and electronic properties which have numerous device applications.[1-5] Recently, we have demonstrated that under certain deposition conditions, single-crystalline thin films of the organic compound 3, 4, 9, 10 perylenetetracarboxylic dianhydride (PTCDA) can be deposited onto a variety of substrate materials including glass, metal, or semiconductors. It has been found that the conductivity of such films is extremely anisotropic[6] due to asymmetries in the crystalline structure of the organic compounds investigated. For example, the in-plane conductivity of PTCDA films is found to be at least six orders of magnitude lower than the conductivity perpendicular to the film plane.

One would expect that the dielectric properties of ordered films would also be anisotropic along different crystalline directions. A unit cell of PTCDA is shown in the inset of Fig. 1. The molecules form tilted planar stacks, with a distance of 3.21 Å between molecules in the stack. The long axes of molecules in adjacent stacks are rotated by 90° to the long axis of a molecule in the stack at the center of the unit cell. Now, the off-resonance dielectric constant for a material is given by

$$\epsilon - 1 = 4\pi N q^2 f_j / [m^*(\omega_j^2 - \omega^2)], \qquad (1)$$

where N is the number density of the material, ω_j is the dipole transition frequency, ω is the frequency of the incident electromagnetic radiation, q is the electronic charge, and m^* is the electron effective mass. The oscillator strength of the dipole transition from level o to j is given by $f_j = 2m^*\hbar\omega|x_{0j}|^2/\hbar^2$, where x_{0j} is the electron position expectation value, and $\hbar$ is Planck's constant divided by 2π. Assuming the largest contribution to the dipole moment of the molecule is due to the π orbitals, and that the electron within a given orbital is completely delocalized, then we can make the approximation $f_{j\perp}/f_{j\parallel} \sim |x_{oj\perp}|^2/|x_{oj\parallel}|^2 \sim d^2/L^2$. Here, $d \cong 3.2$ Å is the extent of the π orbital perpendicular to the molecular plane, and L is its extent in the plane, which is taken as the length of the perylene molecular core of PTCDA (i.e., $L \simeq 6.9$ Å). Due to the weak interaction between molecules in crystalline organic semiconductors, this single molecule approximation also can be accurately applied to bulk crystals.[7] Hence, provided that there is perfect crystalline alignment throughout the thin film, we can expect an anisotropy in ϵ between directions perpendicular and parallel to the thin-film plane of $(\epsilon_\perp - 1)/(\epsilon_\parallel - 1) \sim d^2/L^2 \sim 0.22$. This value is only an approximation, since we are assuming that m^* is isotropic, and that the dipole moment is due to a completely delocalized electron in the extended π system. Nevertheless, it is shown below that this value is close to the measured anisotropy in ϵ for quasi-epitaxial films of PTCDA.

To measure the dielectric constant along different film directions, capacitors oriented along the various film axes were fabricated on quartz substrates. For measuring the capacitance along the in-plane direction, interdigitated patterns of Cr-Au contacts were employed. Here, a thin layer ($\sim$150 Å) of Cr was deposited, followed by a 0.7-μm-thick Au layer which forms a current-blocking contact to

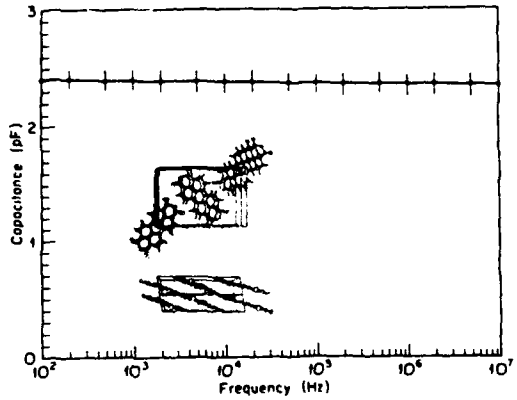

FIG. 1. Capacitance measured vs frequency for a horizontal, interdigitated capacitor with PTCDA serving as the dielectric. Inset: Two views of a unit cell of PTCDA.

 0003-6951/91/320823-04$02.00

PTCDA.[6] Next, the contacts were patterned into 2-mm-long interdigitated electrodes with 2 μm spacing and width. Some electrode sets were positioned perpendicular to others to determine if there were significant asymmetries in the capacitance in the two in-plane directions. Next, purified PTCDA was deposited to a thickness of 0.9 μm via organic molecular beam deposition (OMBD) onto the quartz substrate which was maintained at a temperature of approximately 90 K during growth. As has been discussed previously,[8] deposition under these conditions ensures that the resulting film is single crystalline, independent of the substrate material employed. The capacitance measured between 100 Hz and 10 MHz is shown in Fig. 1. The capacitance is independent of frequency over the measurement range, indicating that the films are free of traps.

It can be shown that the ratio of capacitances of the interdigitated contact pattern measured before (C_{uo}) and after (C_u) deposition of the PTCDA thin film is simply[9] $C_{uo}/C_u = (\epsilon_s + 1)/(\epsilon_s + \epsilon_\parallel)$, where ϵ_s is the dielectric constant for quartz. We note that the small amount of electric field penetration above the PTCDA film can lead to deviations from this expression. However, since the PTCDA thickness was larger than that of the contact fingers, this error is expected to lead to an insignificant underestimate of $\epsilon_\parallel$. By measuring C_{uo} and C_u for these samples, we obtain in-plane dielectric constants for PTCDA of $\epsilon_\parallel = 4.6 \pm 0.2$ and 4.3 ± 0.2 for the two perpendicular orientations of the patterns. Since these values are within each other's error limits, we assume that the dielectric constants along the two directions are not significantly different, leading to $\epsilon_\parallel = 4.5 \pm 0.2$.

To measure $\epsilon_\perp$, a parallel-plate capacitor consisting of a PTCDA film (0.9 μm thick) sandwiched between two Cr-Au contacts was used. Using this geometry, it is found that $\epsilon_\perp = 1.9 \pm 0.1$ over the same frequency range as that used to measure $\epsilon_\parallel$. From these data we obtain $(\epsilon_\perp - 1)/(\epsilon_\parallel - 1) = 0.26$ which is close to our estimate of 0.22 for perfectly oriented crystalline films. In earlier measurements of $\epsilon_\perp$ for PTCDA deposited under conditions leading to polycrystalline growth, it was found that[6] $\epsilon_\perp = 3.6 \pm 0.4$. Assuming a homogeneous medium was being analyzed in that case, then the spatially averaged dielectric constant is $\epsilon \cong (2\epsilon_\parallel + \epsilon_\perp)/3$. Using the values of ϵ obtained here, we find $\epsilon \cong 3.6$, in agreement with the former value. This indicates that the films deposited on room-temperature substrates are structurally randomized, whereas deposition via OMBD on cold substrates results in nearly perfect crystalline order across broad areas.

Since $\epsilon_\infty = n^2$, where n is the refractive index, and ϵ_∞ is the thin-film dielectric constant at optical frequencies, we also expect to observe asymmetries in n as a result of the ordering of the PTCDA films. Previously[5] we measured an in-plane refractive index of $n_\parallel = 2.017 \pm 0.005$. In this work, therefore, we measure only $n_\perp$.

Determination of $n_\perp$ proceeds by measuring the reflectivity from the thin film as a function of beam incident angle using several film thicknesses and light wavelengths. Considering an *isotropic* homogeneous thin film sandwiched between two semi-infinite media, the reflectivity is given by[10]

$$R = \frac{r_{12}^2 + r_{23}^2 + 2r_{12}r_{23}\cos 2\beta}{1 + r_{12}^2 r_{23}^2 + 2r_{12}r_{23}\cos 2\beta}, \tag{2}$$

where $\beta = 2\pi n_2 t \cos\theta_2/\lambda$. Here, n_2 is the refractive index measured along the refractive angle θ_2 in the thin film of thickness t. Also, r_{12} (r_{23}) is the reflectivity at the interface between medium 1 (3) and medium 2. The reflectivity maxima and minima for a given index, n_2, occur at angles θ_2 which satisfy $n_2 t = m\lambda/4\cos\theta_2$, where m is the integer order of the extremum. If the film thickness is accurately determined, the refractive index can thence be obtained by measuring the angles corresponding to reflectivity extrema as predicted by these equations.

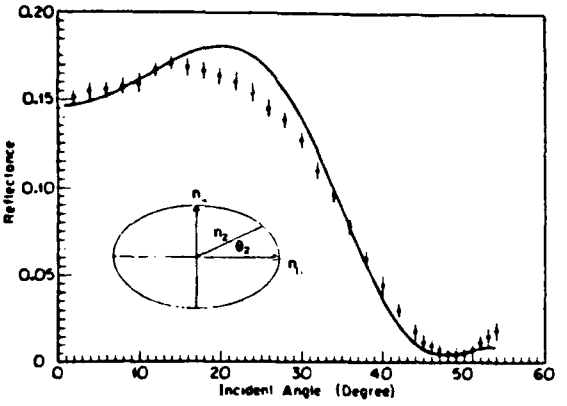

FIG. 2. Reflectance at $\lambda = 1.064$ μm vs incident beam angle for a 1.25-μm-thick PTCDA film on a quartz substrate. Data are shown as closed circles, and theory is shown as a solid line. Inset: Index of refraction ellipsoid for PTCDA showing the relationship between the indices along different thin-film directions.

To extend this technique to anisotropic thin films, the incident light polarization is made parallel to the plane of incidence, i.e., it is a TM-polarized wave. Furthermore, using birefringence measurements,[8] the optical b axis is located, and is also oriented parallel to the incident light polarization vector. When the incident angle (θ_1) of the beam to the film is changed, this rotates θ_2 in an index ellipsoid with axes of length $n_\parallel = n_b$ and $n_\perp$, as shown in the inset in Fig. 2. Here, n_b is the index along the b axis. From this figure, it follows that the index $n_2^2 = n_\parallel^2 + (1 - n_\parallel^2/n_1^2)\sin^2\theta_1$, from which $n_\perp$ is extracted.

A typical measurement result made at $\lambda = 1.064$ μm for a 1.25-μm-thick PTCDA film together with a theoretical calculation using Eq. (2) is shown in Fig. 2. The experimental setup consists of a YAG laser providing the polarized incident beam. A large area detector is positioned near the top film surface to measure the reflected light intensity. The PTCDA is deposited on a quartz substrate at low temperatures. The back surface of the quartz is frosted to minimize reflections from the quartz/air interface. The positions of the theoretical extrema (particularly the minima) can be made to match those obtained experimentally, although the magnitude of the reflected signal is sometimes different from that predicted due to unwanted reflections from surface imperfections and the

TABLE I. Reflectivity data for PTCDA thin films.

$\lambda(\mu m)$	Sample thickness	Incident angle[a]	$n_\perp$ (Cal).
1.064	1.13	29°	1.354 ($m=8$)
1.319	1.25	47°	1.364 ($m=8$)
1.064	1.13	41°	1.343 ($m=6$)
1.319	1.25	55.5°	1.346 ($m=6$)

[a]Corresponding to the reflectivity minima.

quartz/air interface. Similar fits are obtained for a film thickness of 1.13 μm, and at $\lambda = 1.3$ μm, and the data are listed in Table I. From these data, we obtain $n_\perp = 1.36 \pm 0.01$ at $\lambda = 1.064$ μm, giving $\Delta n = n_\parallel - n_\perp = 0.66$, which apparently is the largest value of Δn reported for thin films far from their absorption edge (which for PTCDA lies at $\lambda \cong 6000$ Å[6]). Very little dispersion is observed in n measured at $\lambda = 1.064$ and 1.3 μm, as indicated in Table I.

It is interesting to compare the asymmetries measured for the dielectric constant and the index of refraction. Ignoring dispersion between the frequencies at which these parameters were determined, we find that $\epsilon_\parallel/\epsilon_\perp = 2.4 \cong (n_\parallel/n_\perp)^2 = 2.2$. This is a remarkable agreement given the widely different conditions under which the various measurements were made. Indeed, we see that the low-frequency dielectric constant is approximately equal to n^2 for each of the various film directions.

A waveguide polarizer was fabricated to take advantage of the large birefringence characteristic of OMBD-grown PTCDA thin films. Thus, PTCDA rib waveguides were made of lengths of 1.5 and 10 mm. The guides were fabricated by first spinning a 1-μm-thick film of the photoresist AZ 1400 (with $n_{PR} = 1.61$) onto the (100) surface of an InP wafer (with $n_s = 3.27$ at $\lambda = 1.064$ μm). Next, 2-μm-wide ridges were photolithographically patterned in the AZ 1400, followed by deposition of approximately 1 μm of PTCDA. The regions where PTCDA was deposited onto the photoresist ridges form the guides to TE modes (where $n_\parallel > n_{PR}$), but not to TM modes (where $n_\perp < n_{PR}$). The substrates were cleaved along (110) planes, allowing for coupling into the end facets. Similar guides have been measured to have a loss of < 2.5 dB/cm.[5]

Due to the selective guiding of TE modes, the waveguides form a strongly polarizing medium. To measure the TM/TE extinction ratio, $\lambda = 1.064$ μm light from a diode-pumped YAG laser was coupled into and out of the guides using microscope objective lenses. The input light polarization was continuously rotated through 360° using a quarter wave plate placed between the laser and the sample. In addition, a Glan–Thomson polarizer (GTP) with an extinction ratio > 50 dB was placed in front of the laser. This setup, shown in the inset of Fig. 3, ensures a constant coupling efficiency of a polarized beam along any direction. The outcoupled light was passed through a second GTP which analyzed the light prior to being detected using a Si CCD camera.

Measurements for the 10-mm-long device are shown in Fig. 3. Here, both the TE and TM components of the output light beam are plotted versus the input light polar-

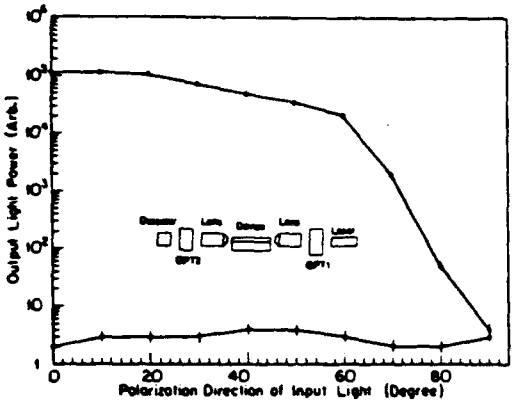

FIG. 3. Transmitted light intensity for TE and TM waves in a 10-mm-long, 2-μm-wide PTCDA rib waveguide as a function of incident angle of polarization. Measurements are made at $\lambda = 1.064$ μm. Inset: Experimental setup used to characterize the PTCDA waveguide polarizer under study.

ization angle. An extinction ratio of TM/TE < -48 dB was obtained, where the measurement accuracy was limited by the GTP. Similar results were obtained for the 1.5 mm guide, where an extinction ratio of TM/TE < -25 dB was measured. The accuracy here was limited by light scattered over the top of the short guide. The propagation loss of the short guide was found to be < 0.4 dB.

In summary, extremely large anisotropies in dielectric properties have been observed in crystalline organic thin films of the compound, PTCDA. The anisotropies in both the dielectric constant and index of refraction for these films is a result of their nearly perfect crystalline order achieved via OMBD on cold substrates. Similar results are expected for other anisotropic organic semiconductor crystals deposited using the OMBD technique. Furthermore, a TE-pass waveguide polarizer with a high TM polarization extinction and low TE propagation loss was demonstrated. Since such polarizing guides can be deposited on semiconductor substrates, these films have uses such as optical isolators integrated with semiconductor lasers or amplifiers.

The authors gratefully acknowledge the Air Force Office of Scientific Research (G. Pomrenke) and 3M Corporation without whose support this work would not have been possible.

[1]F. F. So and S. R. Forrest, IEEE Trans. Electron Devices 36, 66 (1989).
[2]C. L. Cheng, S. R. Forrest, M. L. Kaplan, P. H. Schmidt, and B. Tell, Appl. Phys. Lett. 47, 1217 (1985).
[3]C. Adachi, S. Tokito, T. Tsutsui, and S. Saito, Jpn. J. Appl. Phys. 27, L713 (1988).
[4]J. Simon and J.-J. Andre, *Molecular Semiconductors: Photoelectrical Properties and Solar Cells* (Springer, Berlin, 1985).
[5]D. Y. Zang, Y. Q. Shi, F. F. So, S. R. Forrest, and W. H. Steier, Appl. Phys. Lett. 58, 562 (1991).
[6]S. R. Forrest, M. L. Kaplan, and P. H. Schmidt, J. Appl. Phys. 55, 1492 (1984).
[7]E. A. Silinsh, *Organic Molecular Crystals: Their Electronic States* (Springer, Berlin, 1980), Chap. 2.
[8]F. F. So, S. R. Forrest, Y. Q. Shi, and W. H. Steier, Appl. Phys. Lett. 56, 674 (1990).
[9]W. R. Smythe, *Static and Dynamic Electricity* (McGraw-Hill, New York, 1950), p. 109.
[10]M. Born and E. Wolf, *The Principles of Optics*, 6th ed. (Pergamon, Oxford, 1980), pp. 51–63.